INAF

ISTITUTO NAZIONALE DI ASTROFISICA
OSSERVATORIO ASTROFISICO DI TORINO

Euclid FGS Input Star Catalogue Performance Assessment

SIGNATURE AND APPROVALS ON ORIGINAL

Authors: *S. Perina, R. Drimmel, A. Spagna, P. Re Fiorentin, B. Bucciarelli, R. Morbidelli, R. Smart, M. Lattanzi*

Contract: TASI – OATo, Purchase Order no. 1520060041

Doc: EUCL-OATO-RP-2-004

Issue: 1

Rev: 1

Date: 28/05/2020

APPROVALS:

Program Manager / Techn. Resp.: R. Drimmel

Program Controller / Contractual Resp.: M. Sarasso

DOCUMENT CHANGE RECORD

ISSUE	DATE	REASON FOR CHANGE	AFFECTED PARAGRAPHS
0.0	21/02/2020	Creation	All sections
1.0	05/05/2020	Issued	All sections
1.1	28/05/2020	Revision	Sections 5.2.3, 8.2

TABLE OF CONTENTS

1 SCOPE **4**

2 REFERENCES **4**
2.1 Applicable documents 4

3 DEFINITIONS AND ACRONYMS **5**
3.1 Definitions 5
3.2 Acronyms 5

4 SUMMARY **7**

5 ALL-SKY STATISTICS **9**
5.1 Methodology 9
5.2 Results 9
5.2.1 Magnitude Distribution 9
5.2.2 HEALpix Level 9 Statistics 10
5.2.3 Neighbor Flag statistics 12
5.2.4 Variability and Extended Source Flag Statistics 14
5.2.5 Latitude Distribution 15
5.2.6 Coordinate Errors Distribution 16

6 HEALPix level 2 statistics **17**
6.1 Methodology 17
6.2 Results 19

7 ALL-SKY maps **25**
7.1 Methodology 25
7.2 Results 25

8 Big Extended Sources in ISC **51**
8.1 Methodology 51
8.2 Results 53

9 APPENDIX A **57**

10 APPENDIX B **70**

1. SCOPE

The objective of this performance assessment is to evaluate the ISC performance with respect to some of the key requirements defined in EUCL-TAST-RS-2-056 [AD 1] that may impact the performance of the FGS. This document presents a broader analysis of the ISC performance, taking into consideration the results of the executed verification test cases described in the VTR [AD 2].

2. REFERENCES

2.1 Applicable documents

[AD 1] Bosco A., *Euclid FGS Input Star Catalogue Requirement Specifications*, 21 April 2016, EUCL-TAST-RS-2-056, issue 1

[AD 2] Drimmel R. et al., *Euclid FGS Input Star Catalogue Verification Test Report*, 9 Dec 2019, EUCL-OATO-RP-2-002, issue 1

[AD 3] Perina S., *Euclid FGS Input Star Catalog Generation Approach of Release ISC.R3*, 6 Dec 2019, EUCL-OATO-TN-2-006, issue 2

[AD 4] Morbidelli R., Perina S., *Release Note for Input Star Catalogue R.3 - HEALPix 00 to 191 (all sky)*, 6 Dec 2019, EUCL-OATO-NOTE-2-009, Issue 1

3. DEFINITIONS AND ACRONYMS

3.1 Definitions

In accordance with the SoW [AD 1], the following definitions shall be used.

- **Input Star Catalogue (ISC)**
  Representative of the whole sky. Collecting all the FGS possible targets after a process of target selection driven by the FGS star catalogue requirements. Used as input for the On-ground Algorithm to generate the FGS On-board Catalogue and Triad Database.
- **Reference Star Catalogue (RSC)**
  Representative of the real sky. Limited to selected portions of the sky, collecting all available information in the current databases. Used for pixel-by-pixel simulation, FGS simulator validation and Relative Tracking Mode (RTM) performance analysis.

3.2 Acronyms

Acronym	*Definition*
2MASS	Two Micron All Sky Survey, Extended source catalogue
AD	Applicable Document
ASCII	American Standard Code for Information Interchange
ATM	Absolute Tracking Mode
CCD	Charged Couple Device
DB	DataBase
DDVP	Design Development and Verification Plan
DPAC	Data Processing and Analysis Consortium
DR	Data Release
ESA	European Space Agency
FGS	Fine Guidance Sensor
FOV	Field of View
HEALPix	Hierarchical Equal Area Iso Latitude Pixelation
ICD	Interface Control Document
IDL	Interactive Data Language
INAF	Istituto Nazionale di Astrofisica
ISC	Input Star Catalogue
NGC	New General Catalog
Ns	Number of stars
OATo	Osservatorio Astrofisico di Torino
RD	Reference Document
RSC	Reference Star Catalogue
RTM	Relative Tracking Mode
SDSS	Sloan Digital Sky Survey
SoW or SOW	Statement of Work

SW	Software
TASI	Thales Alenia Space Italy
TAST	Thales Alenia Space Torino
TN	Technical Note
VTR	Verification Test Report

4. SUMMARY

Subject of this report is a detailed and quantitative description of the ISC content.
In section 5 we give summary statistics of the ISC. In Sections 6 and 7 the problem of sparse number of sources is addressed quantifying the impact of the use of the proposed mitigation strategies. In Section 8 the probable number of ISC sources larger than 2.9 arcsec is estimated as a function of R_{FGS} magnitude and in Appendix A and B a sample of such large ISC sources, as identified by the SDSS (Sloan Digital Sky Survey) catalogue, are visually verified an cross-matched with Hubble Space Telescope (HST) archived images to verify their extended nature.

The Verification Test Report (VTR, EUCL-OATO-RP-2-002 [AD 2]) states that the ISC.R3, based on Gaia DR2, does not fulfill all the requirements defined in EUCL-TAST-RS-2-056 [AD 1].
The failed test cases are ISC-TST-REQ-0020-01 and ISC-TST-REQ-0040-01.

Test case ISC-REQ-0020-01 states that

> *the ISC shall contain at least 5 objects suitable for absolute attitude determination for any pointing direction, considering one FGS CCD field of view of 0.11°x0.11°. Among these 5 objects, at least 3 objects shall not have neighbors. An object suitable for absolute attitude determination is defined as having an accuracy better than 0.4" per axis (1 sigma value) at the ISC epoch.*

Relevant to this requirement is the neighborhood flag describing the neighboring conditions of each ISC source:
F=0: no neighbor (isolated source)
F=1: brightest neighbor
F=2: not the brightest neighbor
F=3: unknown neighboring condition
An object shall be considered as having a neighbor (F=1, F=2) if there is any other object closer than 2 arcseconds at the ISC epoch and within 2 magnitudes.

Fields of view (FOVs) with less than 5 sources or with less than 3 objects with no neighbor are the ones not satisfying EUCL-ISC-REQ-0020 and will be named *substandard FOVs* in the rest of the document.

The test case to verify requirement EUCL-ISC-REQ-0020 was expected to fail due to astrophysical reasons. In the VTR [AD 2] three main causes of failure have been identified:

1. Lack of sources in small sky areas due to the patchy completeness caused by the sky scanning pattern of Gaia (e.g. see Figure 14). This problem doesn't have an astrophysical origin, but it is related to the completeness status of the reference survey on which ISC is based. It had already been encountered in ISC.R2, which is based on the less complete Gaia-DR1 data. The higher completeness of the final release of the ISC, based on Gaia-DR2, reduced the extent of the problem even if it is still not enough to entirely remove it. This cause of failure could be completely removed considering a successive version of ISC based on Gaia-DR3 which is expected to further improve the completeness.

2. Lack of sources in small, contiguous sky areas due to high interstellar extinction, in particular near the Galactic plane (e.g. see Figure 16). This is an inherent limitation of the real distribution of dust and stars in the sky, and cannot be resolved.
3. Occasional lack of sources due to sparse number counts of stars at high galactic latitude. Even if this problem only affects a small number of FGS fields, the affected fields are not contiguous, and so cannot be easily mapped and avoided, as can be done for the high extinction areas.

In the VTR [AD 2] some mitigation strategies have been suggested in particular to address the problem of scarce number of sources at high galactic latitudes:

1. treatment of sources with Neighbor Flag F=3 (unknown neighboring condition) as isolated sources;
2. the possibility to choose which FGS CCD should be used during the operation planning phase in order to avoid in advance the FGS failure due to lack of ISC sources for specific target fields. This operation can always be successfully performed in the case of isolated *substandard FOVs*, i.e.*substandard FOVs* surrounded by nominal adjacent FOVs.

We evaluate the efficiency of these mitigation strategies in Section 6 and 7. In Section 6 we find that the fraction of the sky not meeting the requirement EUCL-ISC-REQ-0020 is reduced from 0.0339% to 0.0077% of the sky when these two strategies are used in concert. Furthermore, in Section 7 we show that the remaining parts of the sky that do not have sufficient ISC sources for the FGS is restricted to the part of the sky that is either within 20°of the galactic plane or within 20° of the ecliptic plane, and therefore should have no impact in the Eulid survey area. In any case, the ISC permits such fields to be identified and avoided during the on-ground observation planning phase.

The second requirement found to be not satisfied in the VTR [AD 2] is ISC-TST-REQ-0040-01:

> *the ISC shall not contain objects with estimated size higher than 2.9 arcsecs x 2.9 arcsecs (29 x 29 pixels).*

The failure of this requirement was not foreseen, as it was expected that the onboard source detection algorithm used by the Gaia satellite would filter out large extended sources, as per design. However, published studies indicate that galaxies with a highly peaked luminosity profile could indeed be detected by Gaia. In the VTR [AD 2] this was confirmed by identifying a few such cases as part of the verification test phase (see [AD 2] Section 6.5).

In Section 8 we estimate the total number of ISC sources that may be larger than 2.9 arcsecs to be just over 1 million objects, or about 0.16% of the ISC. This estimate is based on a detailed study of a small fraction of the sky that is also covered by the SDSS survey. Unfortunately, as Gaia DR2 is not an imaging survey, we cannot positively identify and remove these sources. Nevertheless, we show some examples of large ISC sources that were observed by HST. These images confirm that the large extended sources in the ISC have a strong central peak in their luminosity profile, which would make them easily detected by the FGS, so therefore should not cause undue problems for the FGS. In any case, ISC sources flagged as extended should be avoided for tracking purposes.

For more details about the verification phase overall assessment and the possible mitigation strategies we refer the reader to the VTR [AD 2].

5. ALL-SKY STATISTICS

In this section we provide an all-sky statistical summary of ISC.R3.

5.1 Methodology

For all the ISC sources we computed:

1. the all-sky R_{FGS} magnitude distribution;
2. the distribution of the counts in HEALPix level 9 regions (FOVs). The pixel of the HEALPix tessellation scheme at level 9 has size $\theta_{pix} = 0.11°$, approximately equal to the FGS FOV;
3. the number of ISC sources per Neighbor flag value [0,1,2,3];
4. the Galactic Latitude distribution;
5. the coordinate errors distribution.

The analysis has been performed using Python scripts and tools (Healpy, Astropy, Numpy, Pandas, Matplotlib) and TOPCAT (Tool for OPerations on Catalogues And Tables).

5.2 Results

5.2.1 Magnitude Distribution

Figure 1 shows the R_{FGS} magnitude distribution of the ISC sources. The ISC sources span a range in magnitude of $1 < R_{FGS} < 19$. The FGS magnitude range [10 - 19] is plotted in blue.

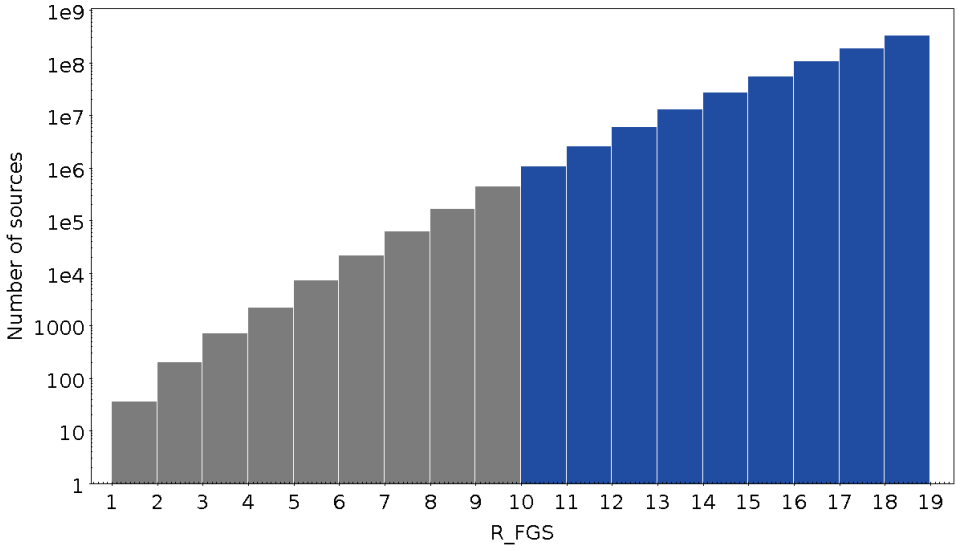


Figure 1: Magnitude distribution of ISC sources (bin width = 1.0)

5.2.2 HEALpix Level 9 Statistics

Figure 2 shows the distribution of the ISC sources counts in HEALPix level 9 regions (FOVs), Figure 3 shows a zoom on the counts range [0,50], and Figure 4 shows the cumulative distribution.
The entire sky contains 3 145 728 FOVs, of which 529 (0.0168%) contain less than 5 stars and 48 are empty (0.0015%). See Table 3 and Table 4 for the complete statistics on the number of sources per FOV inside each of the 192 HEALpixes level 2 in which ISC is subdivided.

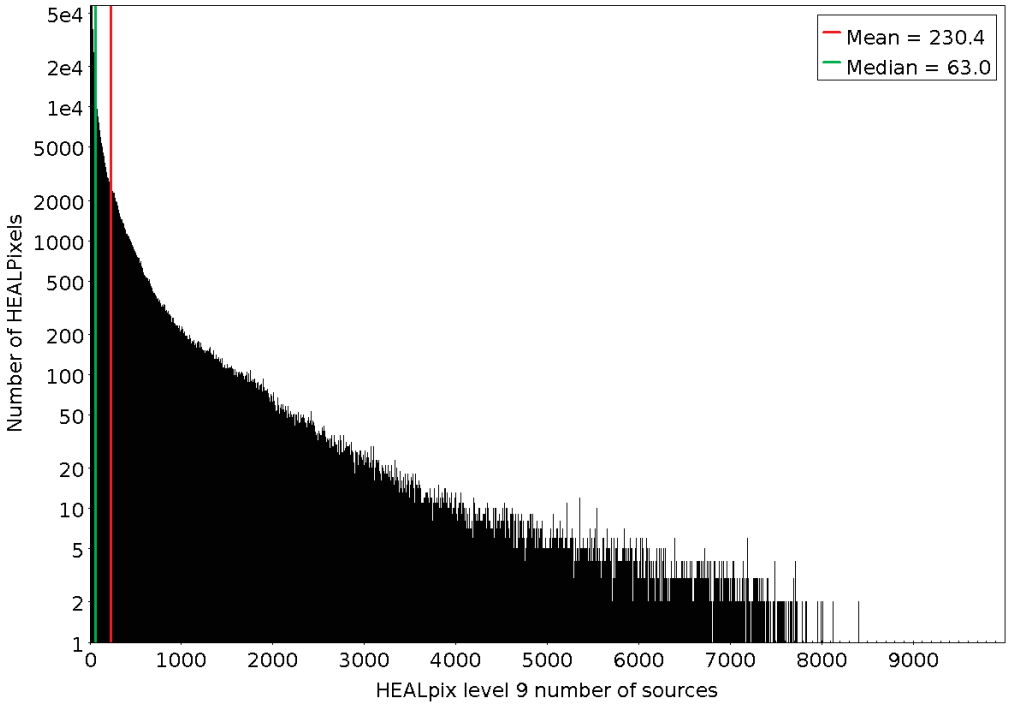


Figure 2: ISC sources distribution in HEALPix level 9 regions (bin width = 1). Mean and median are superposed as red and green lines respectively.

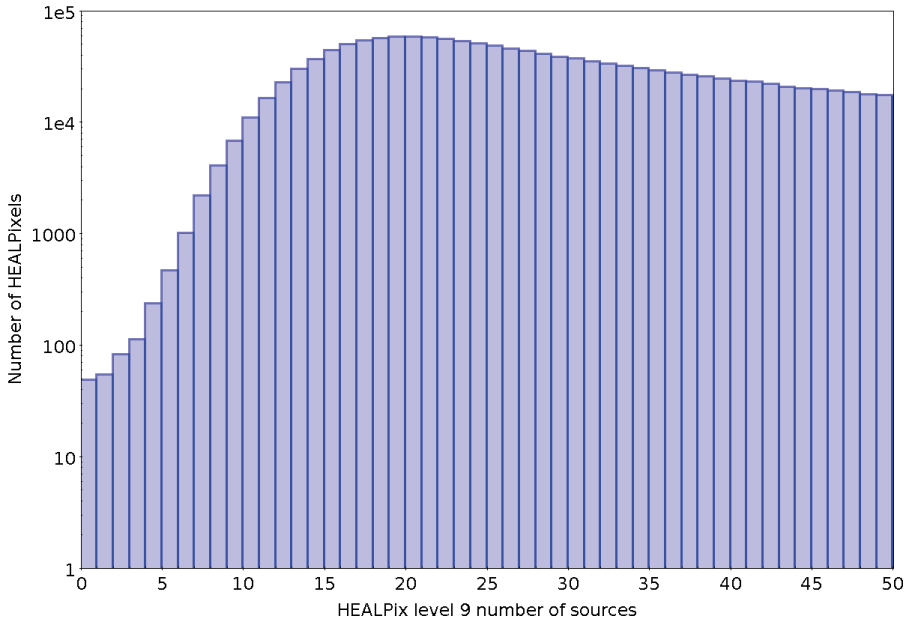


Figure 3: ISC sources distribution in HEALPix level 9 regions in the range [0 - 50] (bin width = 1). Mean and median are superposed as red and green lines respectively.

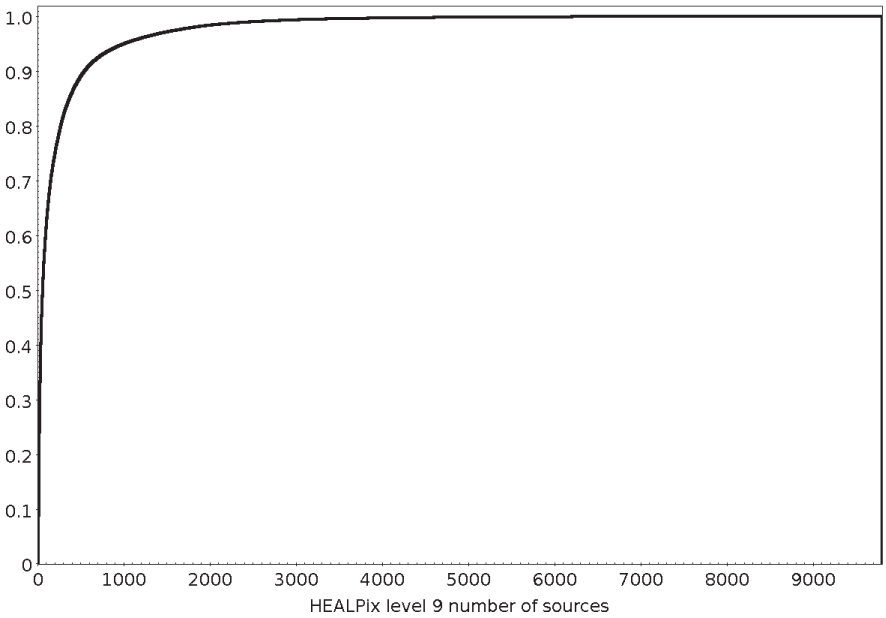


Figure 4: ISC sources cumulative distribution in HEALPix level 9 regions (bin width = 1).

5.2.3 Neighbor Flag statistics

The Neighbor Flag defines the neighboring conditions of each ISC source as described in the Summary (Section 4) and in [AD 3].
Figure 5 shows the number of ISC sources per Neighbor flag value [0,1,2,3].
The ISC contains 724 837 118 sources, 368 499 359 sources have Neighbor flag F = 0 (isolated sources, 50.8%), 62 056 659 sources have Neighbor flag F = 1 (brightest neighbor, 8.6%), 20 209 745 sources have Neighbor flag F = 2 (not the brightest neighbor, 2.8%), 274 071 355 sources have Neighbor flag F = 3 (unknown neighboring condition, 37.8%).
Figure 6 shows the R_{FGS} magnitude distribution of ISC sources for each Neighbor Flag value. The higher number of sources with F=1 with respect to sources with F=2 is common to the whole ISC magnitude range, which is simply a consequence of there being many more faint stars than bright stars: at any given magnitude a star is more likely to have a fainter neighbor than a brighter neighbor. Moreover, as described in [AD 3], the Neighbor Flag has been evaluated considering all the objects in the Gaia DR2 source catalog, hence also sources fainter than 19 that are not present in the ISC. As a consequence, ISC sources fainter than 17 with F = 1 could have fainter neighbors not included in the ISC but whose presence is reflected in the flag value[1].
Figure 7 shows the fractions of ISC sources for each Neighbor Flag value in function of the R_{FGS} magnitude.

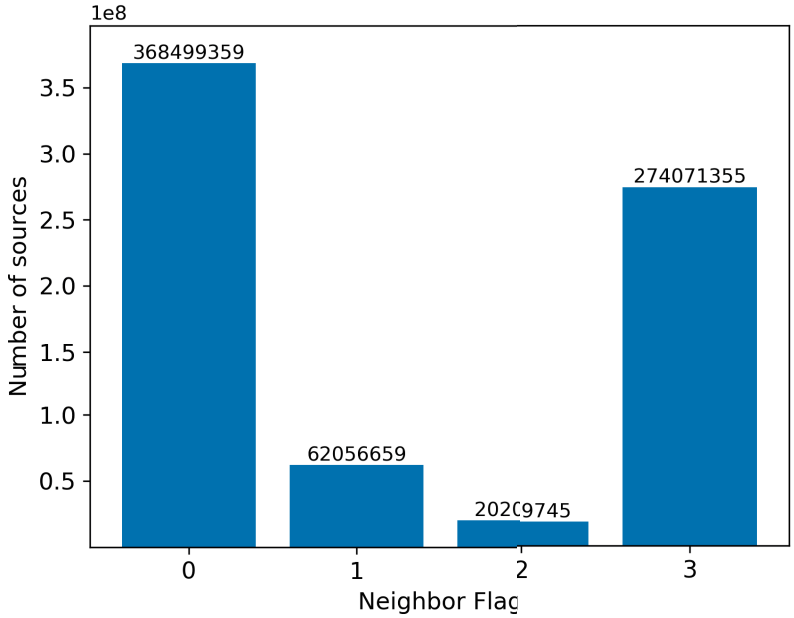


Figure 5: Neighbor Flag values distribution of ISC sources

[1]The Neighbor Flag value reflects also the presence of Gaia DR2 sources with only 2-parameters astrometry not included in the ISC.

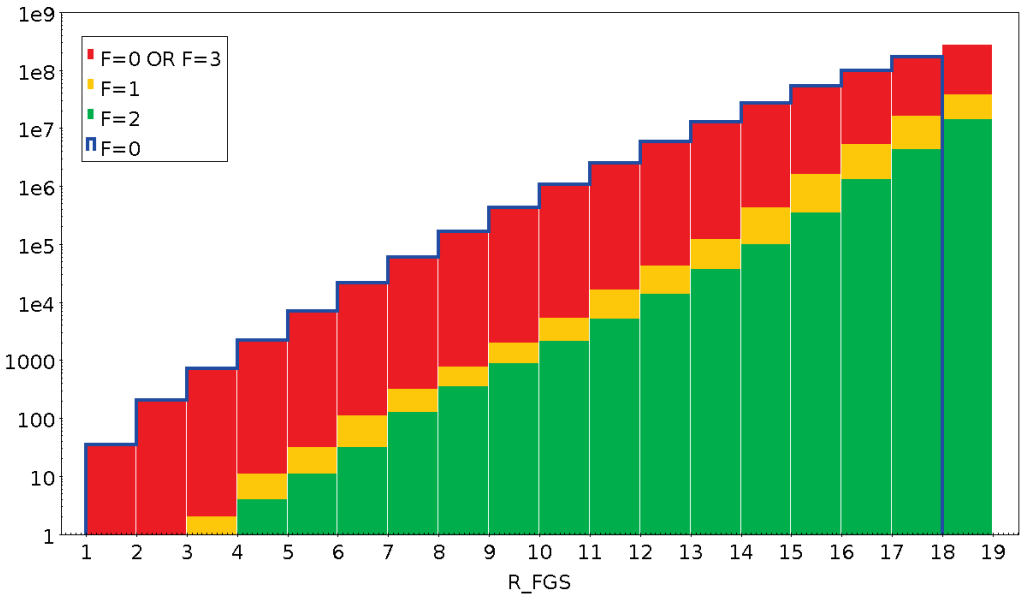


Figure 6: Magnitude distribution of ISC sources with Neighbor flag F = 0 OR F = 3, F=1, and F=2 and F=0. Note that, as defined in [AD 3], all sources fainter than 18 having no neighbors are flagged with F=3 since they are less than 2 magnitudes away from the Gaia DR2 magnitude limit, set to 20, and the neighborhood conditions are unknown due to incompleteness effects.

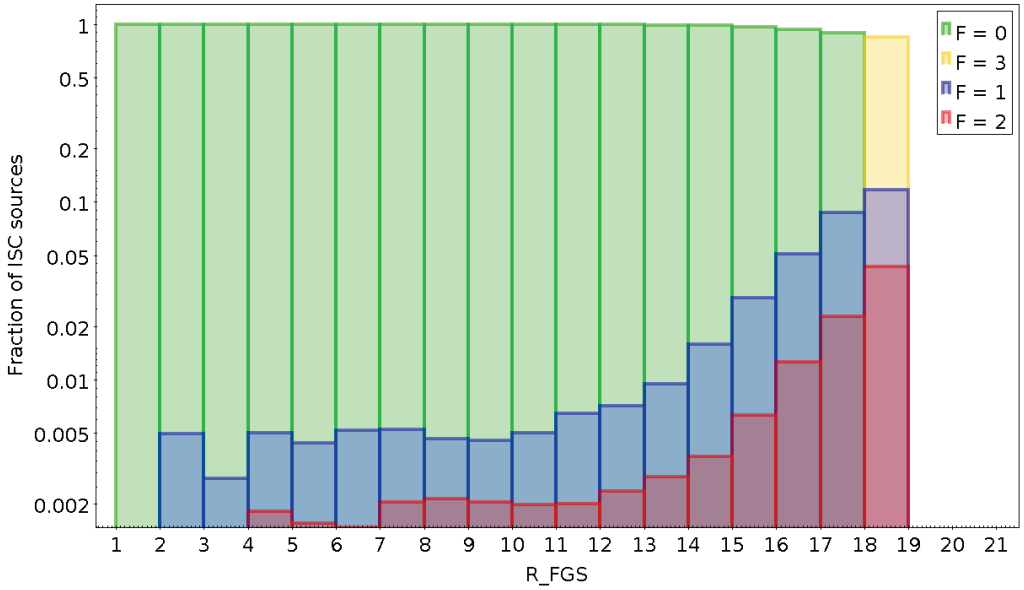


Figure 7: Fraction of ISC sources with Neighbor flag F=0, F=1, F=2 and F=3.

5.2.4 Variability and Extended Source Flag Statistics

Using the criterium defined in [AD 3] 248 760 ISC sources are flagged as variables (0.03%), i.e. they have Gaia G magnitude variation greater than 0.5. The blue histogram in Figure 8 shows the R_{FGS} magnitude distribution of ISC sources flagged as variables (Variability Flag = 1).

In [AD 3] we described the machine learning technique used to generate the Classification Flag needed to discriminate ISC sources as extended (Classification Flag =1) or point-like (Classification Flag =0). The classification has been performed only for ISC sources with Gaia G magnitude greater than 13. All the sources brighter than this limit are assumed to be point-like. In ISC 205 687 140 sources are flagged as extended (28%). The red histogram in Figure 8 shows the R_{FGS} magnitude distribution of ISC sources flagged as extended (Classification Flag = 1).

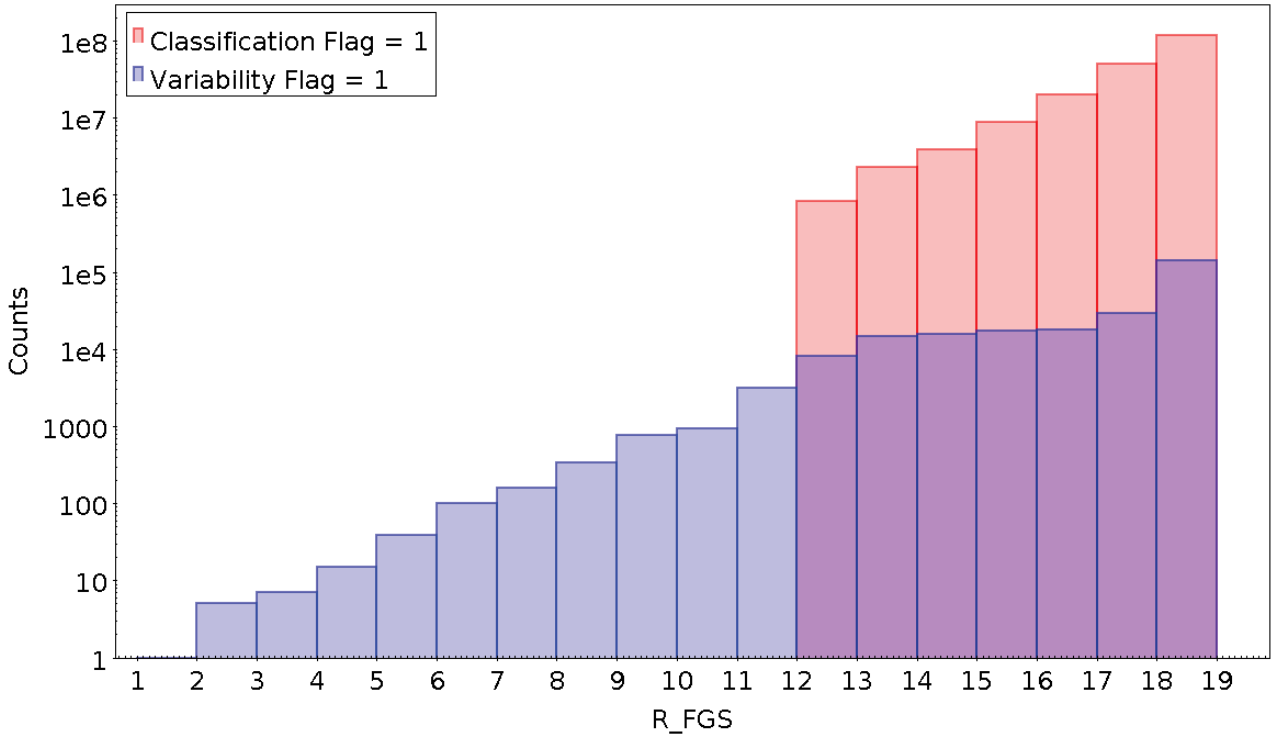


Figure 8: Distribution in R_{FGS} magnitude of ISC sources flagged as extended (red) and flagged as variables (blue).

5.2.5 Latitude Distribution

Figure 9 shows galactic latitude distribution of ISC sources. Galactic latitudes have been computed from ISC ICRS Declinations (Dec_deg). The two highest peaks are generated by the high extinction regions on the galactic plane (b = 0°). The two small peaks on the left are due to the Large and Small Magellanic Cloud.

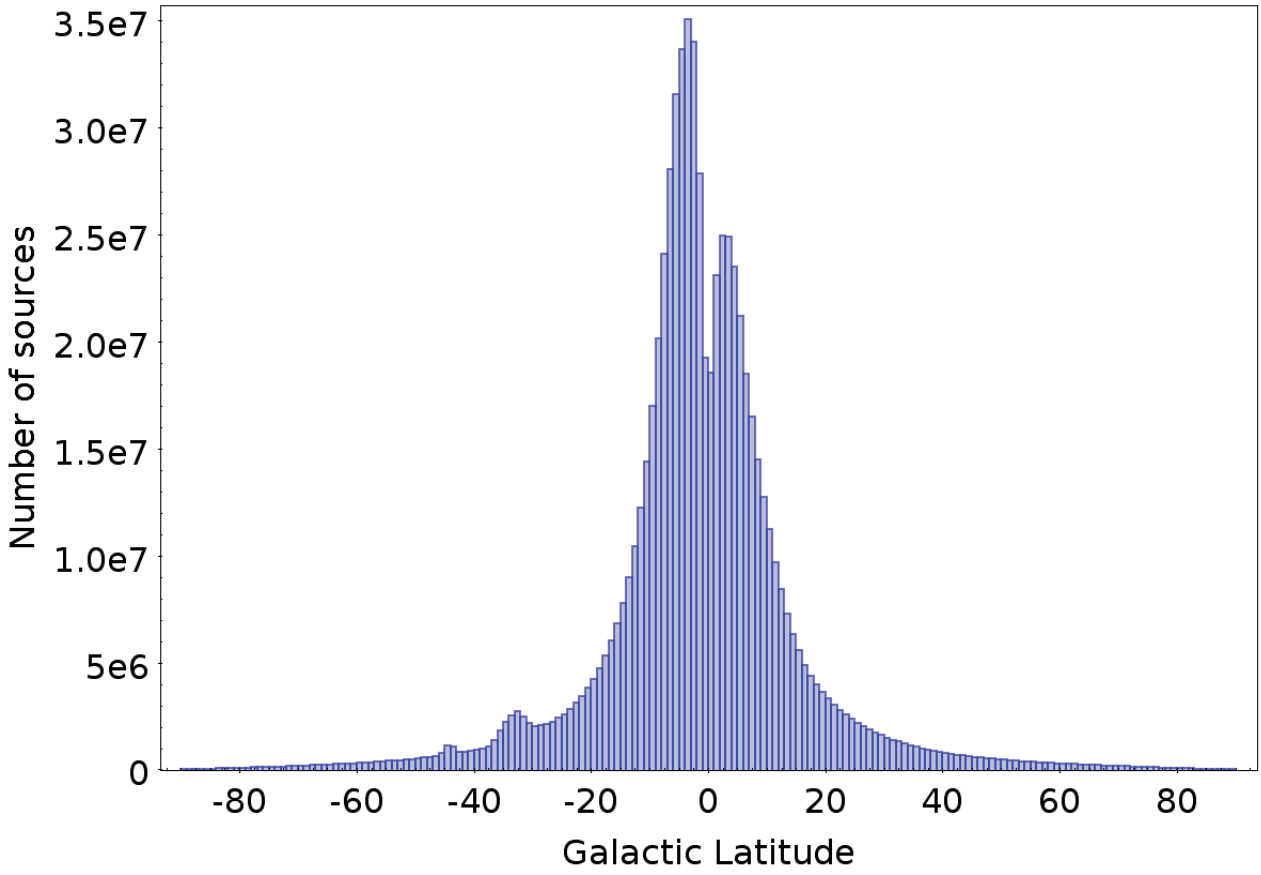


Figure 9: Galactic Latitude distribution of ISC sources (bin width = 1°).

5.2.6 Coordinate Errors Distribution

Figure 10 shows the distribution of errors on right ascension (RA_error) and declination (Dec_error) in arcsec (defined as 1 sigma value). Statistics of data are given in Table 2.
ISC.R3 sources positional errors are the errors on the positions in the Gaia-DR2 catalogue propagated to the Euclid reference epoch 2025, so they take into account the contribution from the proper motion errors and the additional positional error due to parallax effect (see EUCL-OATO-TN-2-006 [AD 3]). Despite this, for the vast majority of the sources the coordinate errors are well below the required 0.4 arcsec requirement. Only for a smallest number of sources (112), the positional error is greater than the limit of 0.4 arcsecs due to a large (and probably erroneous) absolute parallax. See the acceptance tests results in EUCL-OATO-NOTE-2-009 [AD 4].

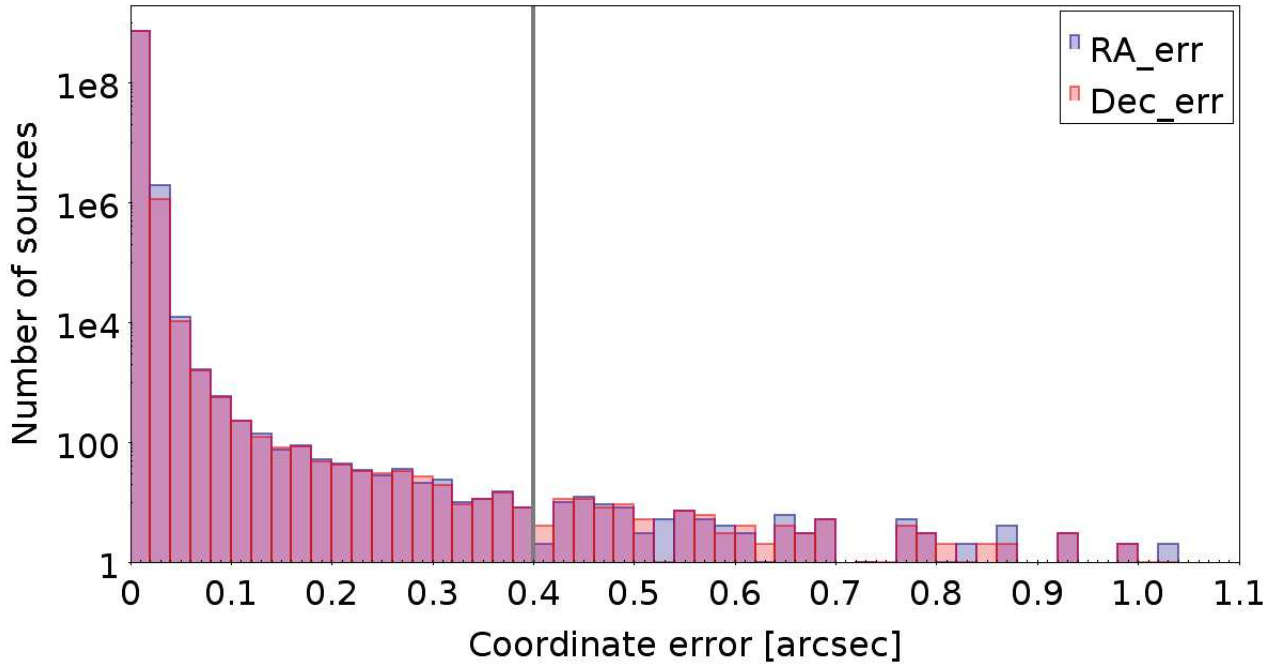


Figure 10: RA_error and Dec_error distributions of ISC sources (bin width = 0.002). The gray vertical line corresponds to the 0.4 arcsec requirement.

Table 2: Statistics of coordinate errors: μ is the mean error. The 99.7th percentile is the error below which 99.7% of sources are found.

	μ [arcsec]	**99.7th percentile** [arcsec]
RA_error	0.004557	0.019740
Dec_error	0.004133	0.018272

6. HEALPix level 2 statistics

The ISC is provided in 192 files, each file corresponding to the 192 HEALPixes of level 2 (pixel size $\theta_{pix} = 14.7°$). Each HEALPix of level 2 is subdivided in 16 384 HEALPixes of level 9 (pixel size $\theta_{pix} = 0.114°$), having size approximately equal to the FGS FOV ($0.116° \times 0.116°$).
In this section we provide ISC summary statistics per HEALPix region of level 2. Also, we computed the statistics resulting from the adoption of the two proposed mitigation strategies:

1. treatment of sources with Neighbor Flag F=3 (unknown condition) as isolated sources;
2. possibility to switch to an adjacent FGS CCD in the case that one of the two FGS CCD FOVs falls in an area of the sky with insufficient sources.

6.1 Methodology

In the following we define:

- FOV each HEALPix of level 9 in which the sky is subdivided;
- **substandard FOV** a FOV not satisfying requirement EUCL-ISC-REQ-0020, i.e. a FOV with less than 5 sources or with less than 3 objects with no neighbor.

From each of the 192 ISC files we computed:

1. the number of sources per HEALpix level 2 region;
2. the number of sources with Neighbor flag F=1 OR F=2;
3. HEALPix level 9 tables (sources grouped by HEALPix level 9 ID) from which we obtained the number of sources per FOV and the number of *substandard FOVs* inside each HEALPix level 2 using the Neighbor flag values;
4. the number of *substandard FOVs* when sources with Neighbor flag F = 3 are treated as isolated sources (mitigation strategy).
   In the ISC all sources fainter than magnitude 18 with no neighbors were assigned a Neighbor flag F = 3 (unknown condition), due to the incompleteness of Gaia-DR2 at magnitudes fainter than 20. The treatment of sources with Neighbor flag F=3 as isolated sources is justified given that, for the brighter sources, only a very small fraction have a neighbor within 2". We can therefore expect that very nearly all the faint sources with F=3 are indeed isolated, or having a neighbor too faint for the FGS to see. Moreover, Figure 7 shows that sources with F=3 has a probability of $\sim$ 90% to be isolated (F=0) and of $\sim$ 10% to be a brightest neighbor, and clearly it can never be a faintest neighbour (F=2);
5. the number of *substandard FOVs* with one or more adjacent *substandard FOVs* (mitigation strategy).
   Isolated *Substandard FOVs* (i.e. *Substandard FOVs* with all nominal adjacent FOVs) can be

avoided switching to the adjacent CCD while maintaining the desired pointing.
For each *substandard FOV* the eight adjacent FOVs have been identified and labeled as substandard or not respect to requirement EUCL-ISC-REQ-0020-01. The *substandard FOVs* having one or more adjacent substandard FOVs are counted.
The left panel of Figure 11 shows a *substandard FOV* with three adjacent *substandard FOVs*: this *substandard FOV* remains critical even when applying this mitigation strategy. The right panel of Figure 11 shows a *substandard FOV* with all nominal adjacent FOVs.

6. the number of *substandard FOVs* with one or more adjacent *substandard FOVs* when sources with Neighbor flag F = 3 are treated as isolated sources (mitigation strategy).

To perform this analysis we used: (1) a combination of STILTS and custom IDL programs and (2) Python scripts and tools (Healpy, Astropy, Numpy, Pandas).

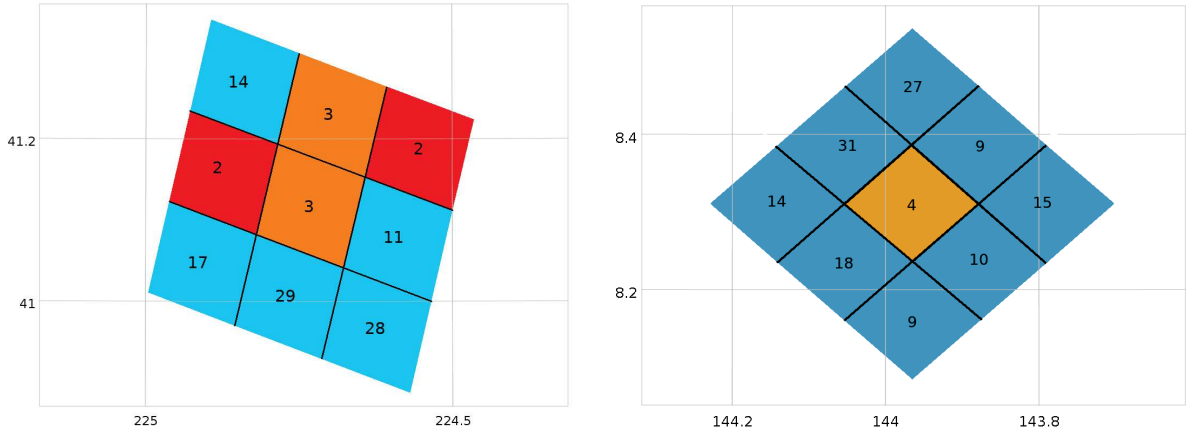


Figure 11: Left Panel: density map at healpix level 9 resolution showing a *substandard FOV* (healpID9=267664, healpID2=16) and its eight adjacent FOVs: there are three adjacent *substandard FOVs* (red and orange) and five nominal adjacent FOVs (cyan). Right Panel: *substandard FOV* (healpID9=267364, healpID2=16) with all eight nominal adjacent FOVs (light blue). For each FOV the number of sources is indicated.

6.2 Results

In Table 3, for each of the 192 HEALPix level 2 regions, numbered from 0 to 191 (column 1), are reported the total number of ISC sources (column 2) , and the number of sources with neighbor flag F=1 OR F=2 (column 3).

Table 4 reports the statistics on the number of sources per FOV inside each of the 192 level 2 HEALpixes:

Column 1. Identification number of the HEALpixes of level 2 (from 0 to 192)

Column 2. Number of FOVs with less than 5 sources

Column 3. Number of empty FOVs (0 sources)

Column 4. **Number of *substandard FOVs***, i.e. FOVs with less than 5 sources or with less than 3 objects with no neighbor (Neighbor flag F=0)

Column 5. Number of *substandard FOVs* with one or more adjacent *substandard FOVs*

Column 6. Number of *substandard FOVs* when sources with Neighbor flag F=3 (unknown condition) are treated as isolated

Column 7. Number of *substandard FOVs* with one or more adjacent *substandard FOVs*, when sources with Neighbor flag F=3 (unknown condition) are treated as isolated.

From Table 4:

- it is interesting to note that column 2 (N<5) and column 6 (N<5 OR N(F=0 OR F=3)<3) are equal. This means that, when we consider sources with Neighbor flag F=3 (unknown neighboring condition) as isolated sources, the requirement that there be at least 3 sources with no neighbor is always satisfied, if there are at least 5 sources in the FOV.
- ***Substandard FOVs***, i.e. FOVs not satisfying requirement EUCL-ISC-REQ-0020 constitute 0.034% of the sky.
- If sources with F=3 are treated as isolated the percentage of failure drops from 0.034% to 0.017%.
- The total number of *substandard FOVs* with one or more adjacent *substandard FOVs* is 288, corresponding to $\sim 27\%$ of the total number of *substandard FOVs* (1 065) and to $\sim 0.009\%$ of the total number of FOVs (3 145 728). So, in 777 *substandard FOVs* ($\sim 73\%$ of the total number of *substandard FOVs*) the FGS has the possibility to use the adjacent CCD to find adequate targets for pointing.
  With this mitigation strategy the number of FOVs where the pointing operations remain critical drops from $\sim 0.034\%$ to $\sim 0.009\%$ over the whole sky. Considering sources with Neighbor flag F=3 as isolated the number of FOVs where the pointing operations remain critical drops from $\sim 0.017\%$ to $\sim 0.008\%$ (best mitigation strategy).

Table 3: Total number of ISC sources, and the number of sources with Neighbor flag F=1 OR F=2 inside each of the 192 level 2 HEALpixes.

HEALPix File	N. of Sources	F=1 OR F=2
00	385430	4661
01	770652	10855
02	450786	5293
03	931503	12391
04	1982488	38043
05	4621778	131435
06	2869388	68266
07	3506863	96395
08	692032	9226
09	1865010	31645
10	1678195	32375
11	4947351	181027
12	4340785	136475
13	2722864	72610
14	5383802	210424
15	1793071	36586
16	602321	7977
17	328976	3437
18	870962	13101
19	436151	6050
20	273283	3086
21	250502	3034
22	323293	4422
23	292700	4387
24	1334418	20239
25	613703	9031
26	2043151	35078
27	1155564	18371
28	431012	6577
29	382272	5861
30	809983	13819
31	657340	10699
32	527519	5171
33	599513	7479
34	350533	3708
35	390088	5043
36	761500	17476
37	979965	17598
38	471732	6291
39	696760	9973
40	287532	8133
41	307499	4335
42	252020	3712
43	286514	4340
44	376989	5160
45	598360	8576
46	365967	5188
47	580074	8803
48	2569186	53866
49	1699908	25382
50	12779768	1286084
51	7455461	393274
52	1621260	27861
53	2261038	51758
54	7429487	385978
55	7749594	377944
56	16769625	2133029
57	9398513	705900
58	2750547	64492
59	2328794	51864
60	7393036	396643
61	5038964	204435
62	1803251	35013
63	1411995	25010
64	315692	3494
65	277446	5215
66	370361	3569
67	311627	3543
68	266885	3240
69	306907	3468
70	296754	3665
71	333943	3878
72	502958	4491
73	413865	4536
74	909649	10577
75	684744	6779
76	386808	4909
77	448880	5804
78	644780	8710
79	795536	12212
80	1360885	25943
81	4659277	158319
82	818074	15191
83	1999909	37874
84	5758335	199398
85	1731857	31770
86	5393575	160259
87	2783026	57521
88	558050	8995
89	1294105	20547
90	419879	5575
91	854942	13047
92	3858218	94636
93	3859852	88511
94	2530935	50483
95	4193115	103636
96	1104823	16005
97	674702	8873
98	665576	8372
99	450688	5134
100	544299	5445
101	514030	5150
102	375164	4124
103	351172	3788
104	508594	5007
105	355171	3702
106	480193	4990
107	316453	3119
108	294886	3178
109	276860	4513
110	260371	2554
111	240668	2731
112	59913423	18924555
113	31333587	6683849
114	21376000	4422850
115	13828242	1731218
116	12041037	1210400
117	4840854	170371
118	18821782	3073505
119	18162147	2342218
120	2175079	42699
121	3340066	94656
122	960178	14506
123	1257228	18482
124	6928677	351014
125	10541857	876333
126	1697017	29396
127	2295394	47167
128	1027731	15356
129	6744609	1699564
130	1718813	258034
131	423973	6947
132	971974	26230
133	722996	13240
134	394534	5884
135	472121	7384
136	404086	5551
137	310310	4678
138	325868	4571
139	269546	3741
140	304355	4734
141	357894	5341
142	261965	3344
143	304717	3751
144	2514114	53937
145	14143350	1502162
146	2693930	74461
147	9565039	659630
148	16052617	1901530
149	3105519	86745
150	6405953	326862
151	1442664	23769
152	2163128	46362
153	7504893	376978
154	1992184	42463
155	7725037	374945
156	4680515	167740
157	1100033	15148
158	5426863	204367
159	1218221	18870
160	5369054	253155
161	15462072	2230142
162	24302938	4326289
163	20106008	2906301
164	23356139	3951067
165	26624929	4903474
166	12086848	1085730
167	13290959	2135656
168	13412421	1444395
169	4779143	152222
170	3027765	77148
171	1393897	17640
172	2645275	50700
173	2236215	40619
174	977803	10480
175	902733	9348
176	1341420	21099
177	796383	11009
178	2161099	41552
179	1078426	14710
180	537278	6959
181	401398	4802
182	697930	8635
183	492799	5044
184	3942421	113533
185	1811153	29001
186	12784581	1227497
187	5942805	286549
188	1100875	14622
189	699029	8085
190	2546271	51330
191	1471791	21157
Total	724837118	82266404

Table 4: Statistics on the number of sources per FOV inside each of the 192 level 2 HEALpixels. Lime color column contains the number of *substandard FOVs* (FOVs not fulfilling requirement ISC-REQ-0020-01).

[a] Substandard FOVs having at least one adjacent substandard FOV.
[b] Substandard FOVs when sources with neighbor flag F=3 are treated as isolated.

HEALPix	N<5	N=0	N<5 OR N(F=0)<3	With adjacent subst. FOV [a]	N<5 OR N(F=0 OR F=3)<3 [b]	With adjacent subst. FOV [ab] (F=3 as isolated)
0	0	0	1	0	0	0
1	0	0	0	0	0	0
2	1	0	2	2	1	0
3	4	0	7	0	4	0
4	17	0	23	13	17	7
5	0	0	0	0	0	0
6	1	0	1	0	1	0
7	0	0	0	0	0	0
8	0	0	0	0	0	0
9	0	0	0	0	0	0
10	0	0	0	0	0	0
11	0	0	0	0	0	0
12	0	0	0	0	0	0
13	0	0	0	0	0	0
14	0	0	0	0	0	0
15	0	0	0	0	0	0
16	51	6	51	42	51	42
17	91	14	98	52	91	49
18	0	0	0	0	0	0
19	0	0	0	0	0	0
20	14	0	29	0	14	0
21	12	0	56	0	12	0
22	0	0	1	0	0	0
23	3	0	11	0	3	0
24	0	0	0	0	0	0
25	0	0	0	0	0	0
26	0	0	0	0	0	0
27	0	0	0	0	0	0
28	0	0	1	0	0	0
29	0	0	0	0	0	0
30	0	0	0	0	0	0
31	0	0	0	0	0	0
32	0	0	0	0	0	0
33	0	0	0	0	0	0
34	0	0	3	0	0	0
35	0	0	0	0	0	0
36	0	0	0	0	0	0
37	0	0	0	0	0	0
38	0	0	0	0	0	0
39	0	0	0	0	0	0
40	2	0	28	0	2	0
41	0	0	3	0	0	0
42	18	0	74	4	18	0
43	12	0	25	0	12	0
44	0	0	1	0	0	0
45	0	0	0	0	0	0
46	0	0	4	0	0	0
47	0	0	0	0	0	0

Table 4: Continue.

HEALPix	N<5	N=0	N<5 OR N(F=0)<3	With adjacent subst. FOV [a]	N<5 OR N(F=0 OR F=3)<3 [b]	With adjacent subst. FOV [ab] (F=3 as isolated)
48	0	0	0	0	0	0
49	0	0	0	0	0	0
50	0	0	0	0	0	0
51	0	0	0	0	0	0
52	0	0	0	0	0	0
53	0	0	0	0	0	0
54	0	0	0	0	0	0
55	0	0	0	0	0	0
56	0	0	0	0	0	0
57	0	0	0	0	0	0
58	0	0	0	0	0	0
59	0	0	0	0	0	0
60	0	0	0	0	0	0
61	0	0	0	0	0	0
62	0	0	0	0	0	0
63	0	0	0	0	0	0
64	3	0	13	0	3	0
65	3	0	30	2	3	0
66	1	0	3	0	1	0
67	0	0	7	0	0	0
68	4	0	22	0	4	0
69	1	0	6	0	1	0
70	0	0	11	0	0	0
71	0	0	4	0	0	0
72	20	3	21	14	20	14
73	0	0	0	0	0	0
74	2	1	2	0	2	0
75	3	0	3	2	3	2
76	0	0	1	0	0	0
77	0	0	1	0	0	0
78	0	0	0	0	0	0
79	0	0	0	0	0	0
80	0	0	0	0	0	0
81	0	0	0	0	0	0
82	0	0	0	0	0	0
83	6	0	8	5	6	2
84	0	0	0	0	0	0
85	0	0	0	0	0	0
86	0	0	0	0	0	0
87	0	0	0	0	0	0
88	0	0	1	0	0	0
89	1	0	3	0	1	0
90	0	0	1	0	0	0
91	2	0	2	2	2	2
92	0	0	0	0	0	0
93	0	0	0	0	0	0
94	0	0	0	0	0	0
95	0	0	0	0	0	0

Table 4: Continue.

HEALPix	N<5	N=0	N<5 OR N(F=0)<3	With adjacent subst. FOV [a]	N<5 OR N(F=0 OR F=3)<3 [b]	With adjacent subst. FOV [ab] (F=3 as isolated)
96	0	0	0	0	0	0
97	0	0	0	0	0	0
98	0	0	0	0	0	0
99	0	0	0	0	0	0
100	0	0	0	0	0	0
101	0	0	0	0	0	0
102	0	0	2	0	0	0
103	0	0	2	0	0	0
104	1	0	1	0	1	0
105	0	0	2	0	0	0
106	102	18	103	73	102	71
107	51	4	58	40	51	33
108	5	0	18	0	5	0
109	3	0	26	0	3	0
110	31	0	62	9	31	7
111	28	0	100	8	28	0
112	0	0	0	0	0	0
113	0	0	0	0	0	0
114	0	0	0	0	0	0
115	0	0	0	0	0	0
116	0	0	0	0	0	0
117	0	0	0	0	0	0
118	3	0	3	2	3	2
119	0	0	0	0	0	0
120	0	0	0	0	0	0
121	0	0	0	0	0	0
122	2	0	2	0	2	0
123	0	0	0	0	0	0
124	0	0	0	0	0	0
125	0	0	0	0	0	0
126	0	0	0	0	0	0
127	0	0	0	0	0	0
128	0	0	0	0	0	0
129	0	0	0	0	0	0
130	0	0	0	0	0	0
131	0	0	1	0	0	0
132	0	0	0	0	0	0
133	0	0	0	0	0	0
134	0	0	1	0	0	0
135	0	0	0	0	0	0
136	0	0	4	0	0	0
137	1	0	8	0	1	0
138	1	0	8	0	1	0
139	5	0	27	0	5	0
140	2	0	12	0	2	0
141	0	0	1	0	0	0
142	5	0	37	0	5	0
143	1	0	5	0	1	0

Table 4: Continue.

HEALPix	N<5	N=0	N<5 OR N(F=0)<3	With adjacent subst. FOV [a]	N<5 OR N(F=0 OR F=3)<3 [b]	With adjacent subst. FOV [ab] (F=3 as isolated)
144	0	0	0	0	0	0
145	0	0	0	0	0	0
146	0	0	0	0	0	0
147	0	0	0	0	0	0
148	0	0	0	0	0	0
149	0	0	0	0	0	0
150	0	0	0	0	0	0
151	0	0	0	0	0	0
152	0	0	0	0	0	0
153	0	0	0	0	0	0
154	0	0	0	0	0	0
155	0	0	0	0	0	0
156	0	0	0	0	0	0
157	0	0	0	0	0	0
158	0	0	0	0	0	0
159	0	0	0	0	0	0
160	0	0	0	0	0	0
161	0	0	0	0	0	0
162	0	0	0	0	0	0
163	0	0	0	0	0	0
164	0	0	0	0	0	0
165	0	0	0	0	0	0
166	0	0	0	0	0	0
167	11	2	18	18	11	10
168	0	0	0	0	0	0
169	0	0	0	0	0	0
170	0	0	0	0	0	0
171	0	0	0	0	0	0
172	0	0	0	0	0	0
173	0	0	0	0	0	0
174	0	0	0	0	0	0
175	0	0	0	0	0	0
176	0	0	0	0	0	0
177	0	0	0	0	0	0
178	0	0	0	0	0	0
179	0	0	0	0	0	0
180	0	0	0	0	0	0
181	2	0	2	0	2	0
182	0	0	0	0	0	0
183	0	0	0	0	0	0
184	0	0	0	0	0	0
185	0	0	0	0	0	0
186	1	0	1	0	1	0
187	0	0	0	0	0	0
188	0	0	0	0	0	0
189	2	0	3	0	2	0
190	0	0	0	0	0	0
191	0	0	0	0	0	0
Total	**529 (0.0168%)**	**48 (0.0015%)**	**1065 (0.0339%)**	**288 (0.0092%)**	**529 (0.0168%)**	**241 (0.0077%)**

7. ALL-SKY maps

We produced all-sky density maps at resolution of HEALPix level 9 (pixel area 0.013 sq.deg) and resolution of HEALPix level 6 (pixel area 0.839 sq.deg).
The entire sky contains 3 145 728 HEALPix of level 9 (FOVs), and 49 152 HEALPix of level 6; one HEALPix of level 6 contains 64 HEALPix of level 9.
The purpose of the maps is to identify the location on the celestial sphere of *substandard FOVs*, i.e. the regions not satisfying requisite EUCL-ISC-REQ-0020, and to quantify their impact on the FGS pointing operations, also considering the proposed mitigation strategies.

7.1 Methodology

From each of the 192 ISC files we computed:

1. HEALPix level 9 tables (sources grouped by HEALPix level 9 ID) from which we obtained the number of sources per FOV and we identified the substandard FOVs using the ISC Neighbor flag values.
2. HEALPix level 6 tables (sources grouped both by HEALPix level 6 ID and by HEALPix level 9 ID) from which we obtained the number of substandard FOVs in each HEALPix level 6.

To perform this analysis we used Python scripts and tools (Healpy, Astropy, Numpy, Pandas) and TOPCAT (Tool for OPerations on Catalogues And Tables).

7.2 Results

Figure 12 shows the all-sky density map of ISC sources at the resolution of HEALPix level 9. The high extinction regions near the galactic plane and the artifacts due to the patchy completeness of Gaia DR2 are promptly identified on the map. These regions of the sky along with areas with sparse sources at high galactic latitudes have been indicated as the three main causes of failure of requisite EUCL-ISC-REQ-0020 in the Verification Test Report EUCL-OATO-RP-2-002 (VTR, [AD 2]).

Figure 13 shows the position of sources with Neighbor flag F=1 and F=2.

Figures 14 and 15 show density maps at HEALpix level 9 resolution of sky regions affected by the patchy incompleteness. Figures from 16 to 21 show density maps at HEALpix level 9 resolution of sky regions located at low galactic latitudes in correspondence of high extinction regions. In all the figures *substandard FOVs* are framed by gray squares and white pixels are empty FOVs.

Figure 22 shows the location on the celestial sphere of *substandard FOVs* and Figure 23 shows the location of *substandard FOVs* when the sources with Neighbor flag F=3 (unknown neighboring conditions) are accepted as isolated sources. Considering this relaxed form of the requirement EUCL-ISC-REQ-0020 the failure rate of FOV fields decreases from 0.0339% to 0.0168% with an evident effect at high galactic latitudes.

The mitigation effect that is obtained by assuming sources with F=3 as isolated for specific regions of the sky is shown in the following maps:
Figures 24 and 25 show the location of *substandard FOVs* in two regions affected by the Gaia scanning law pattern, in the lower panels sources with Neighbor flag F=3 are assumed as isolated.
Figures 26 and 28 show the location of *substandard FOVs* in the North and South polar region, respectively. Figures 27 and 29 show the location of *substandard FOVs* in the North and South polar region, respectively, when the sources with Neighbor flag F=3 (unknown) are accepted as isolated sources.

The probability of failure for lack of ISC sources mapped at an angular resolution of approximately 1 square degree is shown in the following maps:
Figure 30 shows the HEALPix level 6 map (pixel area $\sim$0.8 sq.deg) where the color scale represent the fraction of failure of requirement EUCL-ISC-REQ-002-01 defined as the number of HEALPixes level 9 (FOVs) inside each HEALPix level 6 not satisfying the requisite divided by the total number of HEALPixes level 9 in each HEALPix level 6 (64).
Figure 31 shows the same map of Figure 30 but accepting the sources with Neighbor flag F=3 (unknown) as isolated sources.

The mitigation effect that is obtained considering only *substandard FOVs* with one or more adjacent *substandard FOVs* is shown in the following maps:
Figure 32 shows the location of *substandard FOVs* with one or more adjacent *substandard FOVs*.
Figure 33 shows the location of *substandard FOVs* with one or more adjacent *substandard FOVs* when the sources with Neighbor flag F=3 (unknown) are treated as isolated sources.
Figures 34 and 35 show the location of *substandard FOVs* with one or more adjacent *substandard FOVs* in two regions affected by the Gaia scanning law pattern, in the lower panels sources with Neighbor flag F=3 are assumed as isolated.
Figures 36 and 38 show the location of *substandard FOVs* having one or more adjacent *substandard FOVs* in the North and South polar region, respectively.
Figures 37 and 39 show the location of *substandard FOVs* having one or more adjacent *substandard FOVs* in the North and South polar region, respectively, when the sources with Neighbor flag F=3 (unknown) are accepted as isolated sources.

Figures 40 and 41 show the distribution of *substandard FOVs* in galactic and ecliptic latitude respectively; from top to bottom the different mitigation strategies have been applied: (1) *substandard FOVs*, (2) *substandard FOVs* considering sources with Neighbor flag F=3 as isolated, (3) *substandard FOVs* with adjacent *substandard FOVs*, (4) *substandard FOVs* with adjacent *substandard FOVs* considering sources with Neighbor flag F=3 as isolated.

From the maps we infer that the proposed mitigation strategies have a noticeable effect at high galactic latitudes while, in the regions affected by the patchy incompleteness and by high galactic extinction, they are less effective given the contiguity of the critical FOVs.

However, assuming the galactic and ecliptic planes as secondary target regions for the survey, the

histograms in Figures 40 and 41 show that applying the mitigation strategies:
(1) the number of *substandard FOVs* that are more than 20 degrees away from the galactic plane decrease from 1006 to 487, 250, 220 depending on the adopted strategy;
(2) the number of *substandard FOVs* that are more than 20 degrees away from the ecliptic plane decrease from 503 to 118, 19, 2 depending on the adopted strategy;
(3) the number of *substandard FOVs* that are more than 20 degrees away from both the ecliptic and galactic plane decrease from 491 to 110, 14 or 0 depending on the adopted strategy.

In Table 5 the HEALpix level 9 IDs of *substandard FOVs* having one or more adjacent substandard FOVs when sources with Neighbor flag F=3 are assumed as isolated are reported. These are the *substandard FOVs* that remain critical also adopting the best mitigation strategy.

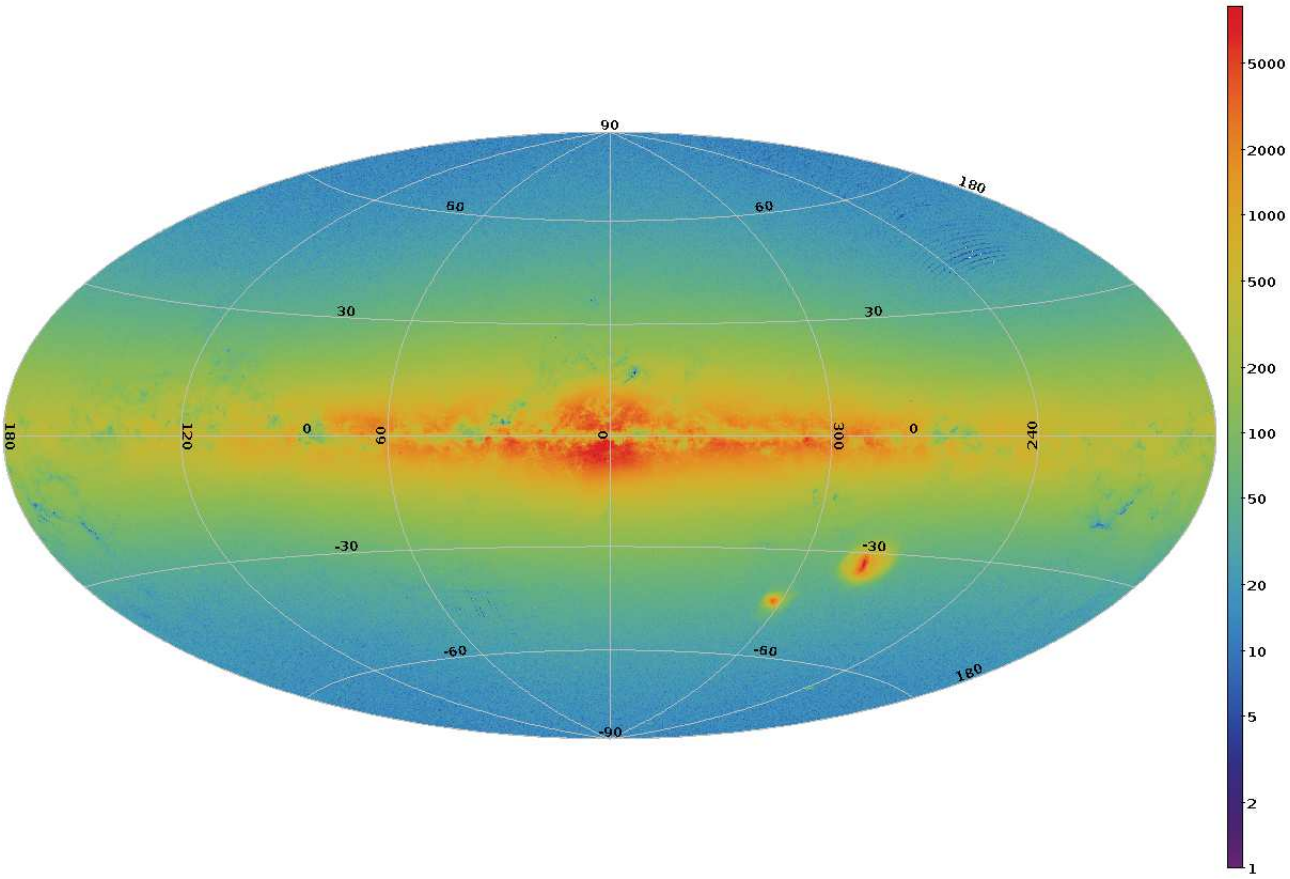


Figure 12: ISC density map in galactic coordinates. The color scale shows the counts inside each HEALPix level 9 region. Empty regions are plotted in white.

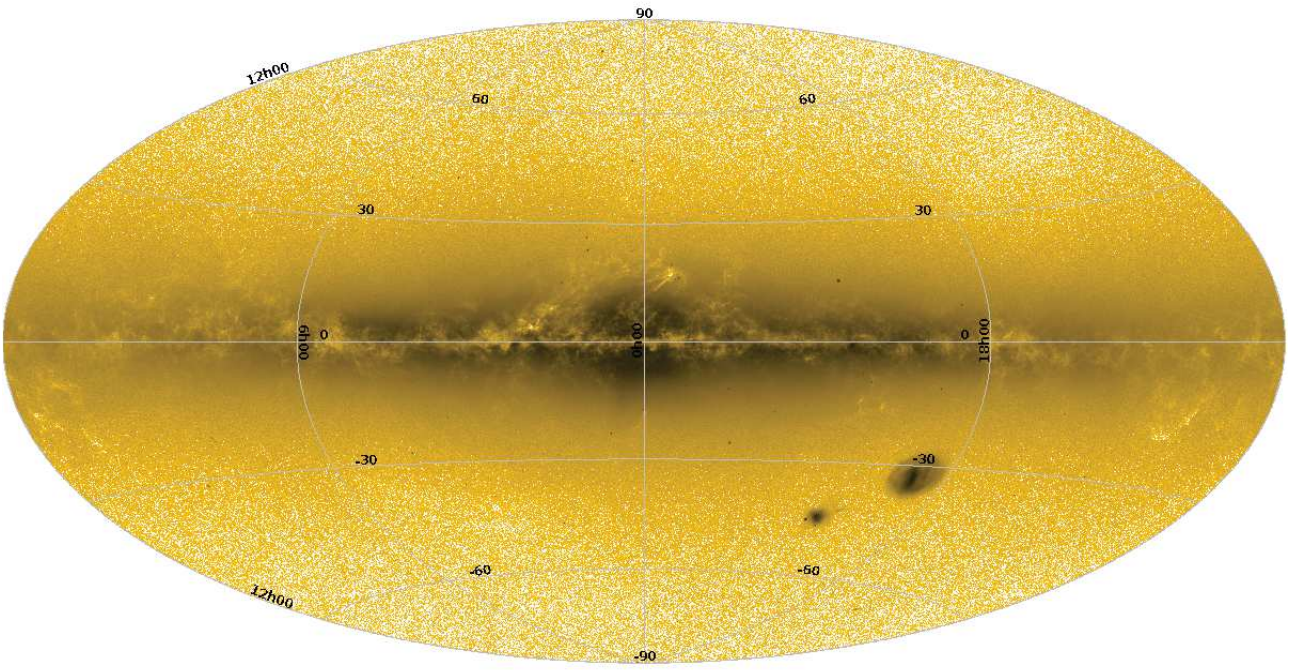


Figure 13: Location of ISC sources with Neighbor flag F=1 OR F=2 (galactic coordinates).

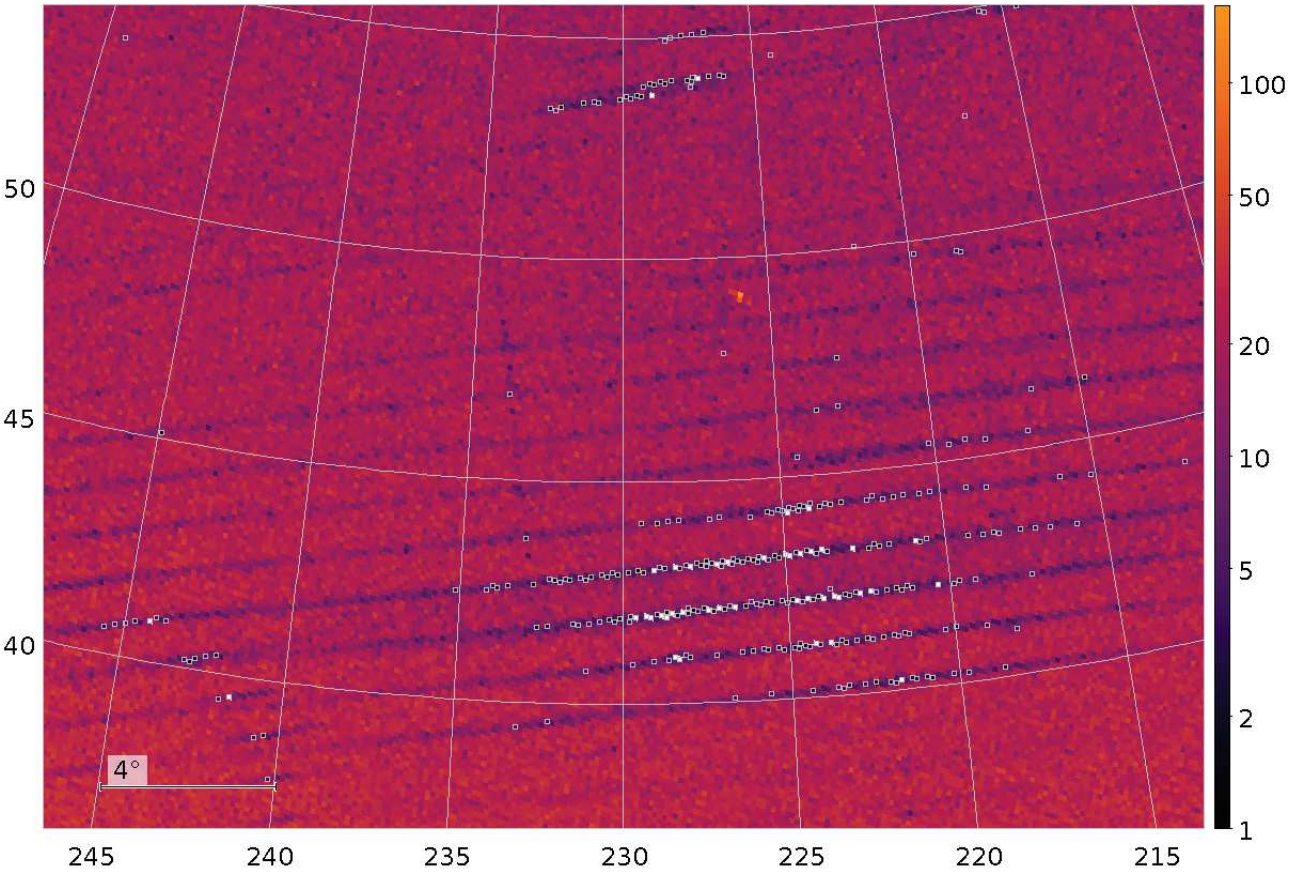


Figure 14: Density map at tessellation level 9 of a sky region spanning HEALpixels 16, 17, 104, 105, 106, 107 (level 2). Each pixel corresponds to one FGS FOV. Gray open squares enclose substandard FOVs. White pixels are empty FOVs within HEALpixels 16, 17, 106,107. The patchy incompleteness due to the sky scanning pattern of Gaia DR2 is visible (galactic coordinates).

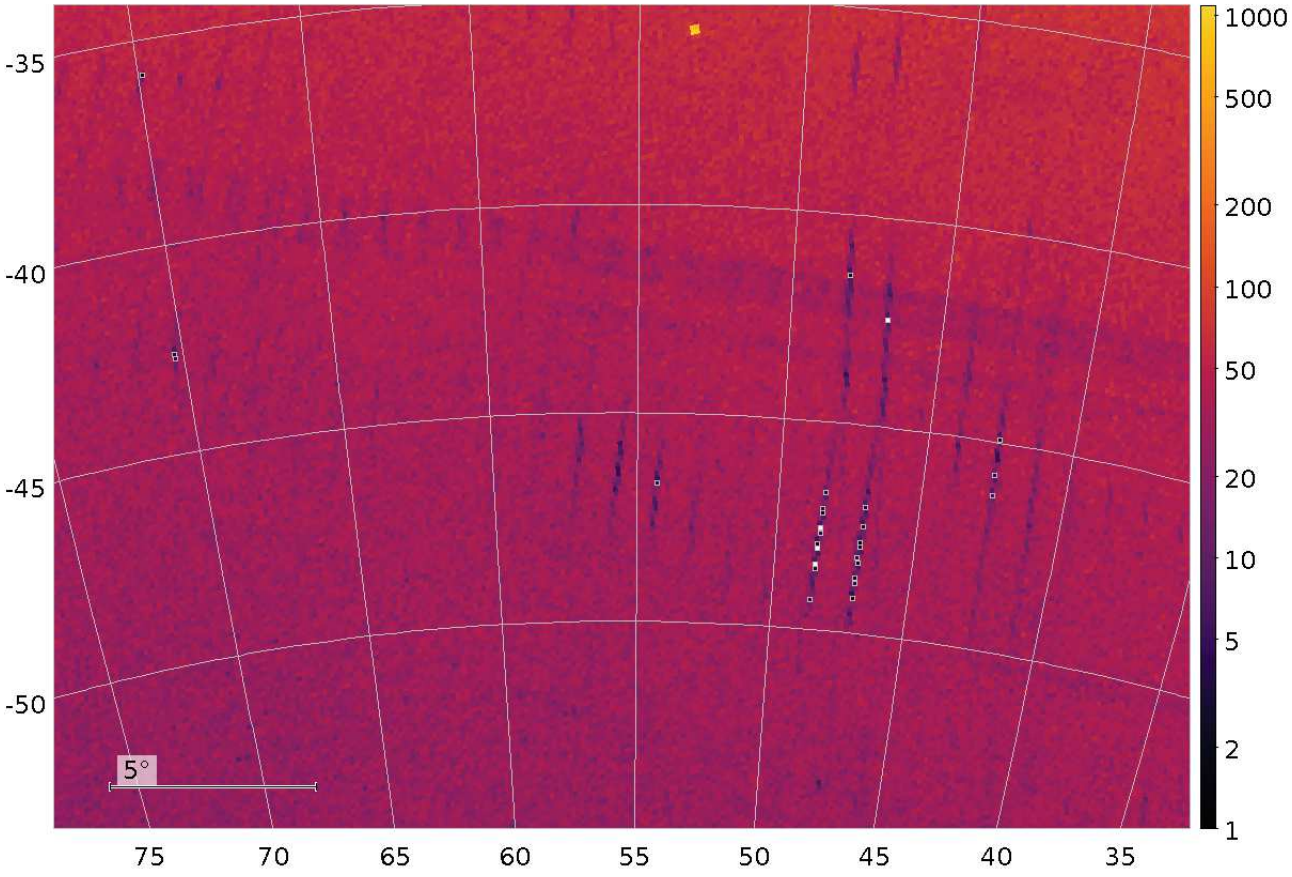


Figure 15: Density map at tessellation level 9 of a sky region spanning HEALpixels 72, 74, 75, 189 (level 2). Each pixel corresponds to one FGS FOV. White pixels are empty FOVs within HEALpixels 72, 74. Gray open squares enclose substandard FOVs. The patchy incompleteness due to the sky scanning pattern of Gaia DR2 is visible (galactic coordinates).

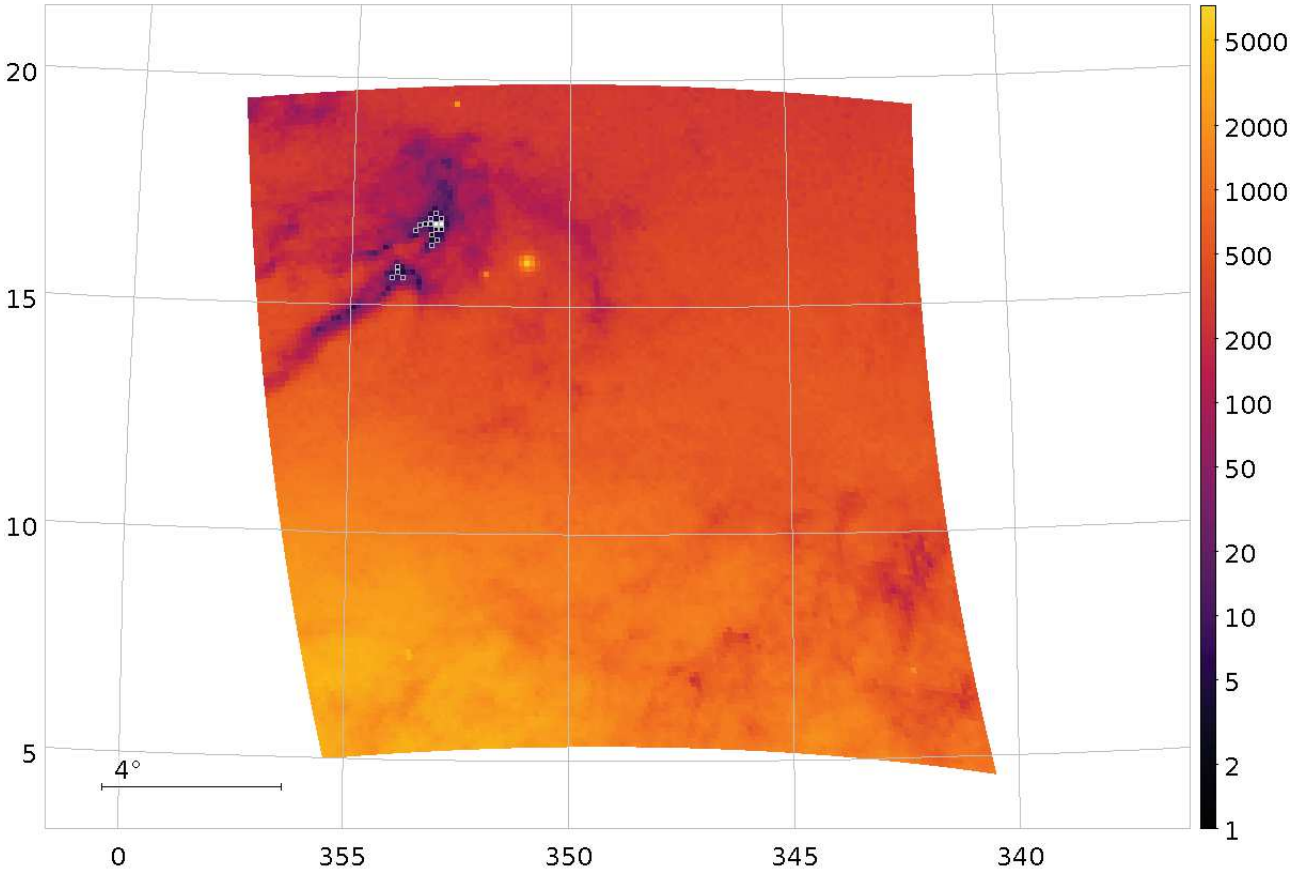


Figure 16: density map at tessellation level 9 of HEALpix 167 (level 2). Each pixel corresponds to one FGS FOV. White pixels are empty FOVs. Gray open squares enclose substandard FOVs. HEALPix 167 is located near the galactic plane. The characteristic high extinction regions are visible (galactic coordinates).

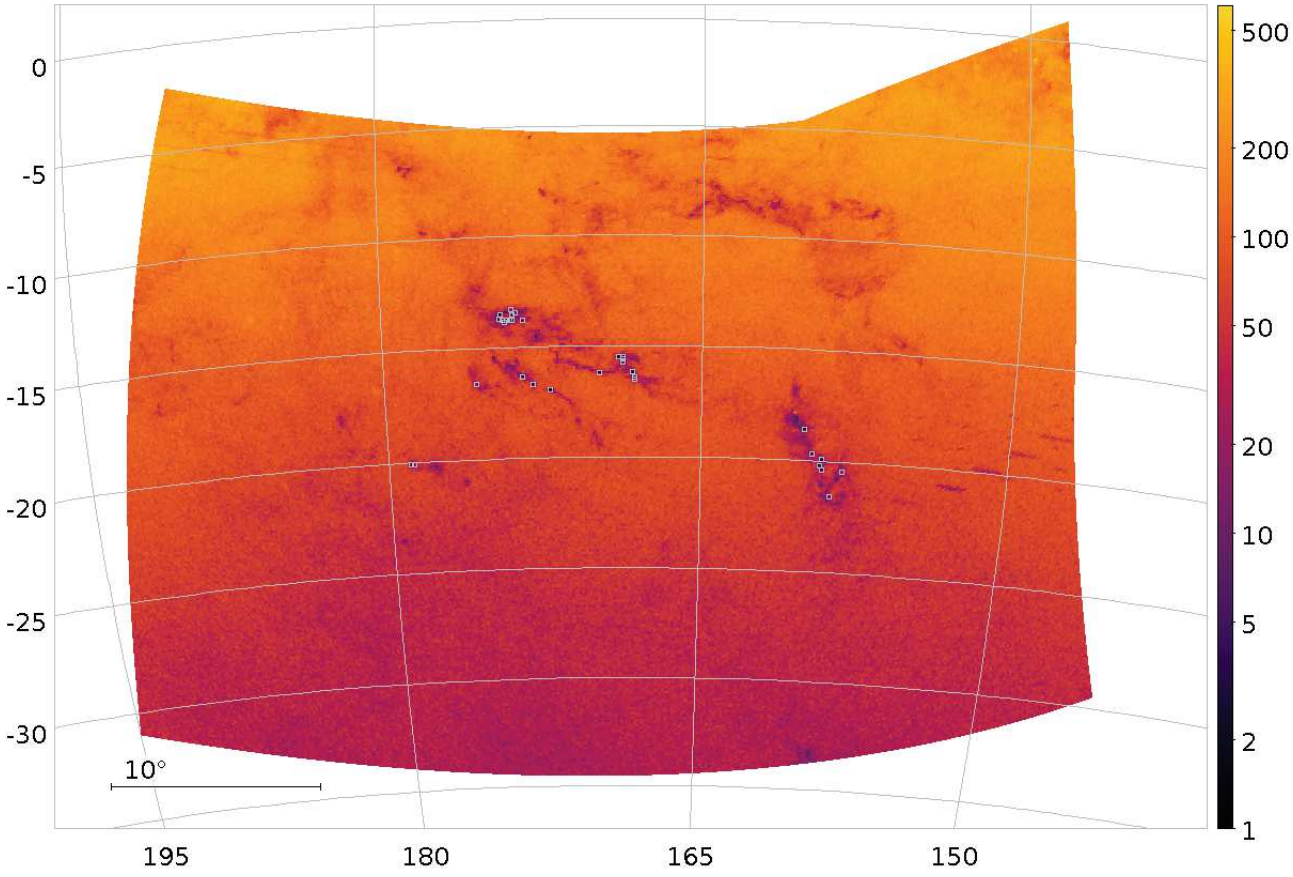


Figure 17: Density map at tessellation level 9 of a sky region at low galactic latitudes spanning HEALpixels 1, 3, 4, 6, 91, 94 (level 2). Each pixel corresponds to one FGS FOV. Gray open squares enclose substandard FOVs. The characteristic high extinction regions are visible (galactic coordinates).

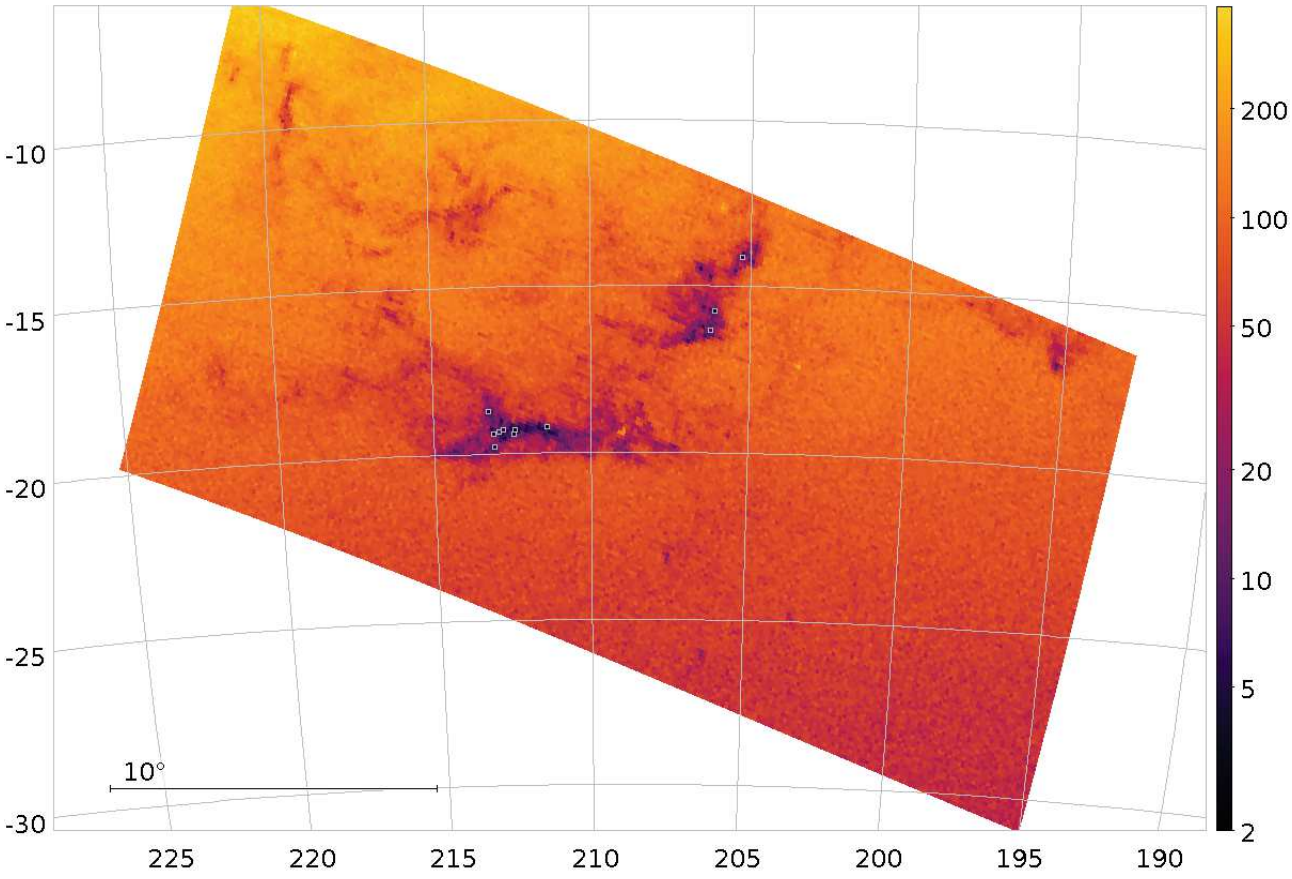


Figure 18: Density map at tessellation level 9 of a sky region at low galactic latitudes spanning HEALpixels 83, 89 (level 2). Each pixel corresponds to one FGS FOV. Gray open squares enclose substandard FOVs. The characteristic high extinction regions are visible (galactic coordinates).

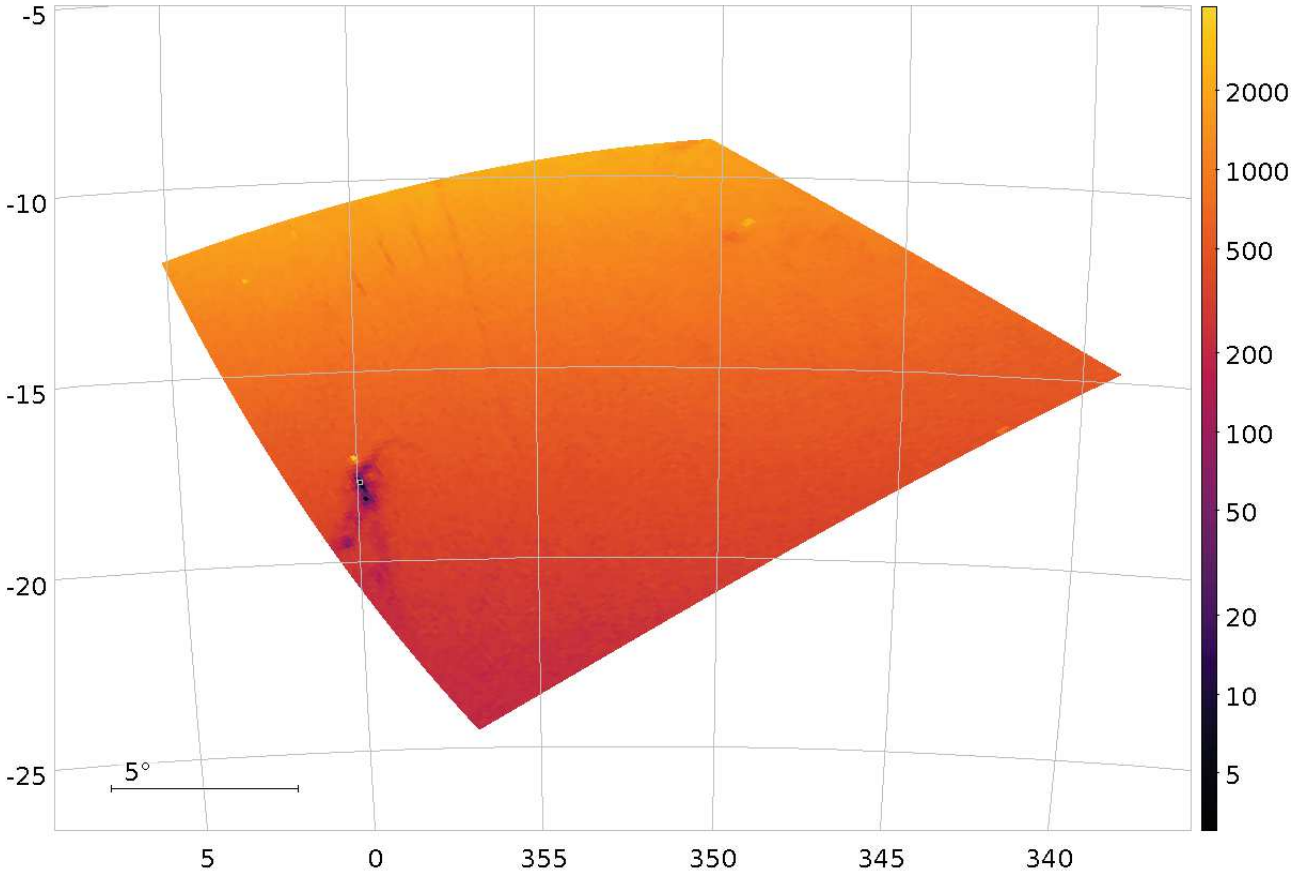


Figure 19: Density map at tessellation level 9 of HEALpix 186 (level 2). Each pixel corresponds to one FGS FOV. Gray open squares enclose substandard FOVs. HEALPix 167 is located near the galactic plane. The Rho Ophiuchi cloud complex is visible (galactic coordinates).

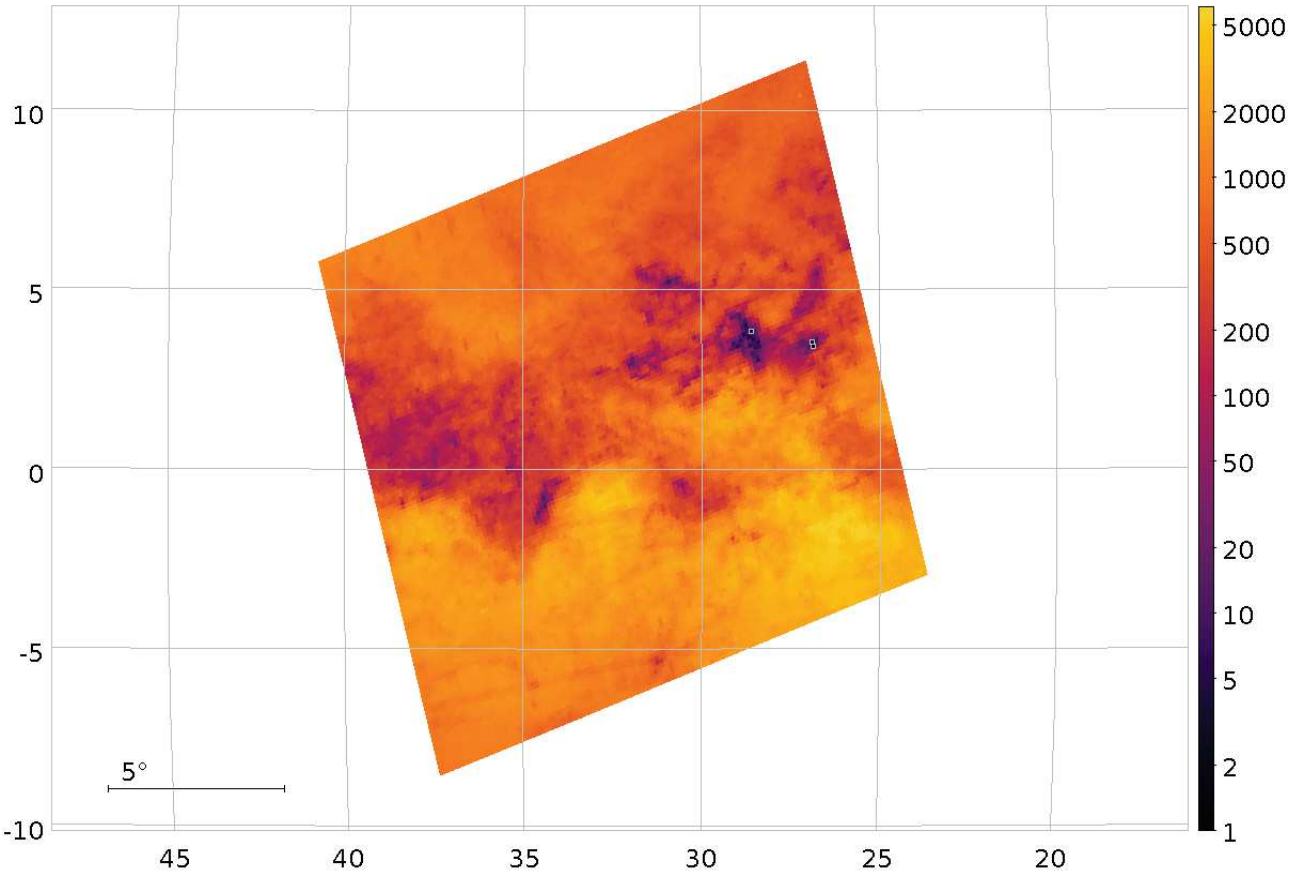


Figure 20: Density map at tessellation level 9 of HEALpix 118 (level 2). Each pixel corresponds to one FGS FOV. Gray open squares enclose substandard FOVs. HEALPix 118 is located near the galactic plane. The characteristic high extinction regions are visible (galactic coordinates).

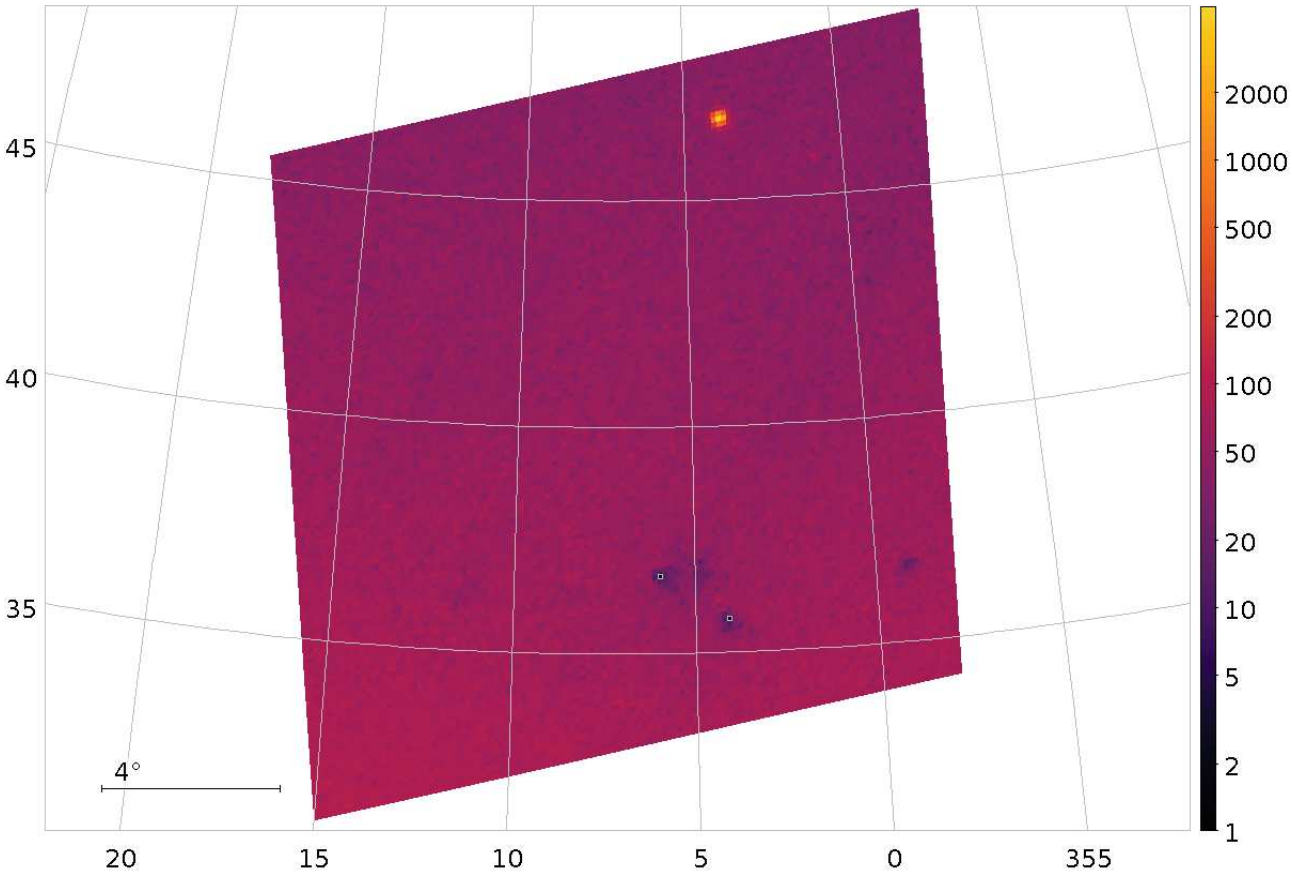


Figure 21: Density map at tessellation level 9 of HEALpix 122 (level 2). Each pixel corresponds to one FGS FOV. Gray open squares enclose substandard FOVs. The high latitude dark cloud Lynds 134 is visible (galactic coordinates).

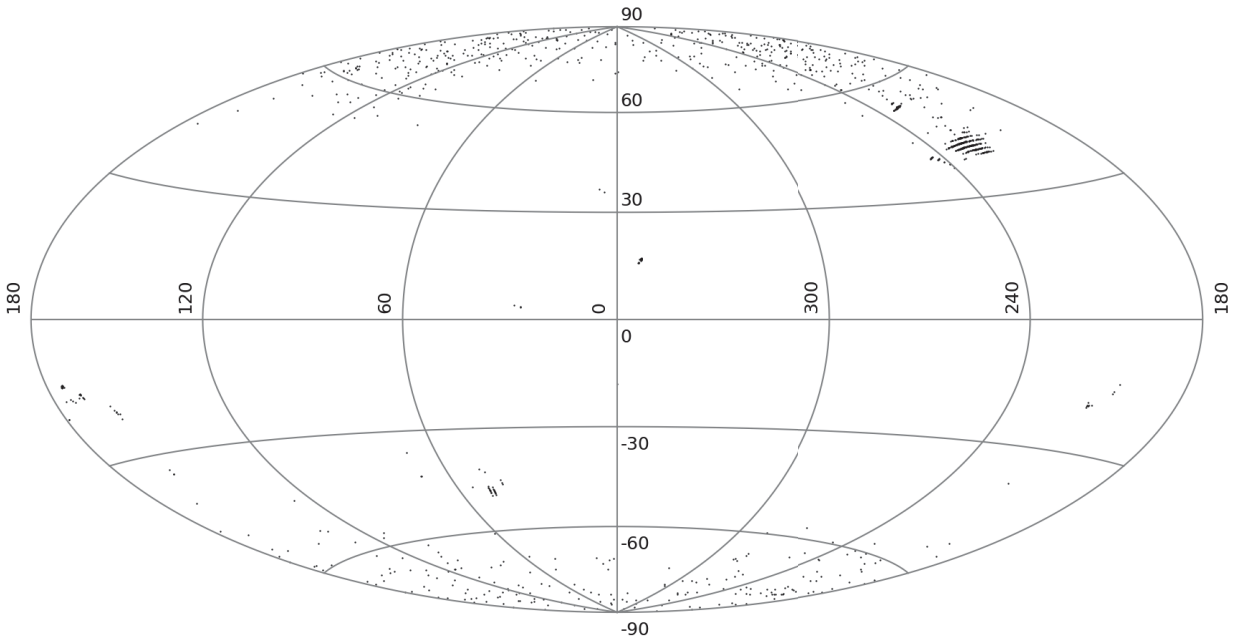


Figure 22: Location of the substandard FOVs (galactic coordinates).

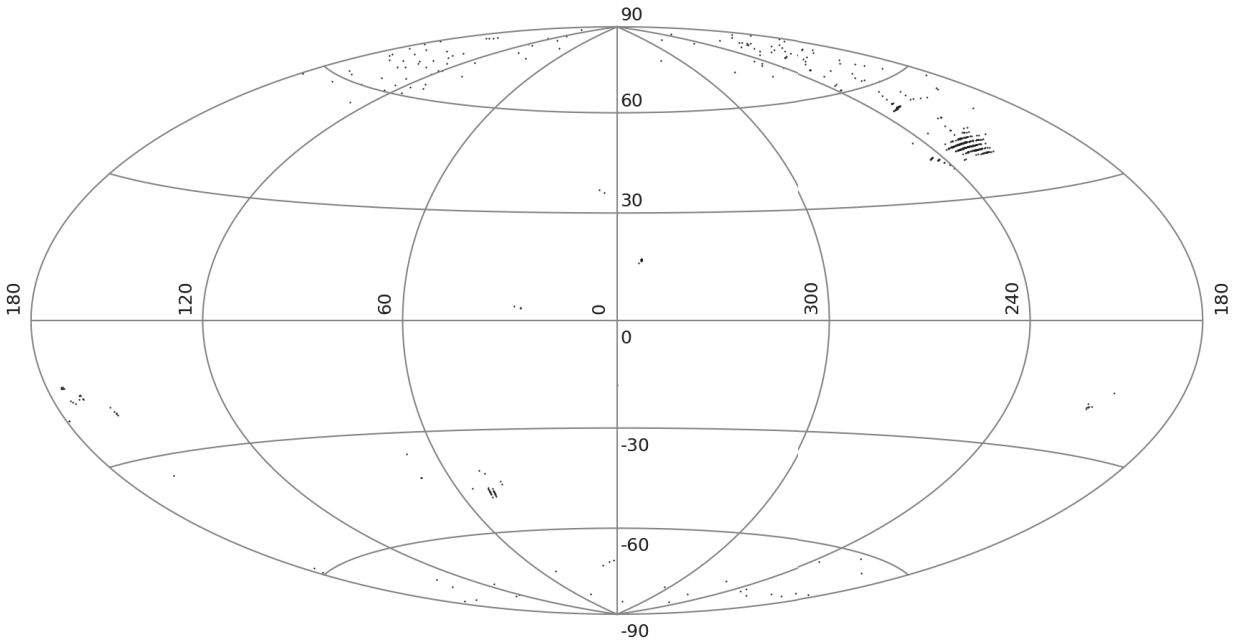


Figure 23: Location of the substandard FOVs when sources with Neighbor flag F=3 are assumed as isolated (galactic coordinates).

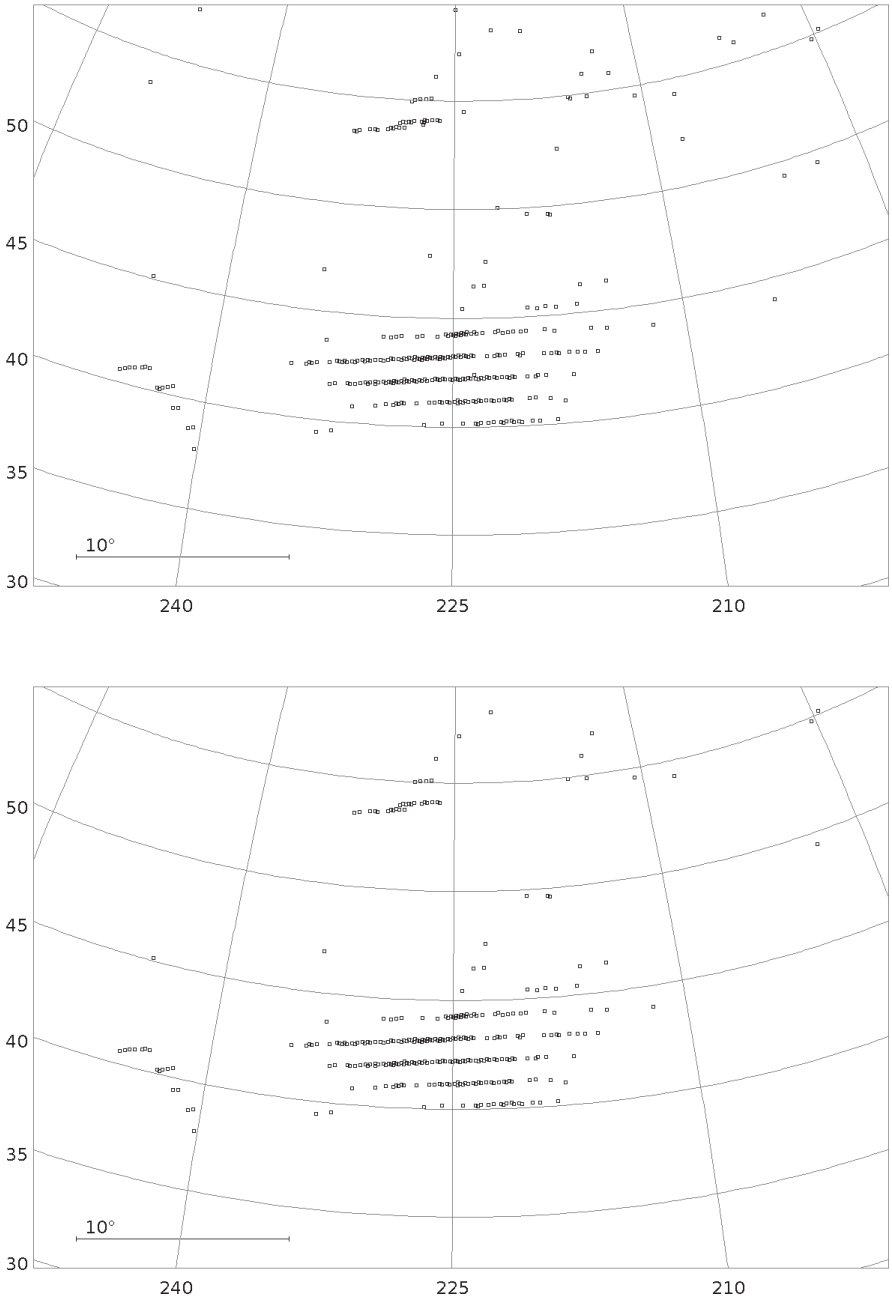


Figure 24: Location of substandard FOVs in a region affected by the Gaia scanning law pattern (see Figure 14). In the lower panel sources with Neighbor flag F=3 are assumed as isolated (galactic coordinates).

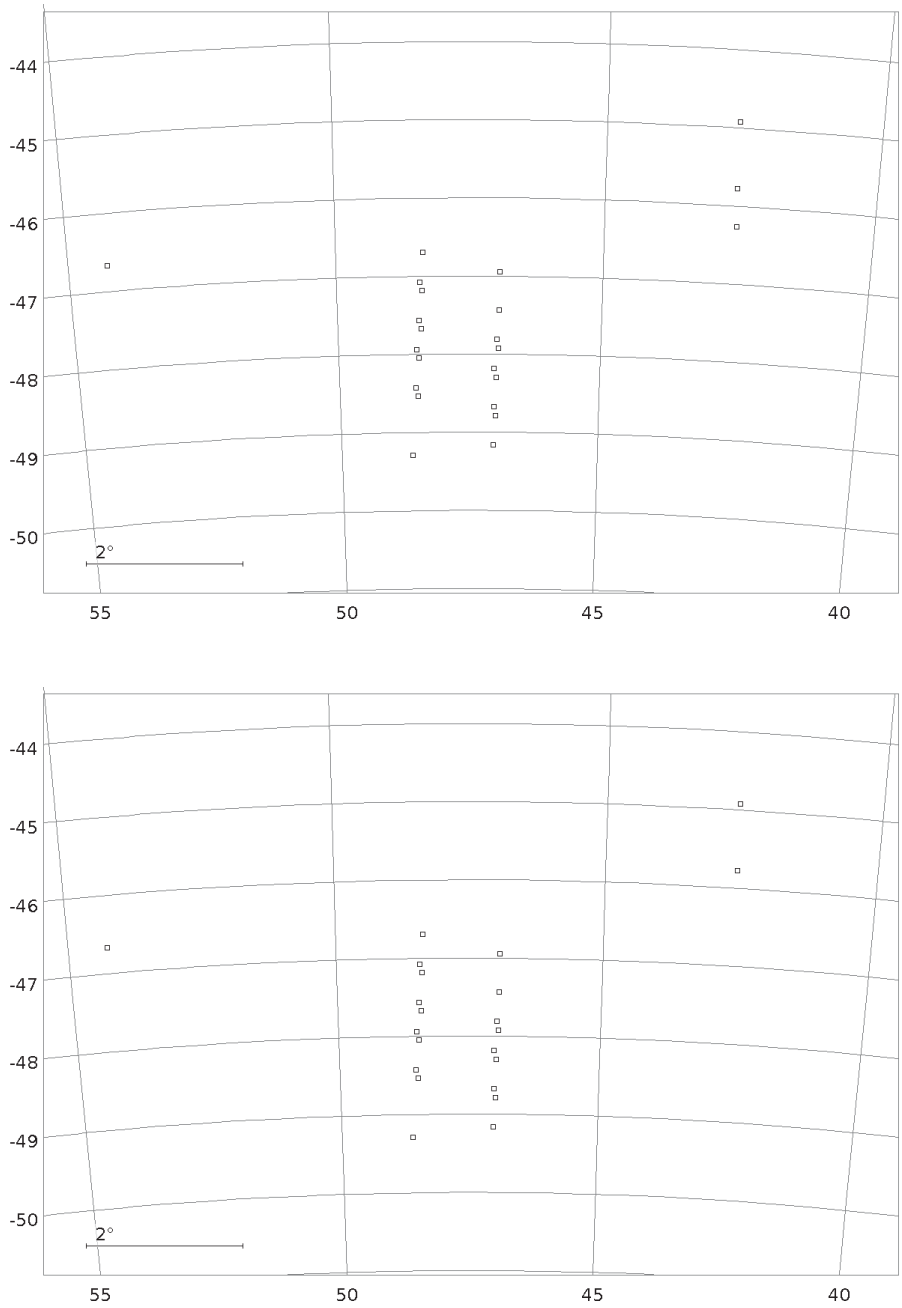


Figure 25: Location of substandard FOVs in a region affected by the Gaia scanning law pattern (see Figure 15). In the lower panel sources with Neighbor flag F=3 are assumed as isolated (galactic coordinates).

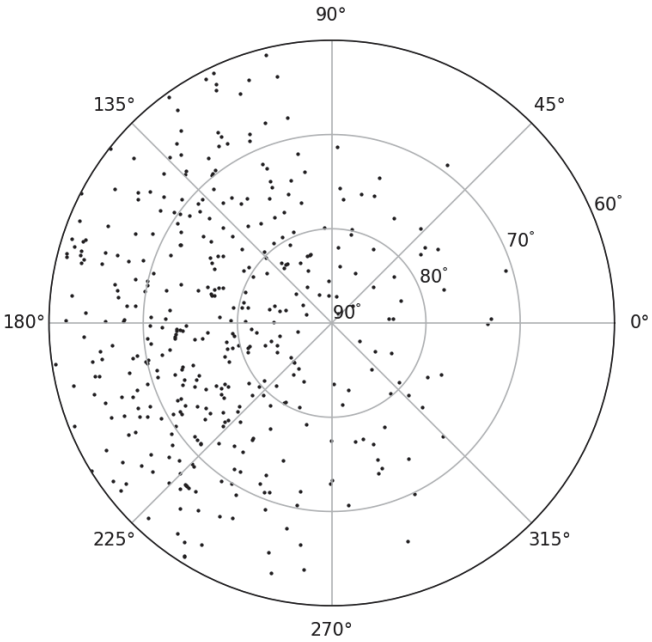


Figure 26: Location of the substandard FOVs in the North polar region (galactic coordinates).

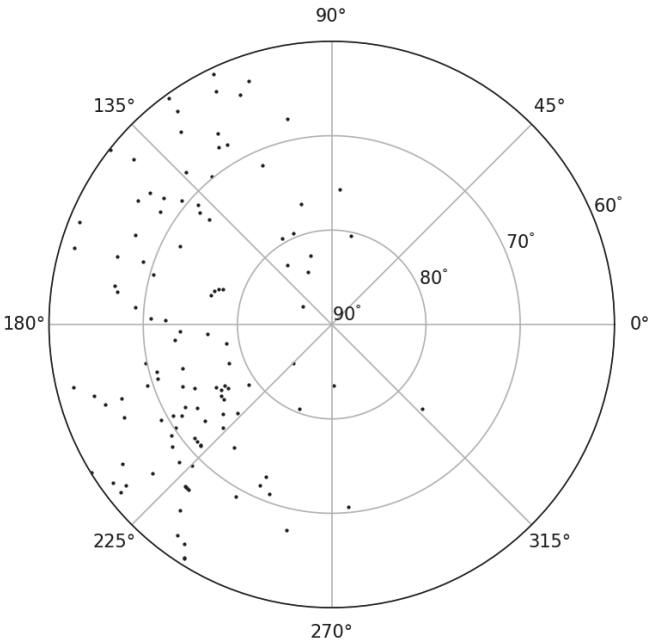


Figure 27: Location of the substandard FOVs in the North polar region when sources with Neighbor flag F=3 are assumed as isolated (galactic coordinates).

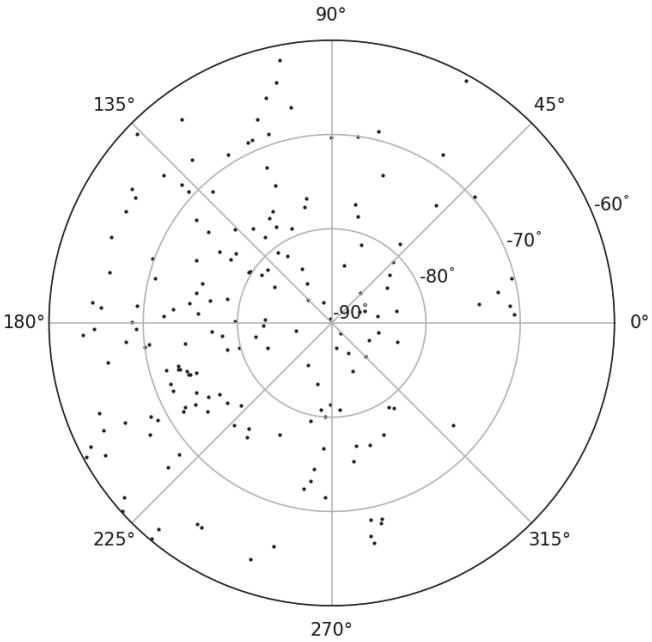


Figure 28: Location of the substandard FOVs in the South polar region (galactic coordinates).

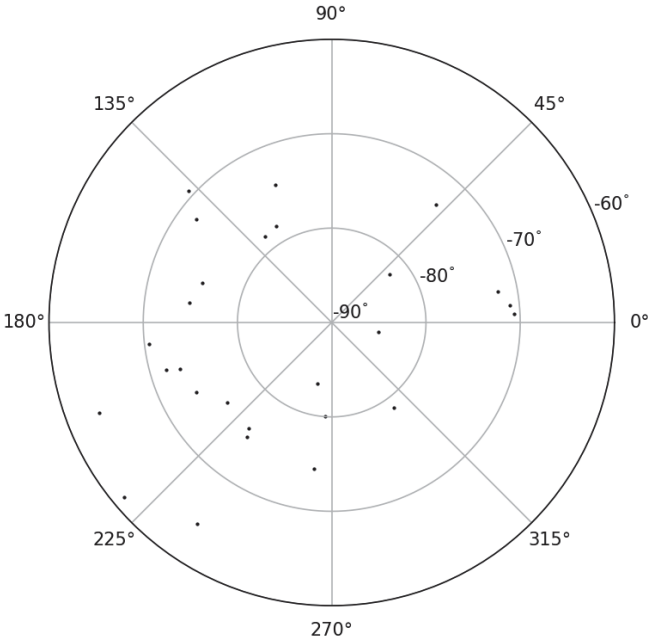


Figure 29: Location of the substandard FOVs in the South polar region when sources with Neighbor flag F=3 are assumed as isolated (galactic coordinates).

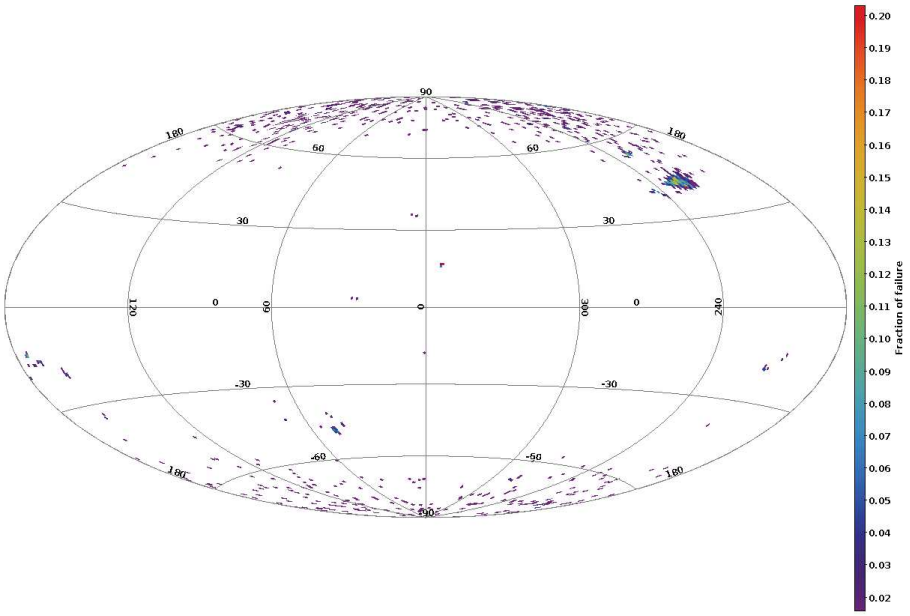


Figure 30: Density map of substandard FOVs at the resolution of HEALpix level 6 (galactic coordinates).

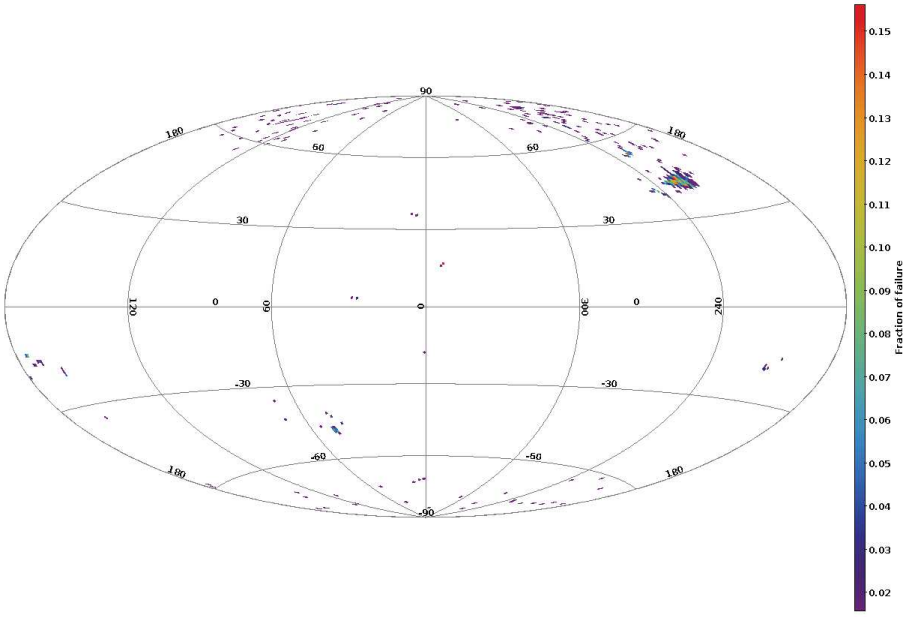


Figure 31: Density map of substandard FOVs at the resolution of HEALpix level 6 when sources with Neighbor flag F=3 are assumed as isolated (galactic coordinates).

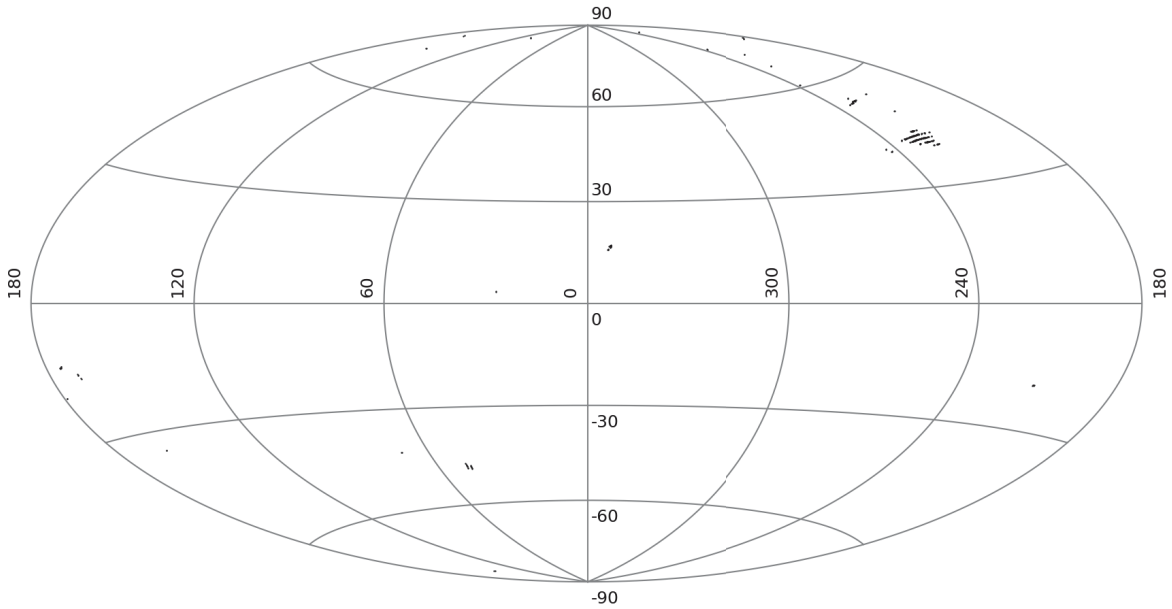


Figure 32: Location of substandard FOVs having one or more adjacent substandard FOVs (galactic coordinates).

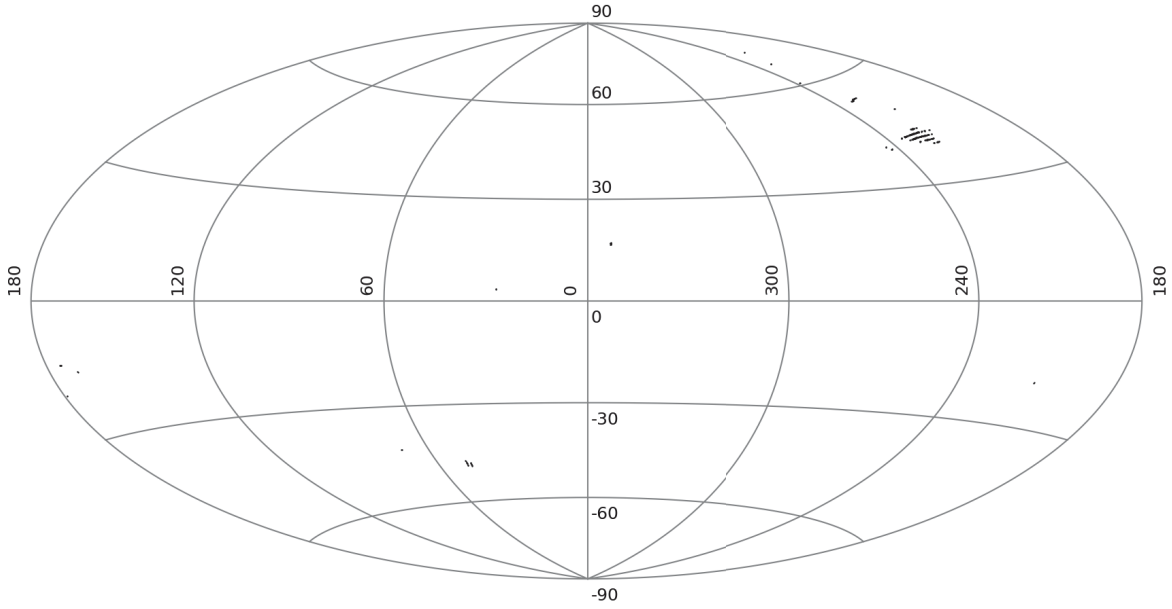


Figure 33: Location of substandard FOVs having one or more adjacent substandard FOVs when sources with Neighbor flag F=3 are assumed as isolated (galactic coordinates).

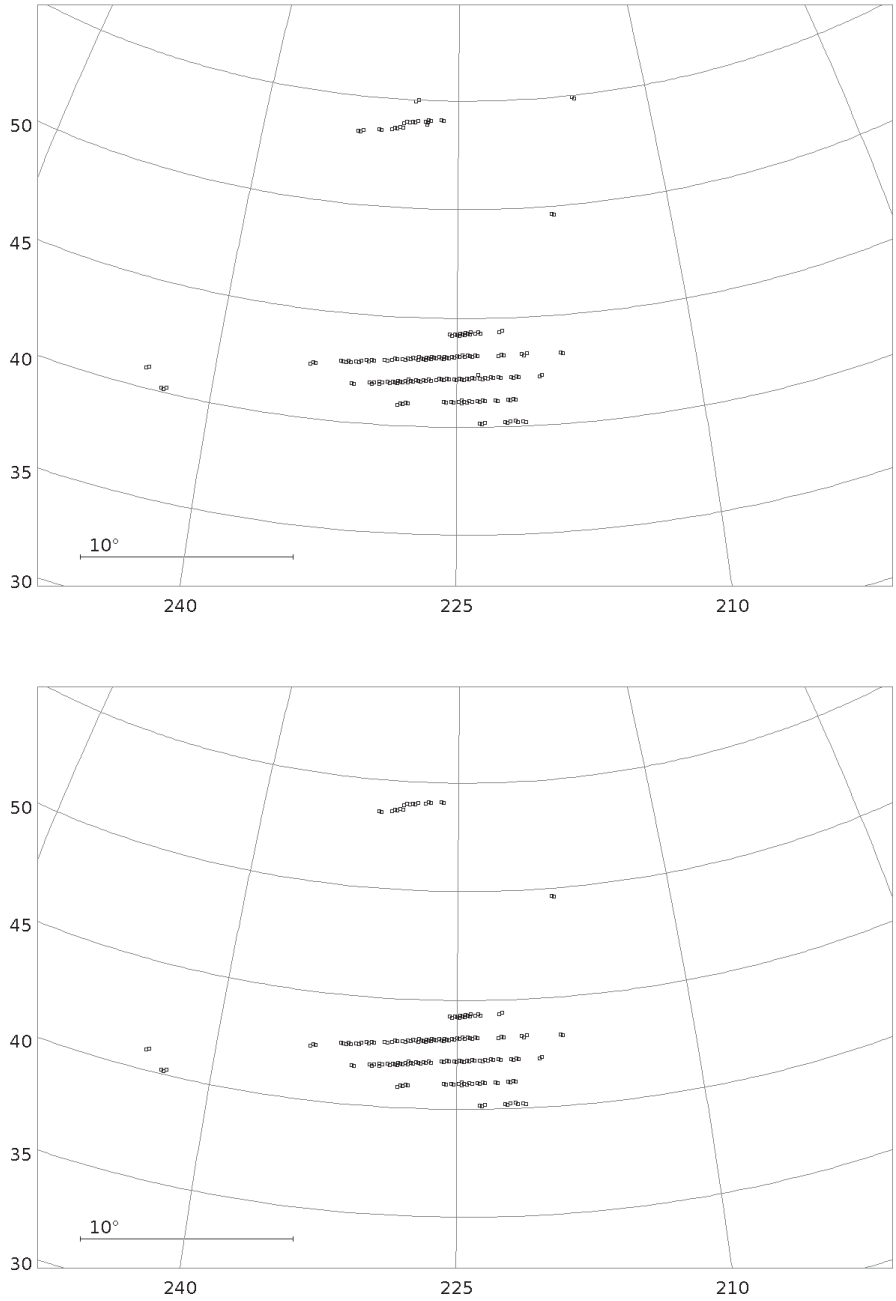


Figure 34: Location of substandard FOVs having one or more adjacent substandard FOVs in a region affected by the Gaia scanning law pattern (see Figure 14). In the lower panel sources with Neighbor flag F=3 are assumed as isolated (galactic coordinates).

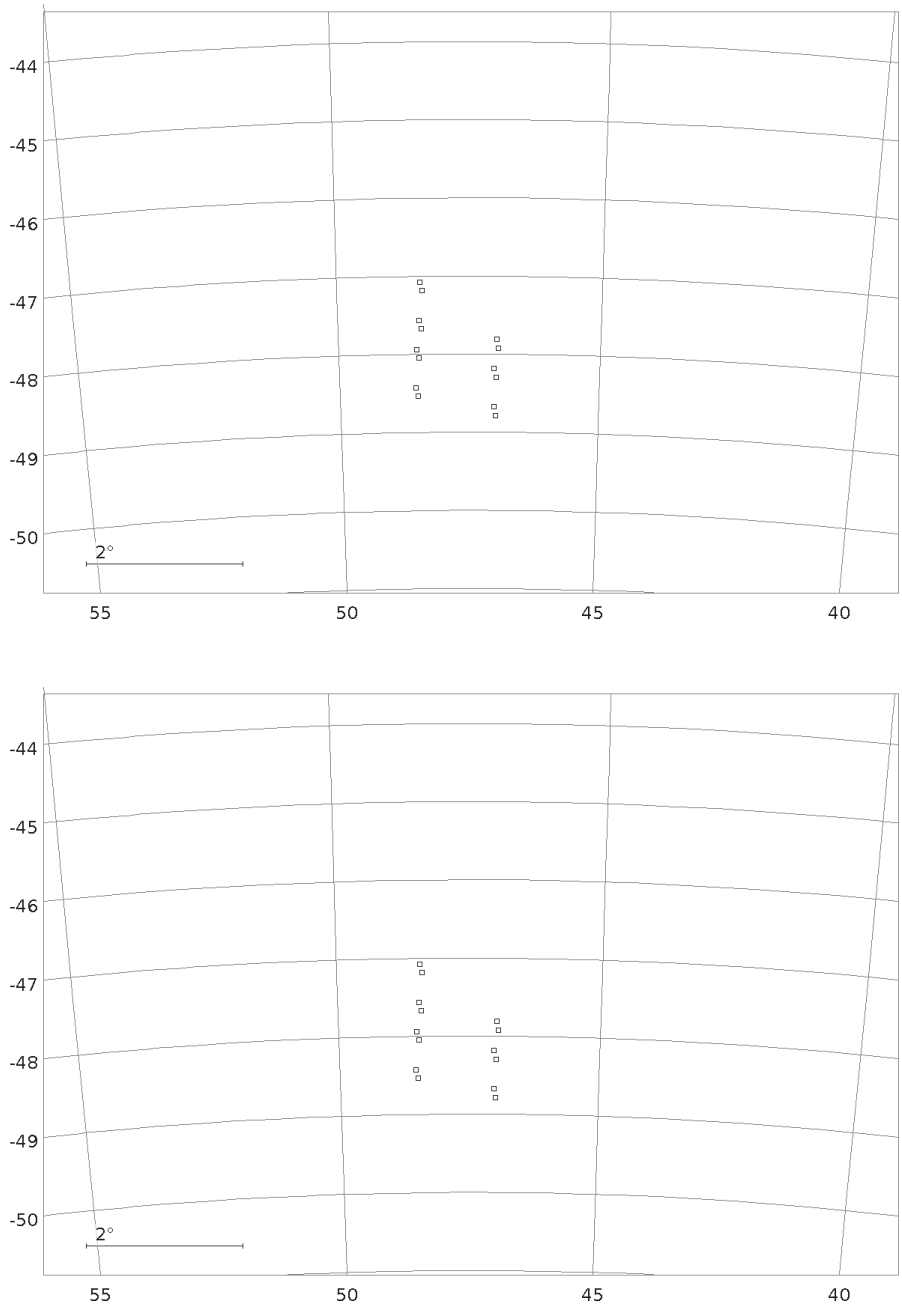


Figure 35: Location of substandard FOVs having one or more adjacent substandard FOVs in a region affected by the Gaia scanning law pattern (see Figure 15). In the lower panel sources with Neighbor flag F=3 are assumed as isolated (galactic coordinates).

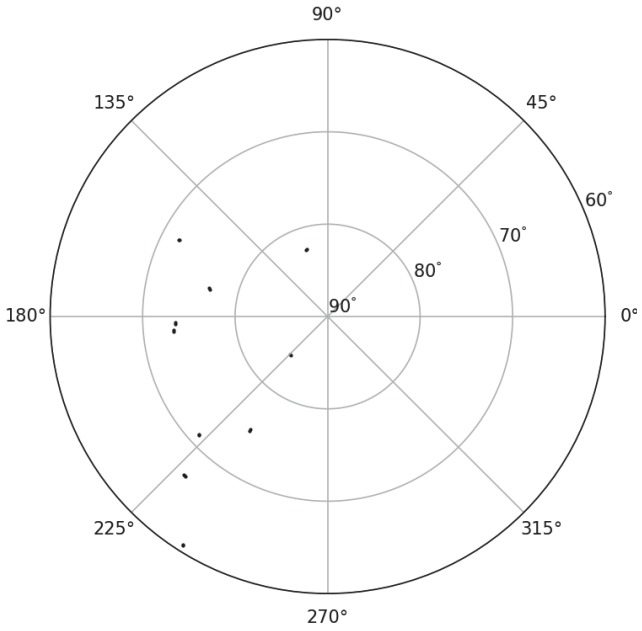


Figure 36: Location of substandard FOVs in the North polar region having one or more adjacent substandard FOVs (galactic coordinates).

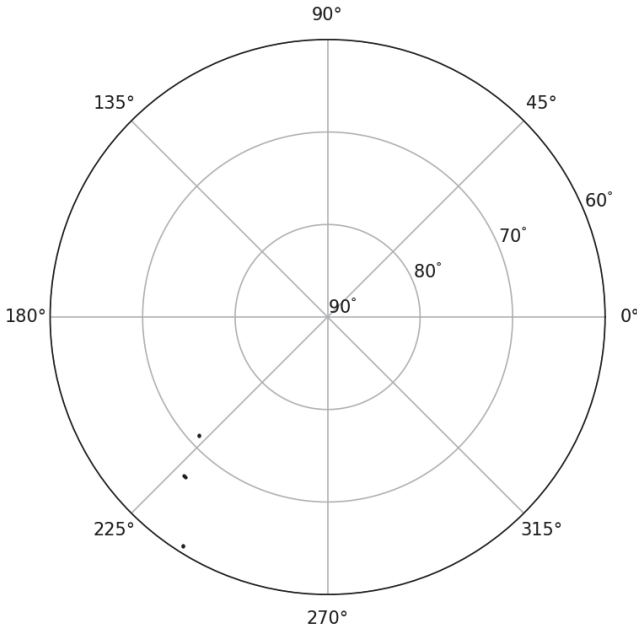


Figure 37: Location of substandard FOVs in the North polar region having one or more adjacent substandard FOVs when sources with Neighbor flag F=3 are assumed as isolated (galactic coordinates).

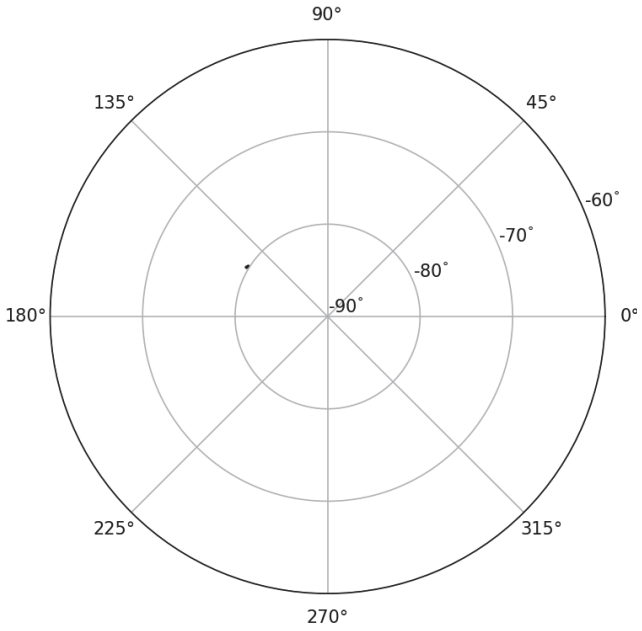


Figure 38: Location of substandard FOVs in the South polar region having one or more adjacent substandard FOVs (galactic coordinates).

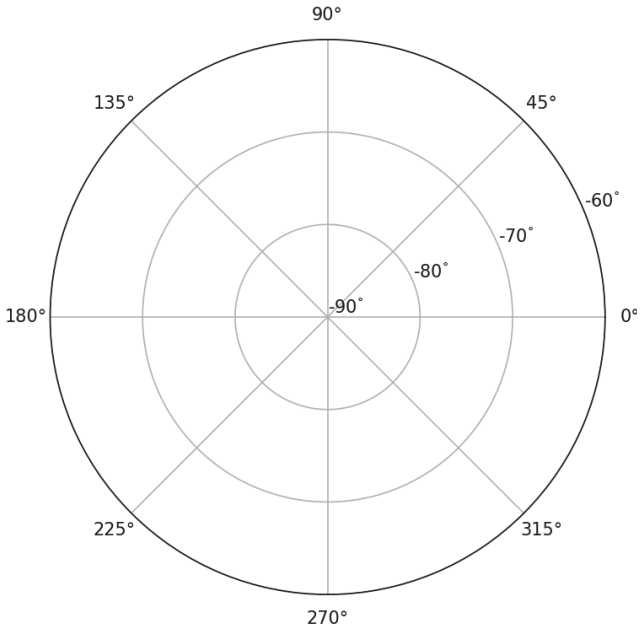


Figure 39: Location of substandard FOVs in the South polar region having one or more adjacent substandard FOVs when sources with Neighbor flag F=3 are assumed as isolated (galactic coordinates).

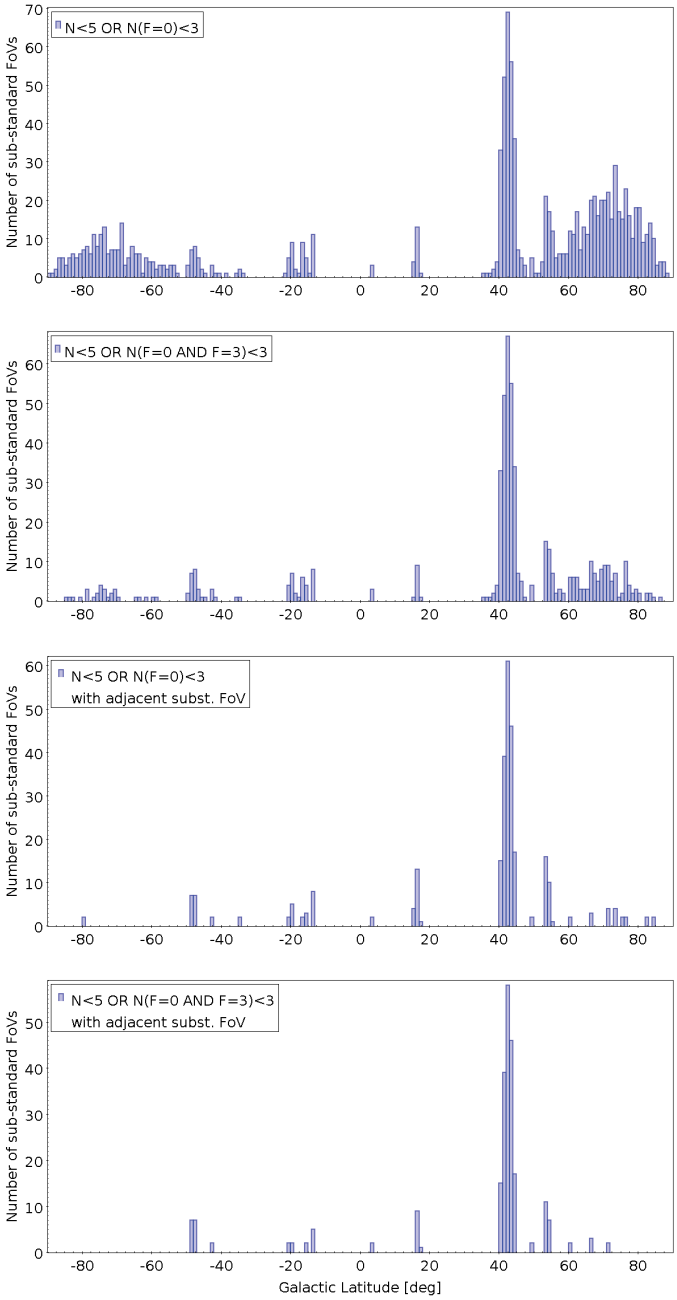


Figure 40: Distribution of *substandard FOVs* in galactic latitude; from top to bottom the different mitigation strategies have been applied.

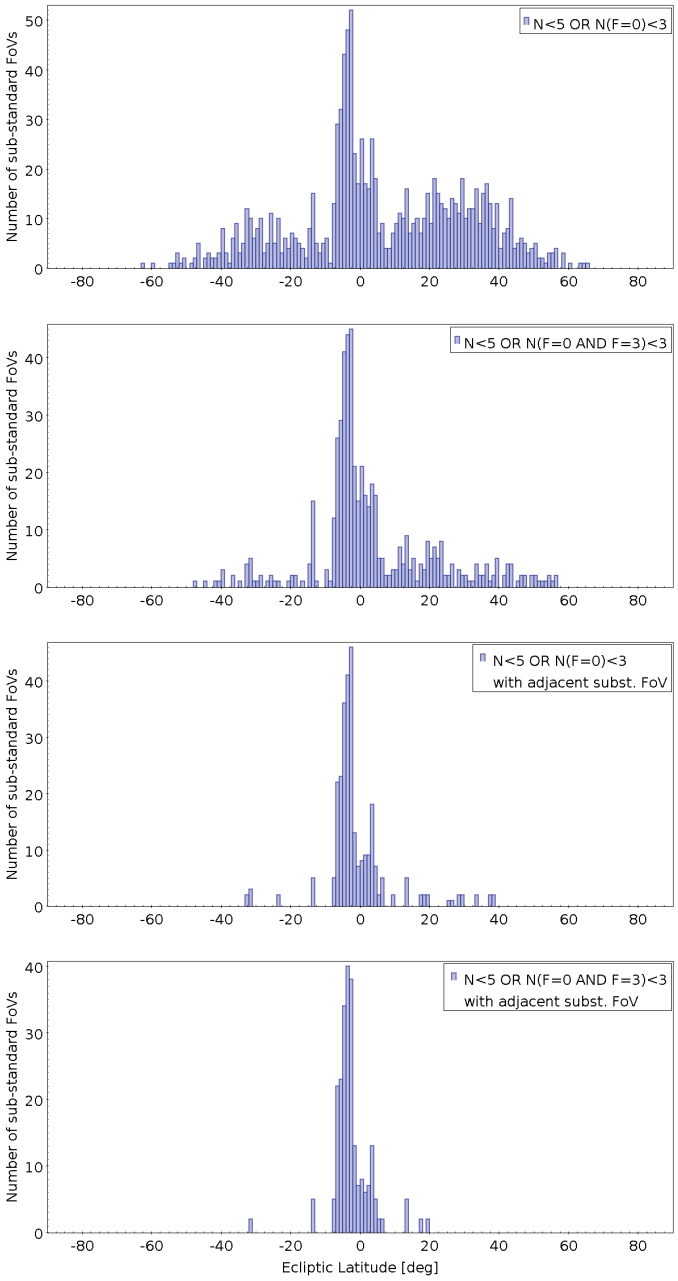


Figure 41: Distribution of *substandard FOVs* in ecliptic latitude; from top to bottom the different mitigation strategies have been applied.

Table 5: IDs of substandard FOVs (Healpix_ID9) having at least one adjacent substandard FOV when sources with Neighbor flag F=3 are assumed as isolated. The first column show the Healpix level 2 ID in which the substandard FOV is located.

Healpix_ID2	Healpix_ID9	Healpix_ID2	Healpix_ID9	Healpix_ID2	Healpix_ID9	Healpix_ID2	Healpix_ID9	Healpix_ID2	Healpix_ID9
4	67378	17	278614	106	1741184	106	1752918	167	2750832
4	67384	17	278620	106	1741187	106	1752924	167	2750834
4	67472	17	278622	106	1741381	106	1752926	167	2750835
4	67474	17	278623	106	1741383	106	1752927	167	2750838
4	67480	17	278645	106	1741400	106	1752949	167	2750842
4	74811	17	278647	106	1750226	106	1752951		
4	74814	17	278677	106	1750233	106	1752957		
16	267526	17	278690	106	1750235	106	1752981		
16	267532	17	278696	106	1750735	106	1753026		
16	267557	17	278699	106	1750757	106	1753032		
16	267559	17	278722	106	1750822	106	1753068		
16	267578	17	278728	106	1750828	106	1753070		
16	267589	17	278818	106	1750830	107	1763880		
16	267591	17	278826	106	1750917	107	1763882		
16	267610	17	278913	106	1750919	107	1763968		
16	267632	17	278915	106	1750938	107	1763969		
16	267635	17	279041	106	1750960	107	1763971		
16	267641	17	279046	106	1750963	107	1763977		
16	267643	17	279052	106	1750974	107	1763982		
16	267664	17	279077	106	1752156	107	1764004		
16	267665	17	279079	106	1752158	107	1764006		
16	267667	17	279117	106	1752181	107	1764007		
16	267673	17	279130	106	1752189	107	1764013		
16	267678	17	279152	106	1752302	107	1764015		
16	267700	17	279187	106	1752340	107	1764082		
16	267709	17	279193	106	1752343	107	1764088		
16	267711	17	279198	106	1752349	107	1764091		
16	267732	17	279220	106	1752360	107	1765620		
16	267734	17	279263	106	1752362	107	1765622		
16	267741	17	279285	106	1752425	107	1766146		
16	267743	17	279312	106	1752427	107	1766153		
16	267863	17	279315	106	1752451	107	1766155		
16	267869	17	279458	106	1752457	107	1766180		
16	268042	17	280673	106	1752462	107	1766182		
16	268096	17	280678	106	1752484	107	1766194		
16	268098	17	280985	106	1752486	107	1766201		
16	268134	17	280987	106	1752487	107	1766203		
16	268140	17	283328	106	1752493	107	1766292		
16	268175	17	283330	106	1752495	107	1766294		
16	268197	72	1188626	106	1752518	107	1766301		
16	268210	72	1188632	106	1752525	107	1766370		
16	268219	72	1188647	106	1752527	107	1766377		
16	268248	72	1188653	106	1752562	107	1766379		
16	268250	72	1188728	106	1752568	107	1767759		
16	268273	72	1188730	106	1752571	107	1767781		
16	268275	72	1188740	106	1752645	110	1804299		
16	269585	72	1188742	106	1752647	110	1804302		
16	269596	72	1188813	106	1752664	110	1806301		
16	269598	72	1188815	106	1752666	110	1809034		
17	278544	72	1188838	106	1752848	110	1809056		
17	278546	72	1188844	106	1752850	110	1810144		
17	278553	72	1190211	106	1752851	110	1810147		
17	278555	72	1190217	106	1752857	118	1936124		
17	278580	75	1231220	106	1752859	118	1936126		
17	278582	75	1231222	106	1752884	167	2750808		
17	278589	83	1371227	106	1752886	167	2750811		
17	278591	83	1371230	106	1752892	167	2750821		
17	278609	91	1507171	106	1752895	167	2750823		
17	278611	91	1507177	106	1752913	167	2750829		

8. Big Extended Sources in ISC

In the VTR [AD 2] we have pointed out that the delivered ISC does not comply the requirement EUCL-ISC-REQ-040 which states that all the objects must have a size smaller than the FGS tracking window size. In practice, this means that the catalog should not contain objects with estimated size larger than 2.9 arcsec x 2.9 arcsec (29x29 pixels).
We demonstrated the presence in the catalog of these objects showing the SDSS images of a few ISC extended sources classified as large extended sources in the Sloan Digital Sky Survey (SDSS), i.e extended sources with estimated size larger than 2.9 arcsec x 2.9 arcsec (see EUCL-OATO-RP-2-002 [AD 2] for details about the executed tests).
We concluded that objects larger than 2.9 arcsec in ISC will be extremely rare, and in any case, will be characterized by a very peaked flux distribution, as required by the Gaia onboard detection algorithm.
In this section we provide an estimate of the probable number of ISC sources larger than 2.9 arcsec as a function of magnitude.

8.1 Methodology

We selected from a test set of 178 310 ISC extended sources located in a sky strip covering all latitudes (SDSS stripe 1188, $l = 94^\circ$, $\delta l = 2.5^\circ$) and having a counterpart in the SDSS-DR9 catalog a sample of 4964 possibly big extended sources still present in ISC. This sample is defined by the objects with size larger than $2.9''$, as estimated by the SDSS-DR9 parameter deVRad_g (see [AD2], [AD3]) and having probability to be extended P1>0.7.
The cut in probability has been done in order to remove from the sample of big sources the ones having photometric properties most common to point-like sources. The color-color diagrams bp_g vs. g_rp in Figures 42 and 43 show that big sources with probability to be extended less than 70% fall on the point-like sources locus, whereas big sources with probability greater than 70% have colors most similar to the sources already filtered from ISC (i.e. sources with P1>0.95 and phot_bp_rp_excess_factor>1.8 [AD3].)

We visually inspected 1717 (out of 6514) SDSS images of big extended sources (P1>0.5, 4$*$deVRad_g > 2.9), in order to verify their extended nature and establish if they can be problematic or not for the FGS. The results of this analysis are shown in the Appendix A of this document.
Moreover, an all-sky sample of big extended sources has been cross-matched with high-resolution HST archived images to verify if they are effectively bigger than the FGS tracking window. In Appendix B the images of 20 of the 169 matched sources are shown.
We used the SDSS-strip sample to compute the fraction of extended sources that are possibly big and could be problematic for the FGS. The computed fractions have been applied to the whole ISC in order to obtain an estimate of the real number of problematic big-extended objects still present in ISC.

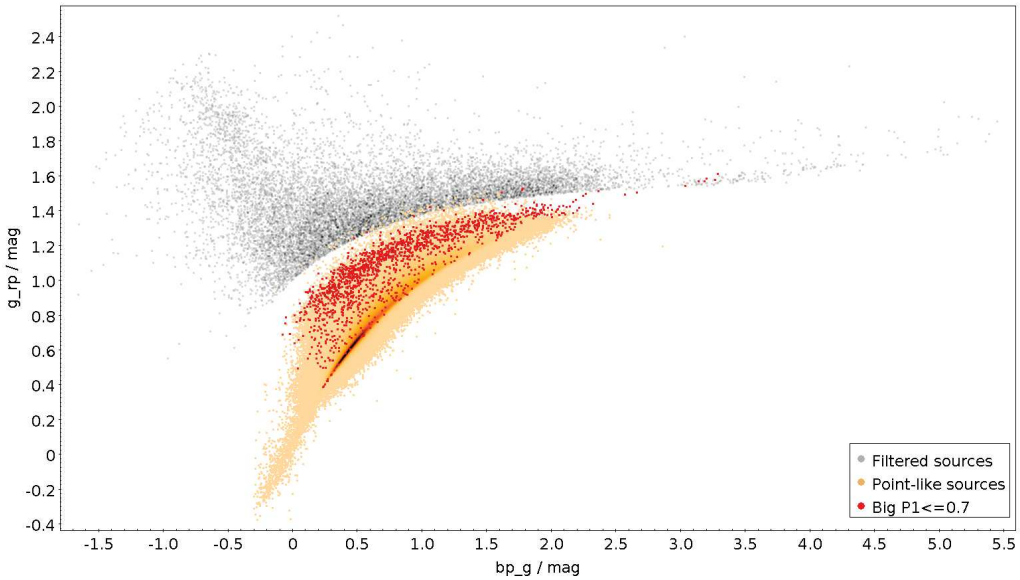


Figure 42: Color-color diagram of the SDSS strip sample. Big extended sources with probability to be extended P1$\leq$0.7 (red dots) are compared with the distribution of point-like sources (heat color map) and the distribution of already filtered big extended sources (grayscale color map).

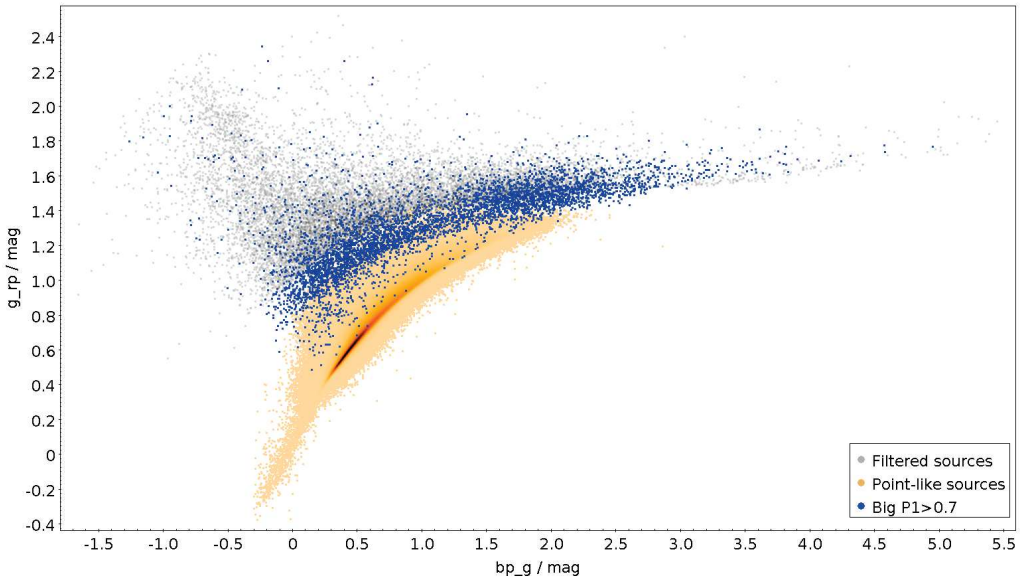


Figure 43: Color-color diagram of the SDSS strip sample. Big extended sources with probability to be extended P1>0.7 (blue dots) are compared with the distribution of point-like sources (heat color map) and the distribution of already filtered big extended sources (grayscale color map).

8.2 Results

From the analysis of the color-color diagram and of the SDSS images we defined as bona-fide sample of big extended sources the sample of sources with size larger than $2.9''$ and having probability to be extended P1>0.7.
On the base of the inspected SDSS images we classified these sources as problematic or not problematic for the FGS, where problematic is for possibly bigger than the FGS tracking window.
In appendix A we divided problematic sources in three groups based on their morphological appearance:

- galaxies: ellipticals or bulges of spirals (e.g. see Figure 48);
- disturbed objects (disturbed_2): sources in the field of a background galaxy, or in the field of star forming regions, HII regions or planetary nebulae. They could be foregrounds stars, not resolved globular clusters, or massive stars in very young clusters. In any case, the diffuse light surrounding these sources makes them potentially problematic for the FGS (e.g. see Figure 58 and Figure 59 central and right panel.);
- unknown objects (unknown_2): the inspected images prevent to define the physical nature of these sources. They belong to two groups: (1) isolated, red, visually big sources with $R_FGS \lesssim 18.0$ located on the galactic plane (abs(b)<10) (e.g. see Figure 51); (2) sources associated with a weak diffuse light, having $R_FGS \gtrsim 18.0$ and located at abs(b)>20 (e.g. see Figure 60).

In general all these sources are characterized by a highly peaked flux distribution, as can be inferred from the high resolution HST image in Figure 52. This is the main reason why these big extended sources have been detected by Gaia, a survey optimized for point-like sources.
In appendix B HST images of nineteen more sources of various morphological types located outside the SDSS strip are shown with superposed brightness contours and the FGS tracking window.

According to the analysis in Appendix A problematic sources are most common within big objects with probability to be extended P1>0.7. The sample of SDSS strip sources with size larger than $2.9''$ and having probability to be extended P1>0.7 was than used to compute the fractions of extended sources that are problematic, and these fractions have been used to estimate the number of problematic big-extended objects still present in ISC.

Figure 44 show fractions of extended sources that are big (blue histogram) and problematic (red histogram) in R_{FGS} magnitude bins. Note that we computed the fractions of objects with high probability to be big that are effectively problematic from the sample of inspected images, and we computed the fractions of extended sources that have high probability to be big from the SDSS strip sample (blue histogram); the red histogram is then obtained as a combination of these two fractions.
Problematic sources constitute less than 1% of the extended sources on the entire magnitude range.

Figure 45 shows the distribution in R_{FGS} magnitude bins of the ISC extended sources (gray histogram) compared with the distribution of big sources (blue histogram), and of big problematic sources

(red histogram). To obtain counts in Figure 45, the fractions in Figure 44 have been multiplied by the number of extended sources in ISC in each magnitude bin. The sum of the counts in the magnitude bins of the red histogram gives the number 1 173 873 i.e. the estimated number of possibly problematic sources still present in ISC. These sources correspond to $\sim 0.57\%$ of ISC extended sources and to $\sim 0.16\%$ of all ISC sources.

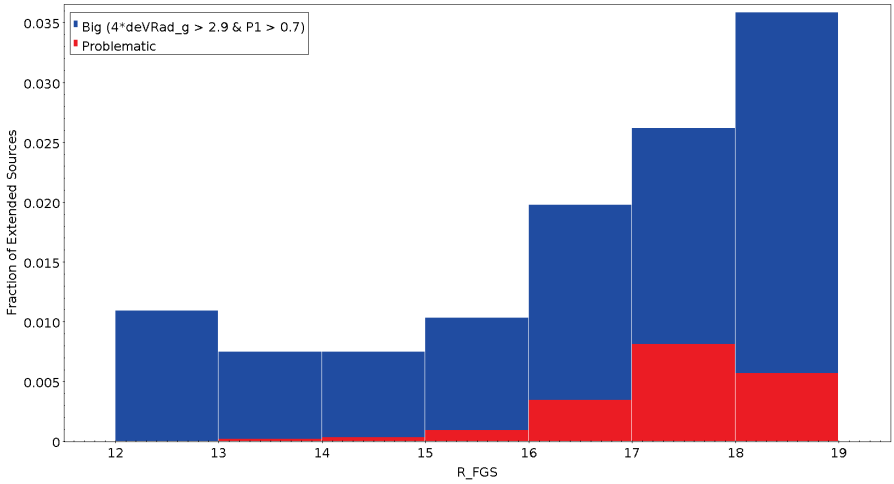


Figure 44: Fractions of extended sources in R_{FGS} magnitude bins that might be big (blue) and problematic for the FGS (red). The fractions have been computed from the SDSS strip sample.

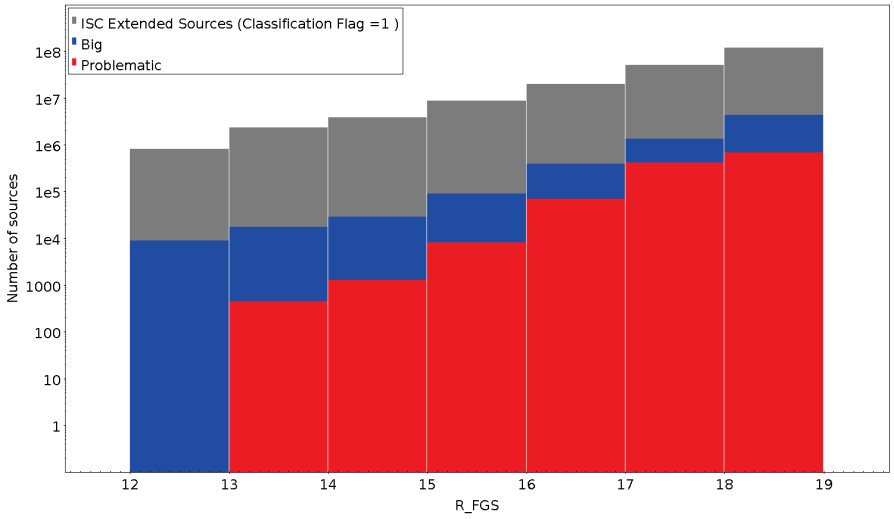


Figure 45: Histograms in R_{FGS} magnitude bins of the estimated number of possibly big-extended sources (blue) and big problematic sources (red) still present in ISC, compared with the distribution of ISC extended sources (gray).

Figure 46 shows the position in galactic coordinates of all ISC extended sources (Classification Flag = 1). Figure 47 shows the positions of ISC extended sources with probability to be extended P1>0.7 (47% of ISC extended sources). As a result of this analysis, only $\sim$ 1.2% of the plotted sources is possibly problematic for FGS.

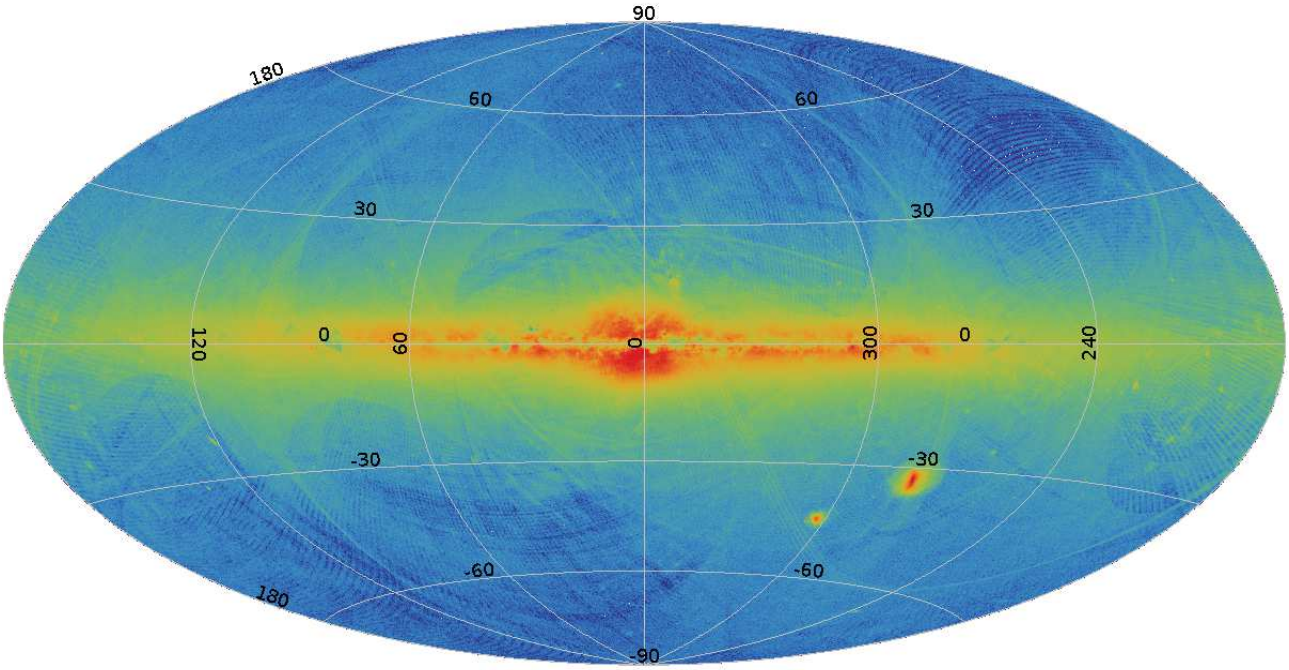


Figure 46: All-sky map (positions) of ISC sources flagged as extended (Classification Flag = 1) (galactic coordinates).

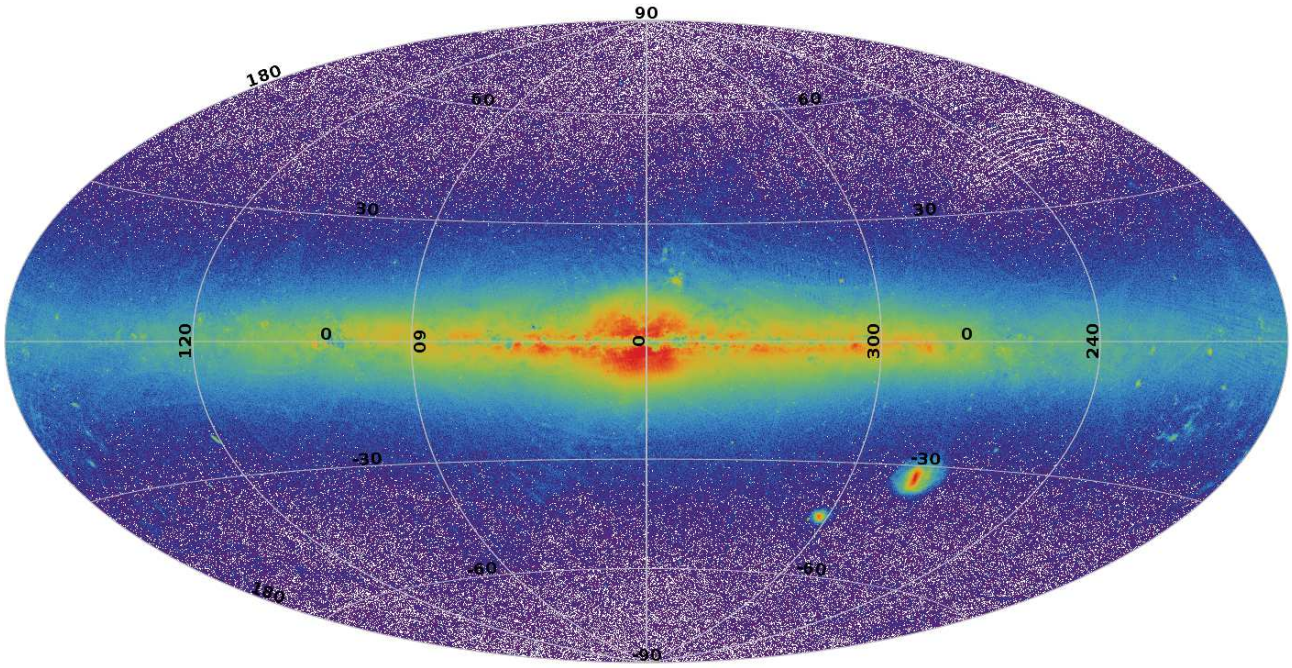


Figure 47: All sky density map (positions) of ISC extended sources (Classification Flag = 1) with probability to be extended P1>0.7 (galactic coordinates).

9. APPENDIX A

We selected from a test set of 178310 ISC extended sources located in a sky strip covering all latitudes and having counterpart in the SDSS-DR9 catalog a sample of 6514 possibly big extended sources still present in ISC. The sample is defined by the objects with size larger than $2.9''$, as estimated by the SDSS-DR9 parameter deVRad_g (see [AD2], [AD3]).
In order to provide a statistic of the kind of objects belonging to this sample we inspected their SDSS DR9 images.
The sample of 6514 objects has been subdivided in four sets. For each set a table with the numbers of objects per type and some example images are shown.

In the images we identified seven morphological types:

- big stars: a single very bright star with spikes;
- blends: faint stars blended with very bright stars, stars in crowded regions;
- disturbed sources type 1 (disturbed_1): sources nearby a very bright star with spikes;
- disturbed sources type 2 (disturbed_2): sources with a galaxy in the background or sources in star forming regions, HII regions, or planetary nebulae;
- galaxies: elliptical, bulges of spirals;
- unknown objects type 1 (unknown_1): sources that cannot be classified. They look as faint (visually small), red, isolated objects. The few that are in Simbad are classified as low mass stars or high proper motion stars.
- unknown objects type 2 (unknown_2): sources that cannot be classified. They look as objects with an associated extended emission, or as bright (visually big), red, isolated objects. The few that are present in Simbad are classified as galaxies, carbon stars, or high proper motion stars.

We divided these seven types in two main classe:

- problematic for FGS: galaxies, disturbed_2, unknown_2
- not problematic for FGS: big stars, blends, disturbed_1, unknown_1

Problematic sources are the ones that are possibly bigger then the FGS tracking window ($2.9''$ x $2.9''$).

BRIGHT_HIGH_P1 (R_{FGS}<16 and P1>0.7).
Total number of objects = 274, inspected images = 274.

object type	**n**	%	%
All	274	100	
Big star	10	4	94
Blend	234	85	
Disturbed_1	14	5	
Unknown_1	0	0	
Galaxy	3	1	6
Disturbed_2	1	<1	
Unknown_2	12	4	

$\sim 6\%$ of bright big extended objects with high probability to be extended are problematic for FGS (lime cell).

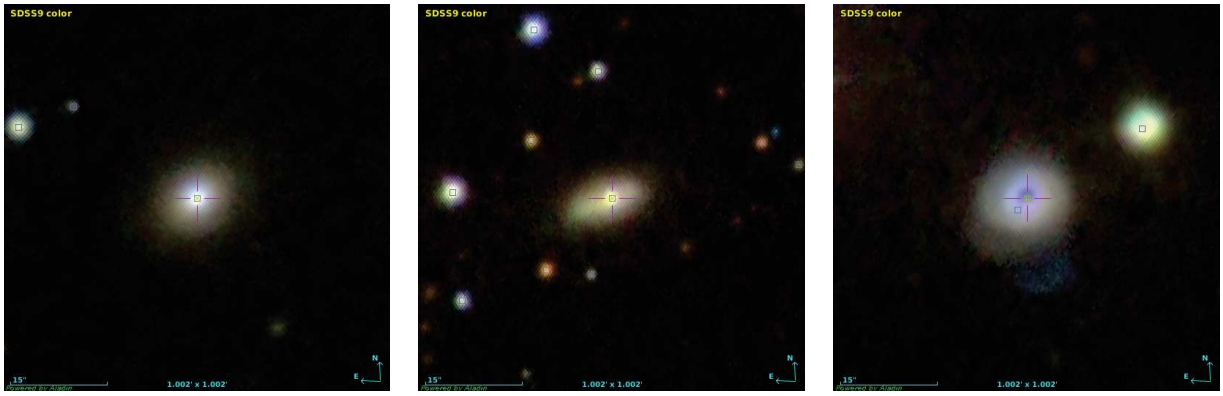


Figure 48: SDSS images of the three galaxies detected in this set. The first and the third are classified as Seyfert I and Seyfert II in Simbad.



Figure 49: Left panel: very bright isolated star. Central and right panels: Images of blends.

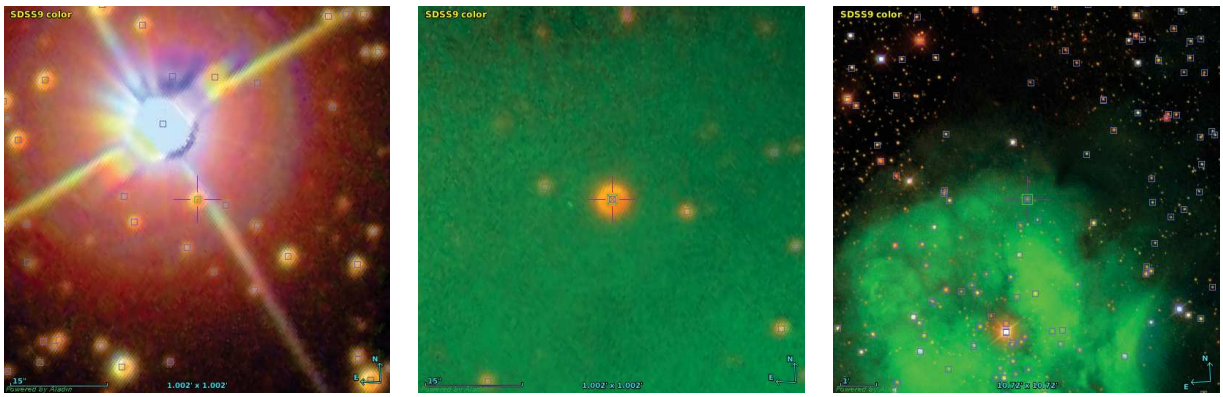


Figure 50: Left panel: image of a disturbed_1 object. Central and right panels show the same disturbed_2 object at different scales; this object is classified as a star in Simbad and it is located in the field of the Cocoon nebula.

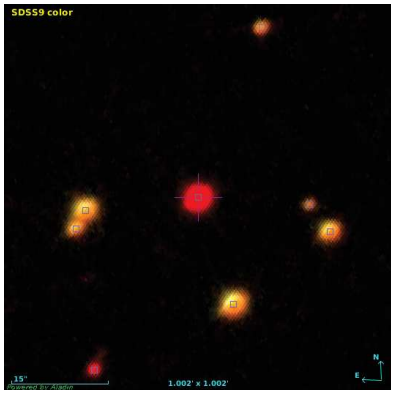


Figure 51: Object of unknown_2 type classified as a possible carbon star in Simbad.

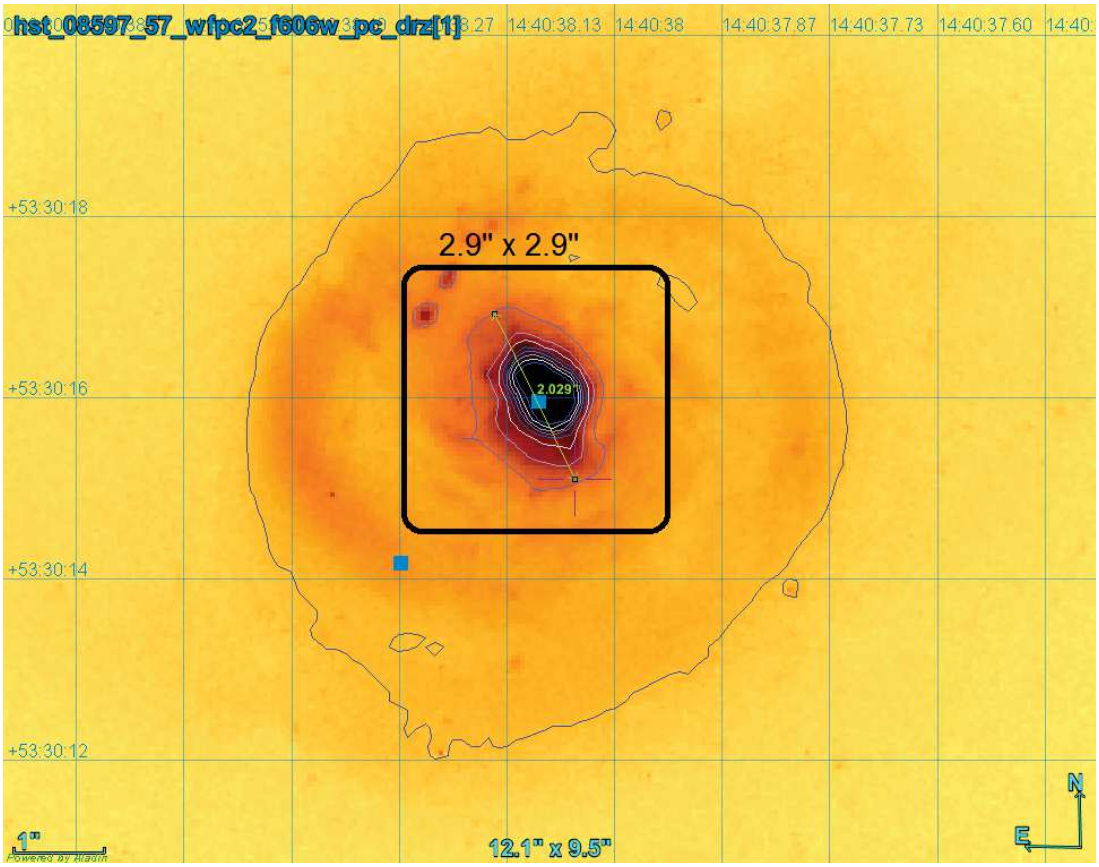


Figure 52: HST-WFPC2 image of the galaxy in the right panel of Figure 48 (Seyfert 2 Galaxy Mrk 477, R_{FGS}=16.136606). This is the only HST image in this set. The black squared box has dimensions of the FGS tracking window.

BRIGHT_LOW_P1 (R_{FGS}<16 and P1$\leq$0.7).
Total number of objects = 143, inspected images = 143.

object type	n	%	%
All	143	100	
Big star	24	17	100
Blend	77	54	
Disturbed_1	37	26	
Unknown_1	4	3	
Galaxy	0	0	<1
Disturbed_2	1	<1	
Unknown_2	0	0	

Less then 1% of bright big extended objects with low probability to be extended are problematic for FGS (lime cell).

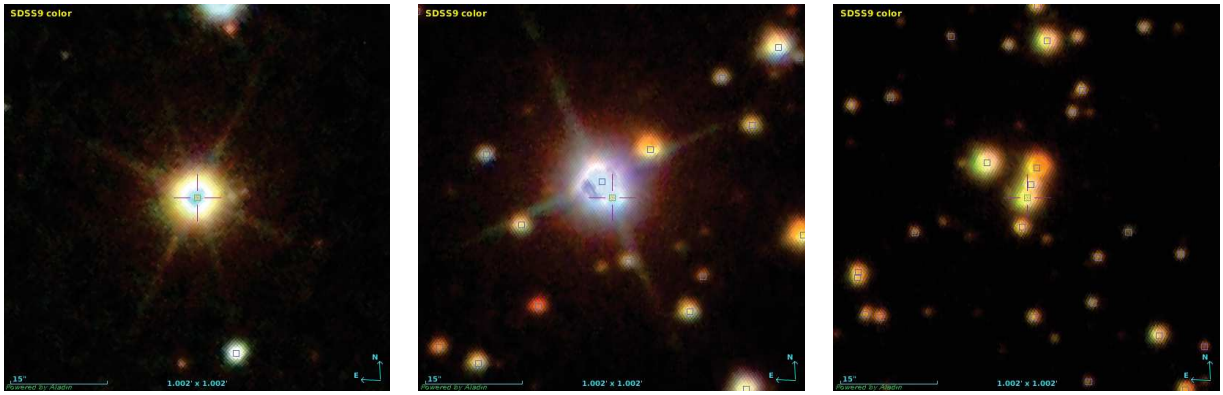


Figure 53: Left panel: a very bright isolated star. Central and right panels: images of blends.

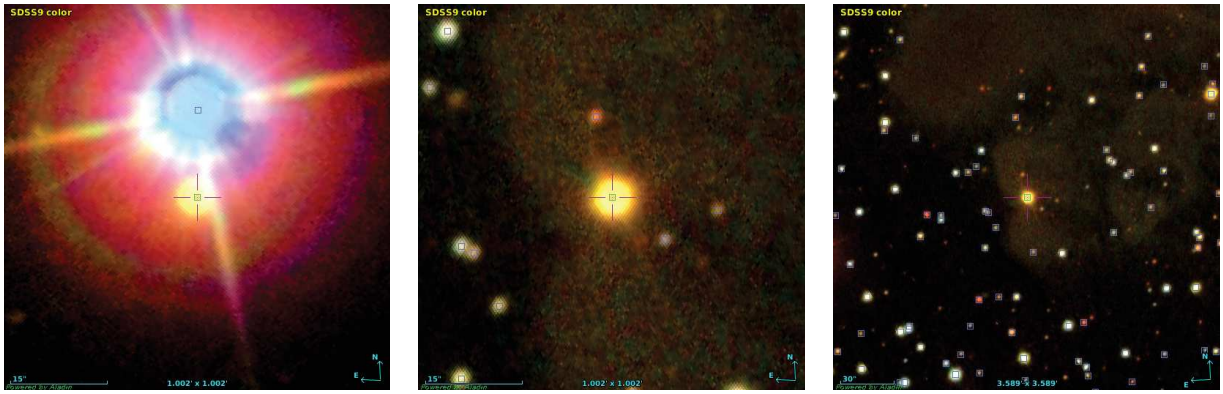


Figure 54: Left panel: disturbed_1 object. Central and right panels show the same disturbed_2 object at different scales; it is a star in a molecular cloud.

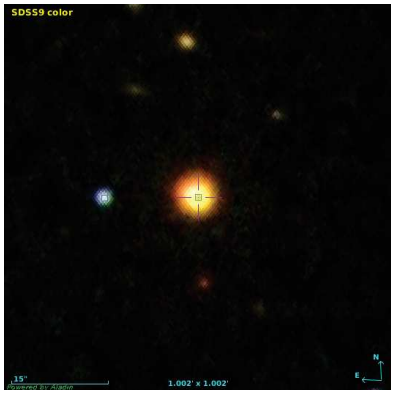


Figure 55: Object of unknown_1 type.

FAINT_HIGH_P1 (R_{FGS} $\geq$16 and P1>0.7).
Total number of objects = 4690, inspected images = 875.

The inspected images in this set belong to three groups: (1) 265 objects with abs(b)$\geq$20 (100% of the sample), (2) 310 objects with abs(b)<20 and R_{FGS}<17 (100% of the sample), (3) 300 objects with abs(b)<20 and R_{FGS} $\geq$17 (random selection, 7% of the sample).

	(1)			(2)			(3)		
object type	**n**	%	%	**n**	%	%	**n**	%	%
All	265	100		310	100		300	7	
Blend	118	44		233	75		112	37	
Disturbed_1	55	21	72	21	7	82	64	21	88
Unknown_1	19	7		0	0		90	30	
Galaxy	3	1		1	<1		0	0	
Disturbed_2	15	6	28	2	<1	18	3	1	11
Unknown_2	55	21		53	17		31	10	

Combining the data of the three groups we obtain that $\sim 13\%$ of faint big extended objects with high probability to be extended are problematic for FGS (lime cells) and $\sim 87\%$ are not problematic.

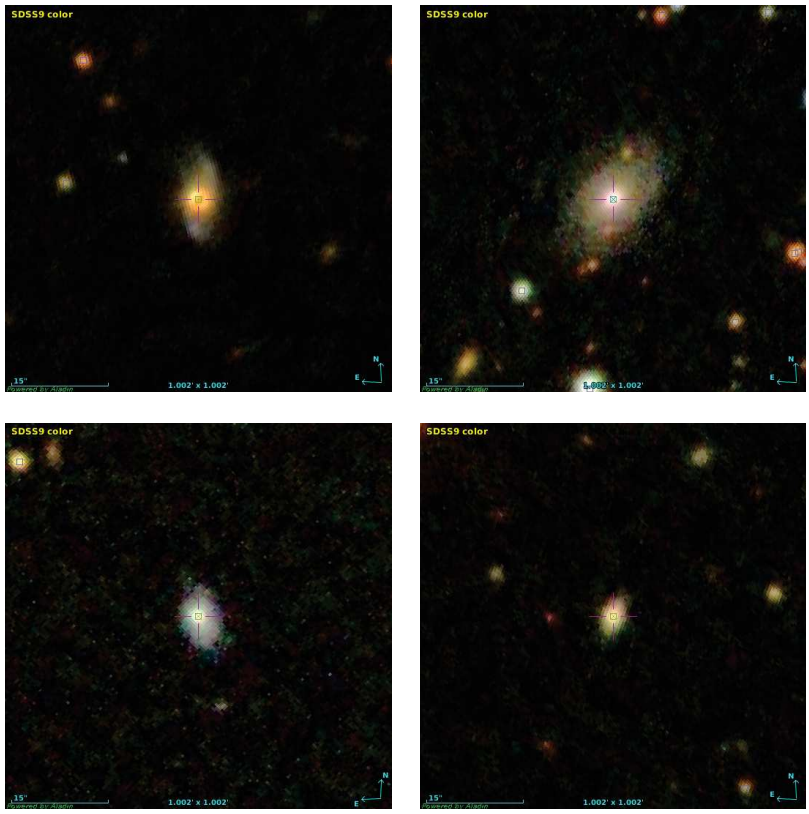


Figure 56: SDSS images of the four galaxies detected in this set. The galaxy in the upper right panel is also classified as galaxy in Simbad.

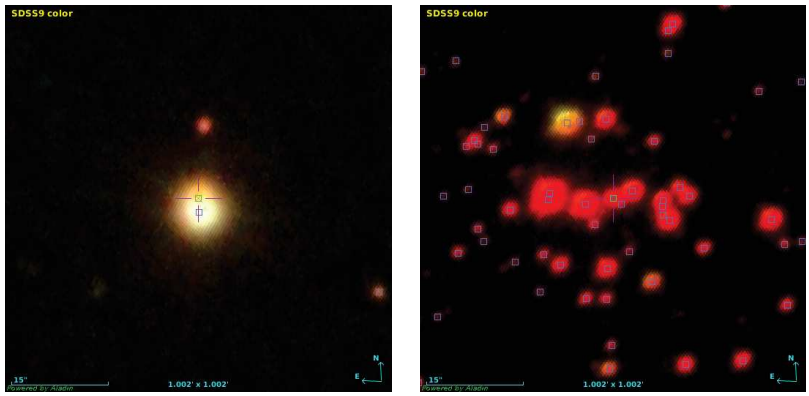


Figure 57: Images of blends. The right panel shows the galactic open cluster Kronberger 80.

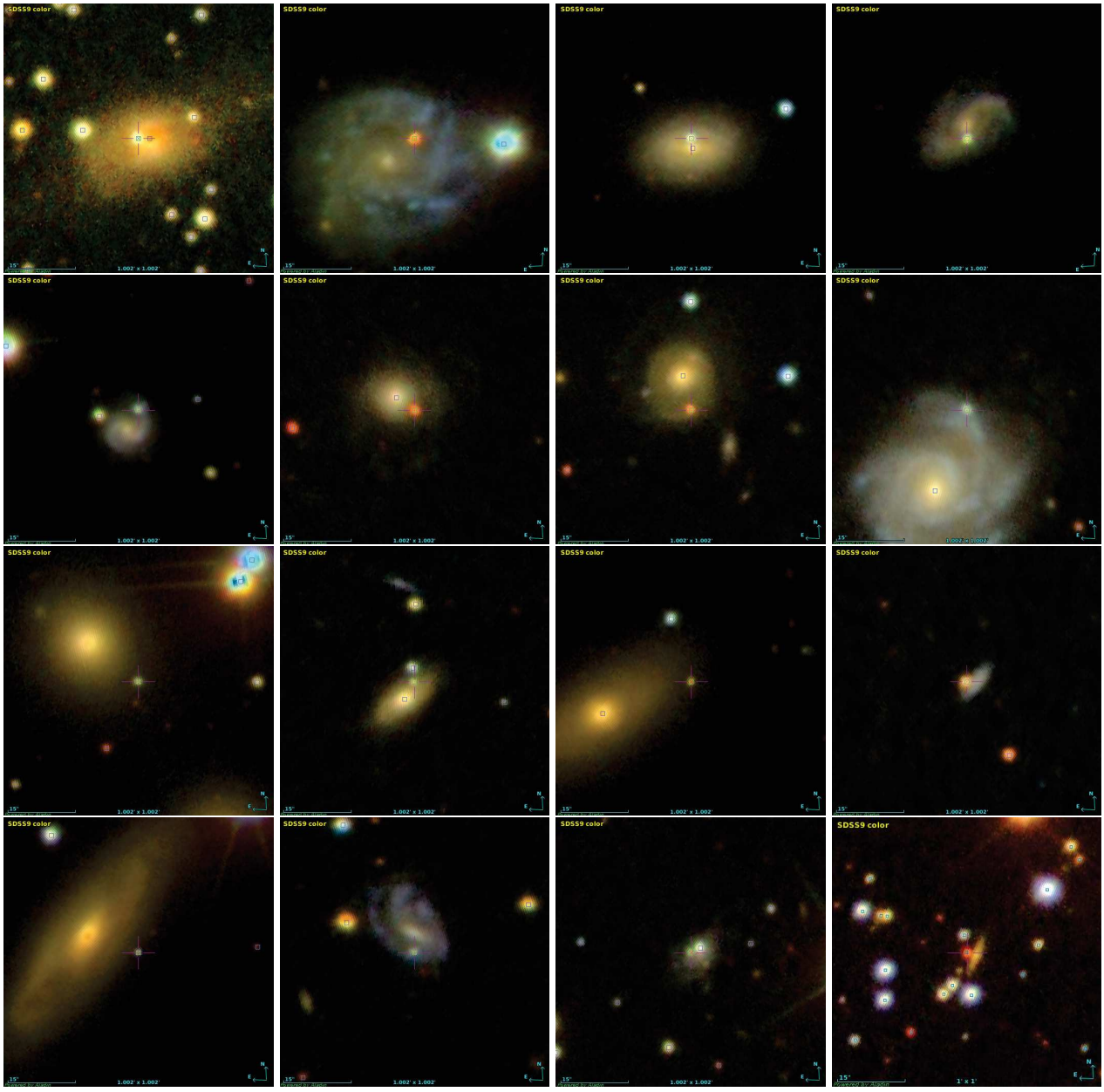


Figure 58: Images of disturbed_2 objects.



Figure 59: Left panel: Images of disturbed_1 object. Central and left panels show the same disturbed_2 object at different scales; this object is classified as an emission-line star in Simbad and it is located in the field of the Cocoon nebula.

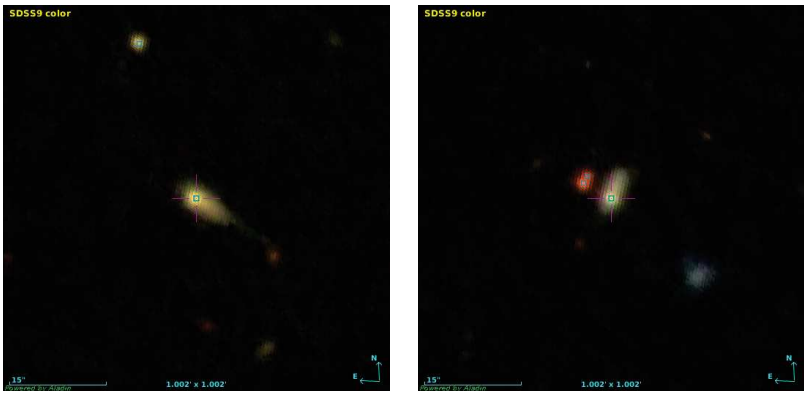


Figure 60: Unknown_2 objects classified as galaxy in Simbad.

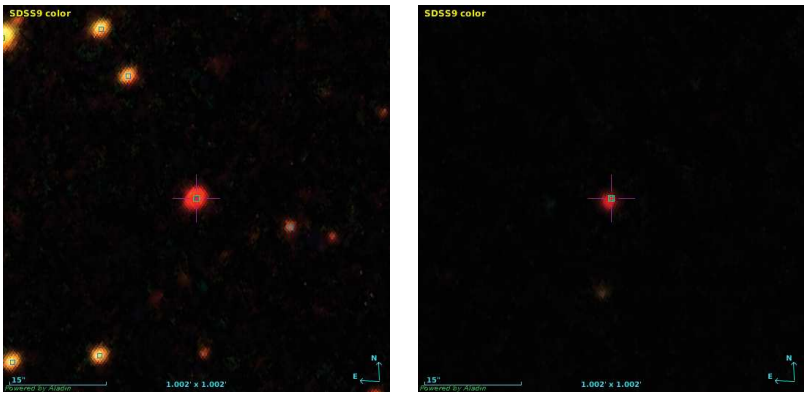


Figure 61: Left panel: unknown_2 object classified as star in Simbad. Right panel: unknown_1 object classified as high proper motion star in Simbad.

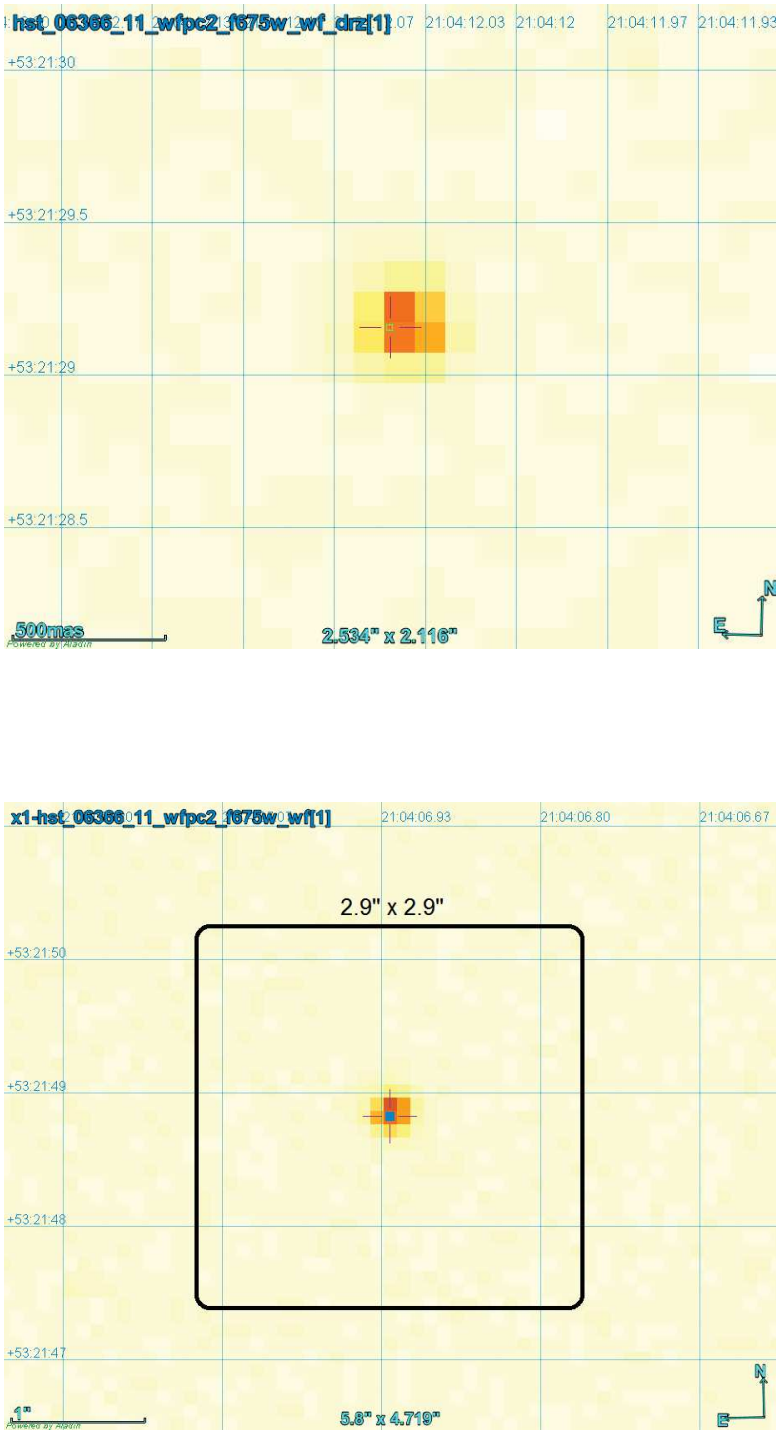


Figure 62: HST_WFPC2 images of two sources in this set. They belong to group (3) and have been classified as unknown_1 objects in the SDSS images (faint red sources). The black squared box has dimensions of the FGS tracking window.

FAINT_LOW_P1 (R_{FGS} $\geq$16 and P1$\leq$0.7).
Total number of objects = 1407, inspected images = 425.

The inspected images in this set belong to two groups: (1) 125 objects with abs(b)$\geq$20 (100% of the sample), (2) 300 objects with abs(b)<20 (random selection, 23% of the sample).

	(1)			(2)		
object type	**n**	%	%	**n**	%	%
All	125	100		300	23	
Blend	14	11	77	121	40	96
Disturbed_1	60	48		110	37	
Unknown_1	22	18		58	19	
Galaxy	1	<1	23	0	0	4
Disturbed_2	1	<1		5	2	
Unknown_2	27	22		6	2	

Combining the data of the two groups we obtain that $\sim 6\%$ of faint big extended objects with low probability to be extended are problematic for FGS (lime cells) and $\sim 94\%$ are not problematic.

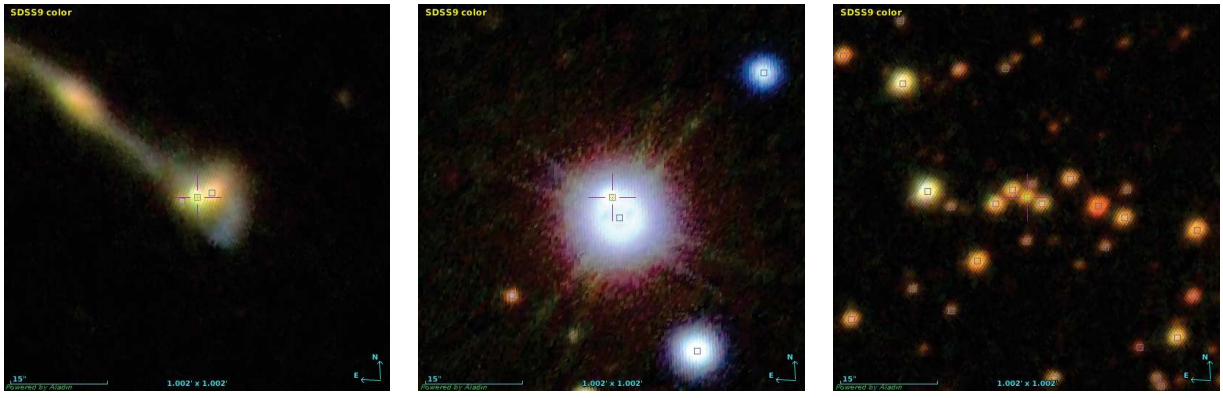


Figure 63: Left panel: SDSS image of the only galaxy detected in this set (this object is 24 arcsec away from a Simbad source classified as group of galaxies). Central and right panels: images of blends.

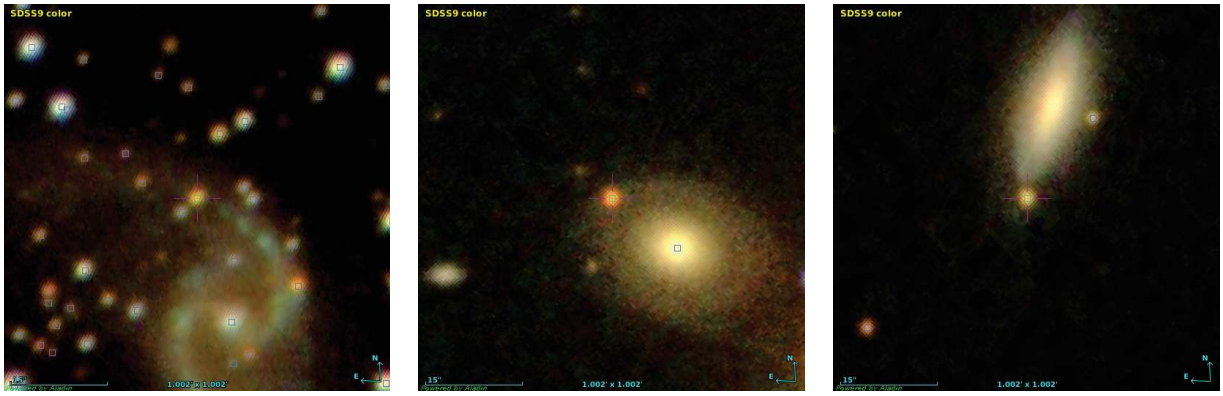


Figure 64: Images of disturbed_2 objects.

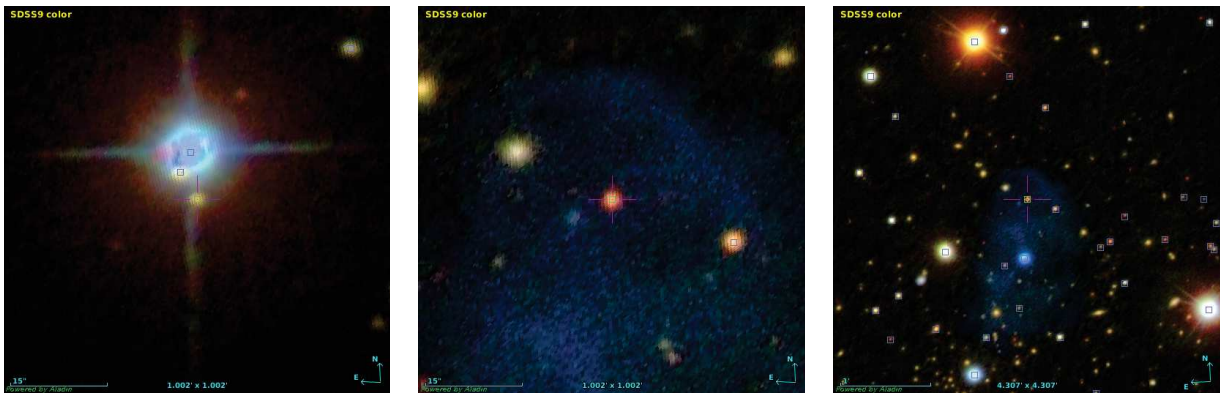


Figure 65: Left panel: image of disturbed_1 object. Central and right panels show the same disturbed_2 object at different scales; it is located in the field of the planetary nebula PN K 1-16.

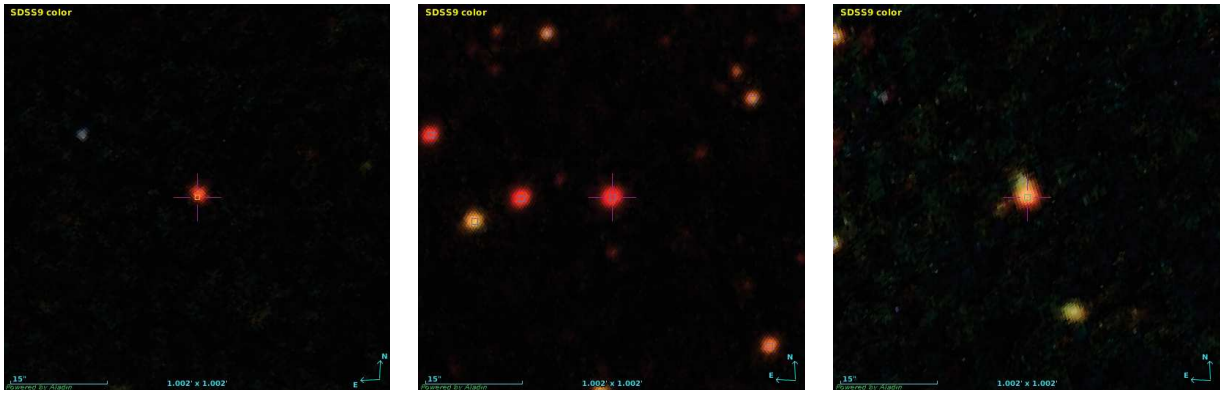


Figure 66: Left panel: image of unknown_1 object. Central and right panels: images of unknown_2 objects.

10. APPENDIX B

An all-sky sample of ISC possibly big extended sources brighter then R_{FGS} 18 (i.e. ISC sources with Classification Flag=1 and R_{FGS}>18 having the SDSS size parameter deVRad_g > 2.9/4.0) has been cross-matched with high-resolution Hubble Space Telescope (HST) archived images to verify if they are effectively bigger then the FGS tracking window.
In this appendix twenty HST images on a total of 169 matched objects are shown.

In each of the following figures the left panel shows the HST image of the source and the right panel shows the SDSS image of the same target on a larger field. In both panels the field dimension and a scale-bar are indicated. Brightness contours and a black squared box representing the FGS tracking window are also superposed to the HST images. In the figures caption the Simbad identifier (if it exists) is reported along with the type of the source, its R_{FGS} magnitude and the P1 value (probability to be extended).

The HST images are cutouts from WFPC2-WF (~ 0.1 arcsec/pixel), WFC3-UVIS (~ 0.04 arcsec/pixel), ACS-WFC (~ 0.05 arcsec/pixel) images.
The SDSS images pixel scale is ~ 0.4 arcsec/pixel.

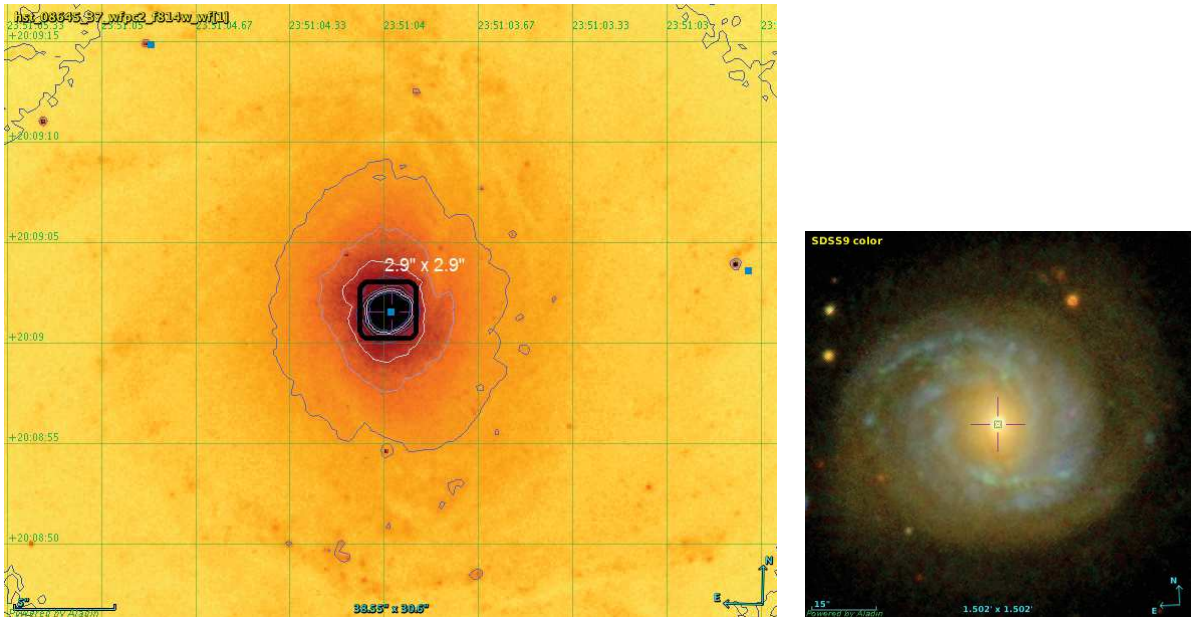


Figure 67: NGC 7769 – LINER-type Active Galaxy Nucleus
source_id=2823242193058306048, G=15.20, R_{FGS}=14.83, P1=0.86

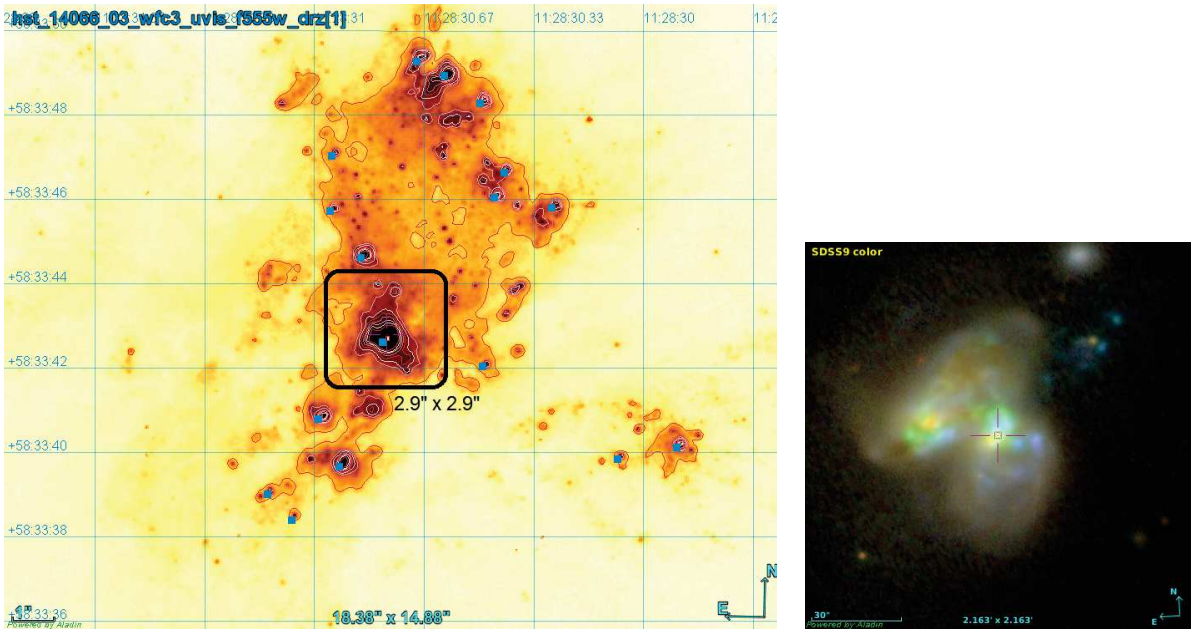


Figure 68: SDSS J112830.77+583342.9 – Interacting Galaxy (Star Formation Region)
source_id=858231978679564160 , G=15.46, R_{FGS}=15.10, P1=0.84

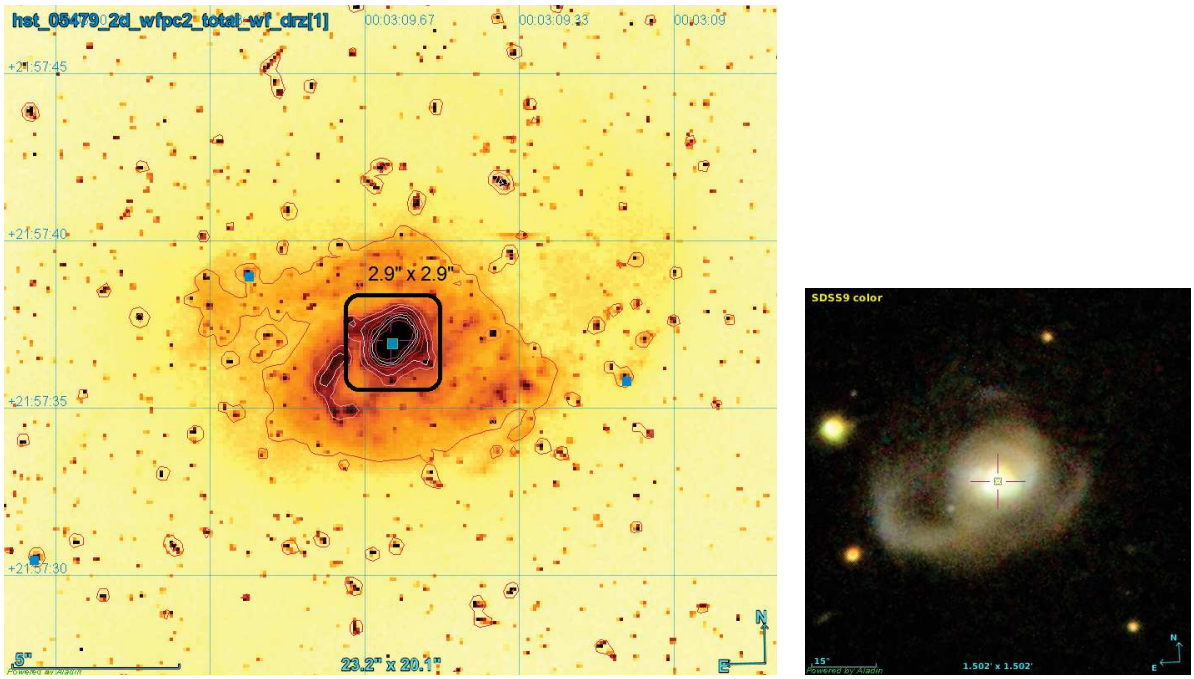


Figure 69: Mrk 334 – Seyfert 1 Galaxy
source_id=2847176568328836736, G=15.83, R_{FGS}=15.39, P1=0.92

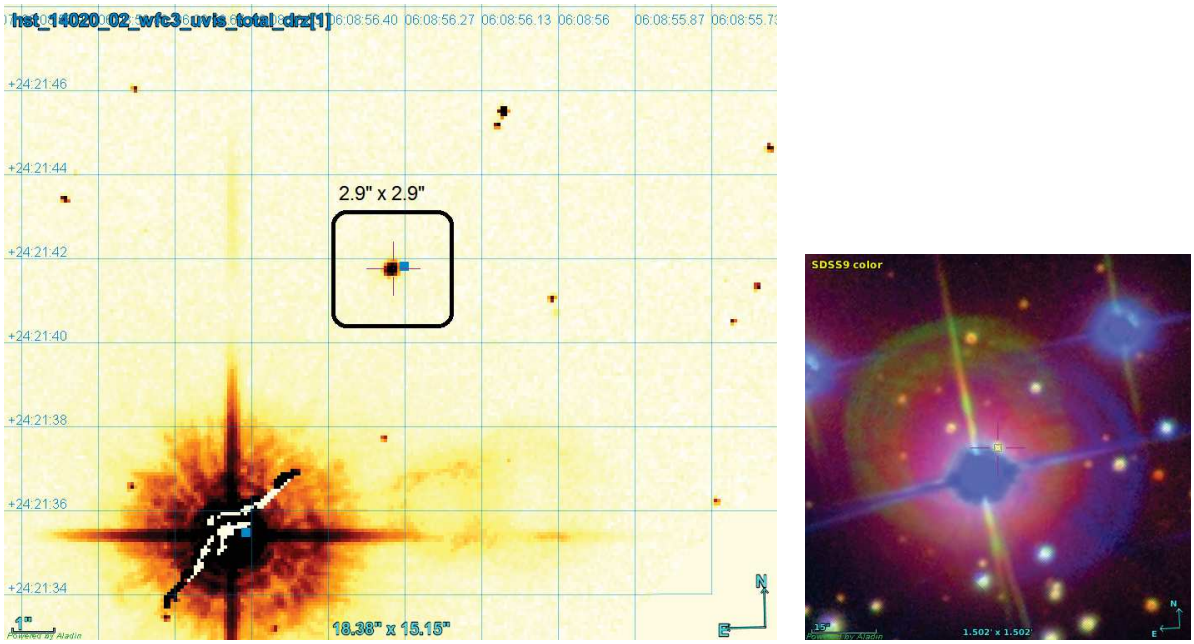


Figure 70: Cl* NGC 2168 BSB 5173 – Star in open cluster
source_id=3426270715411638912, G=15.81, R_{FGS}=15.49, P1=0.83

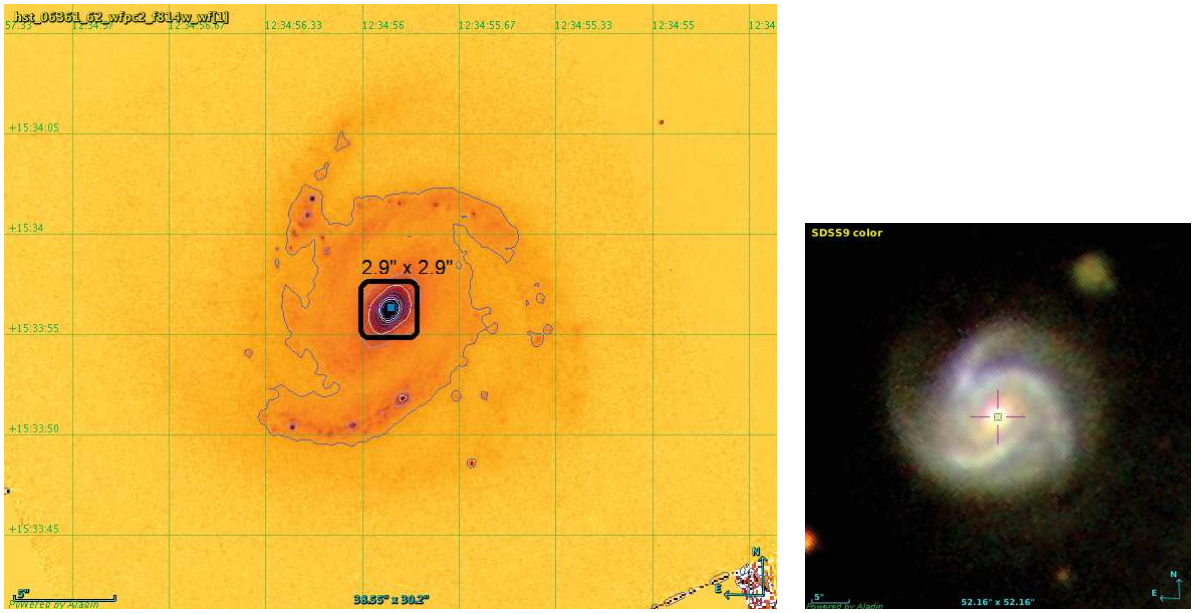


Figure 71: IC 3528 – Seyfert 1 Galaxy
source_id=3933547692122711936, G=16.99, R_{FGS}=16.61, P1=0.95

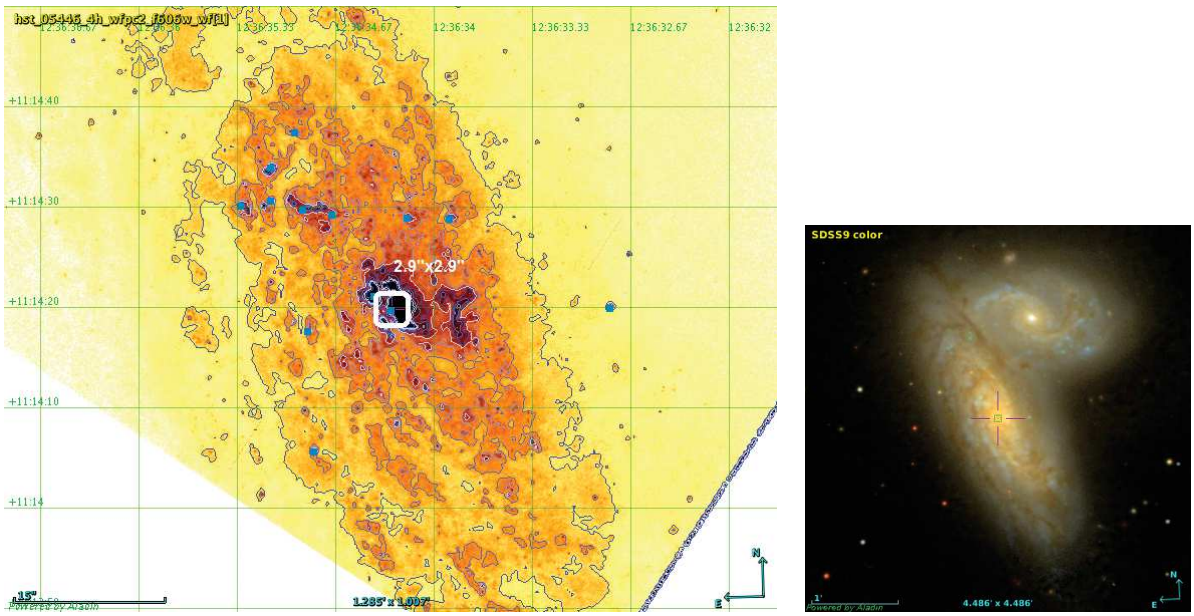


Figure 72: NGC 4568 – Galaxy in Pair of Galaxies
source_id=3904332671739848192, G=17.00, R_{FGS}=16.62, P1=0.88

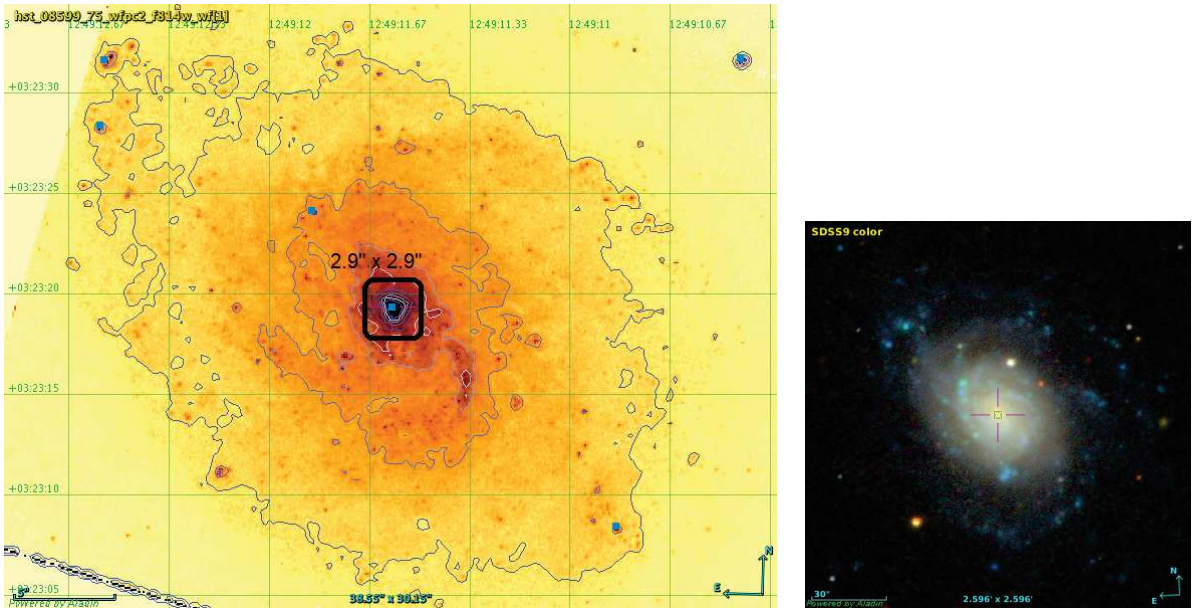


Figure 73: NGC 4701 – Galaxy
source_id=3703825422062498816, G=17.11, R_{FGS}=16.76, P1=0.92

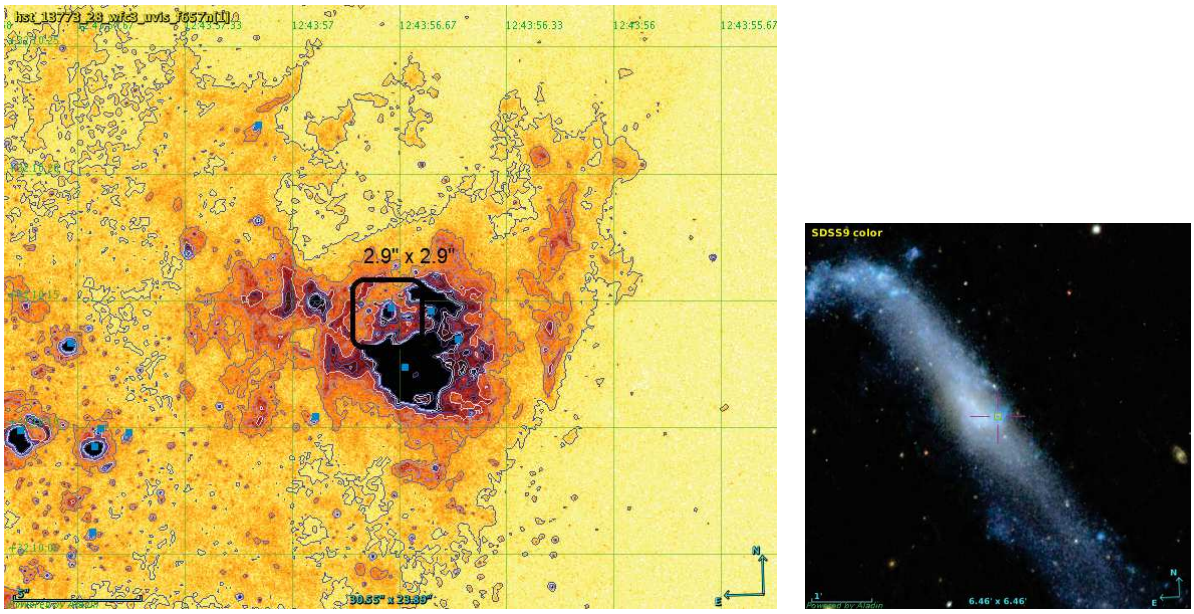


Figure 74: 2MASS J12435666+3210138 – Active Galaxy Nucleus
source_id=1513717414809812992, G=16.74, R_{FGS}=16.79, P1=0.85

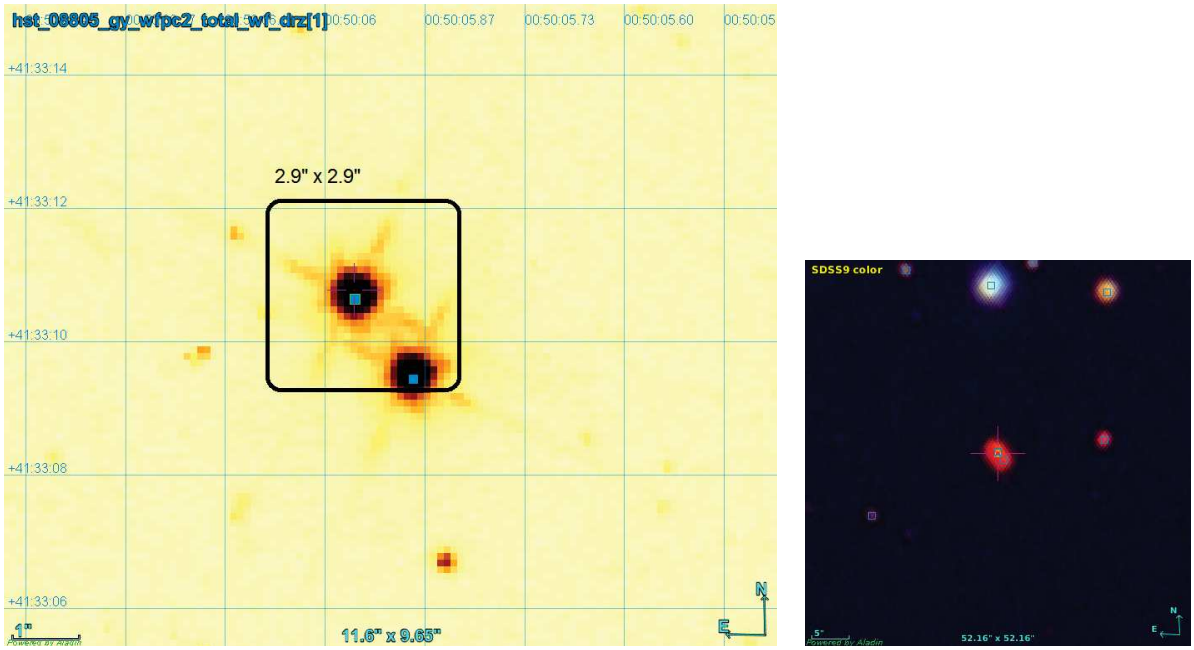


Figure 75: Star (not in Simbad)
source_id=375055480798867328 , G=17.60, R_{FGS}=16.95, P1=0.93

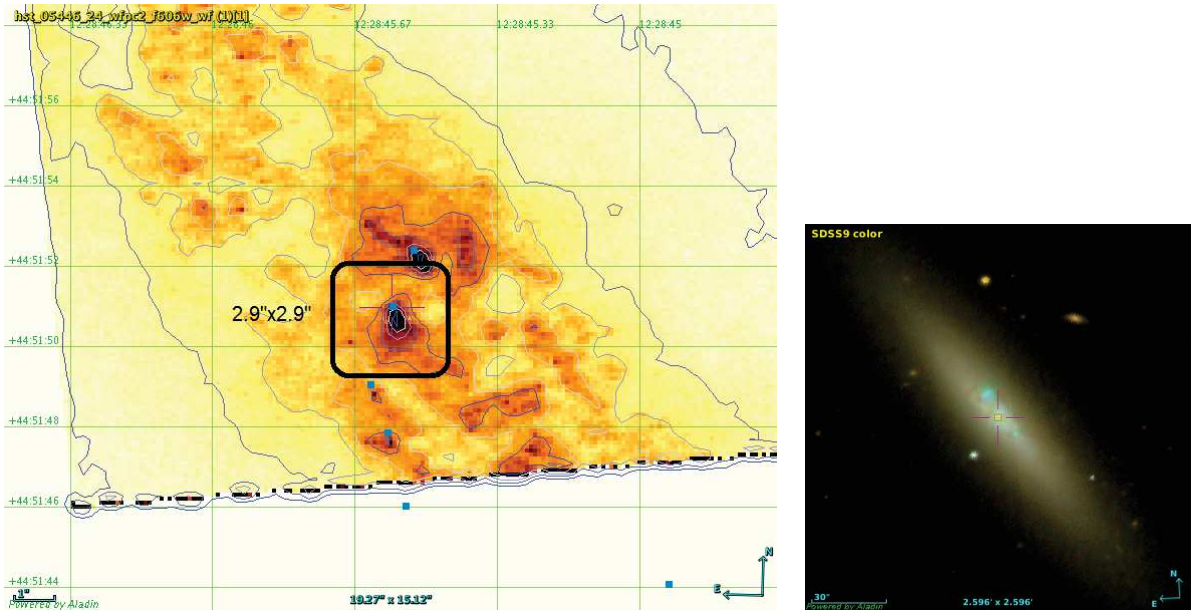


Figure 76: NGC 4460 – HII Galaxy
source_id=1541681362762025728, G=17.50, R_{FGS}=17.12, P1=0.80

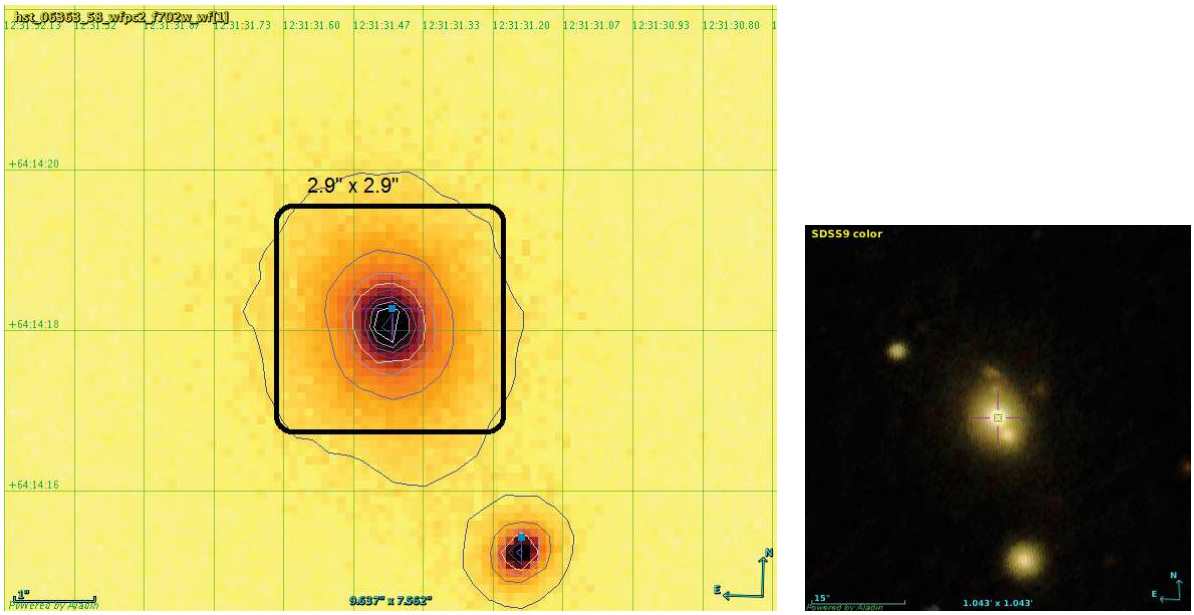


Figure 77: QSO B1229+6430 – BL Lacertae-type object
source_id=1679936845347969920, G=17.89, R_{FGS}=17.47, P1=0.95

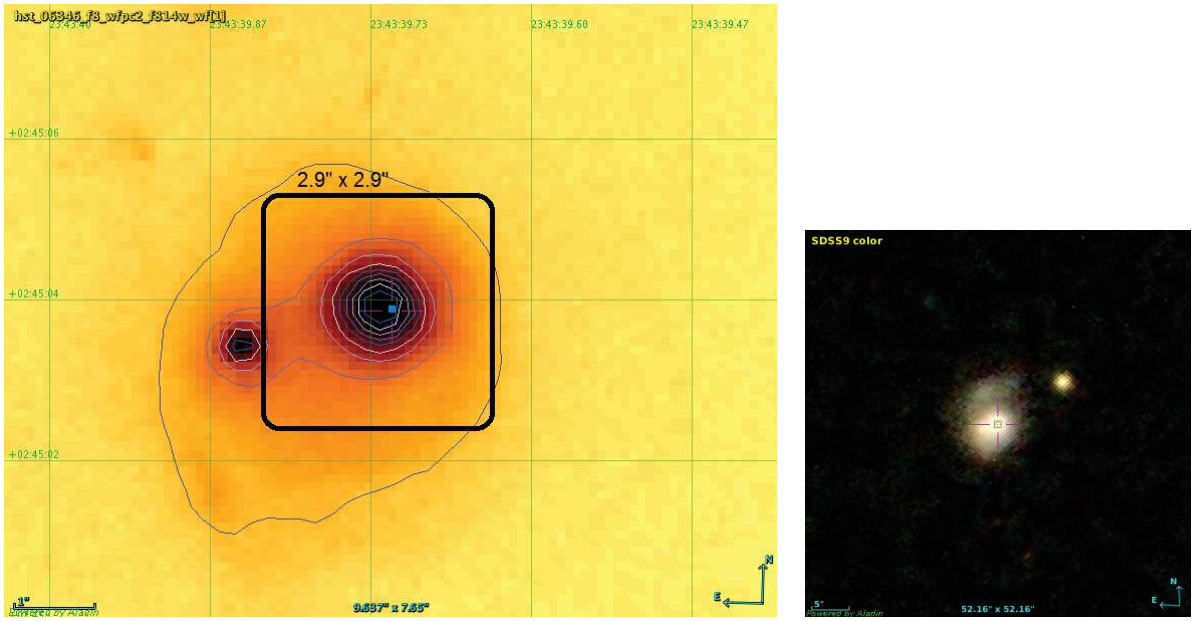


Figure 78: 2MASX J23433974+0245036 – Seyfert 1 Galaxy
source_id=2646866543548019072, G=17.97, R_{FGS}=17.59, P1=0.92

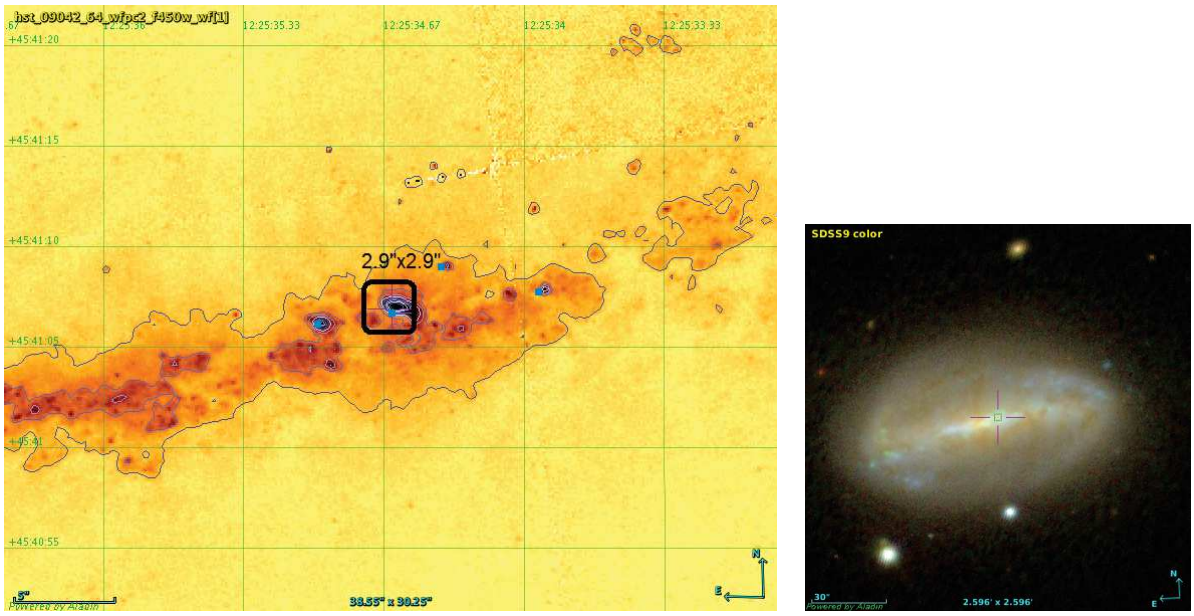


Figure 79: [BKD2008] WR 284 – Part of Galaxy NGC4389 (HII region)
source_id=1541868043512095104, G=17.79, R_{FGS}=17.61, P1=0.93

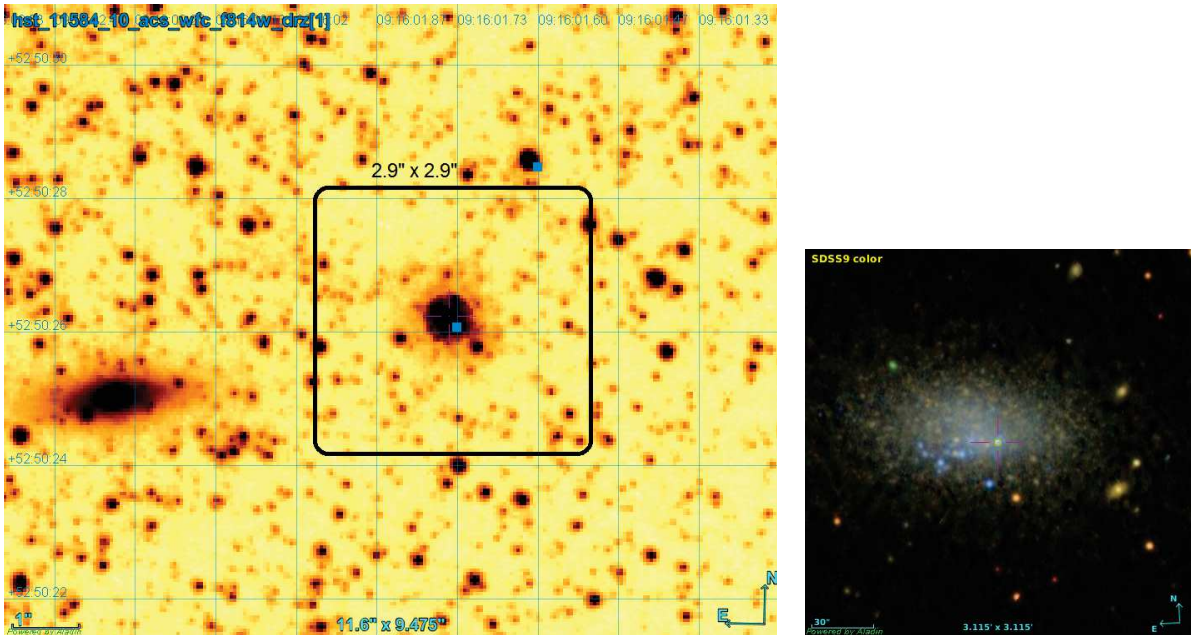


Figure 80: SDSS J091601.73+525026.0 – Star (foreground star on dwarf galaxy UGC 4879)
source_id=1022549082303411584, G=17.97, R_{FGS}=17.72, P1=0.55

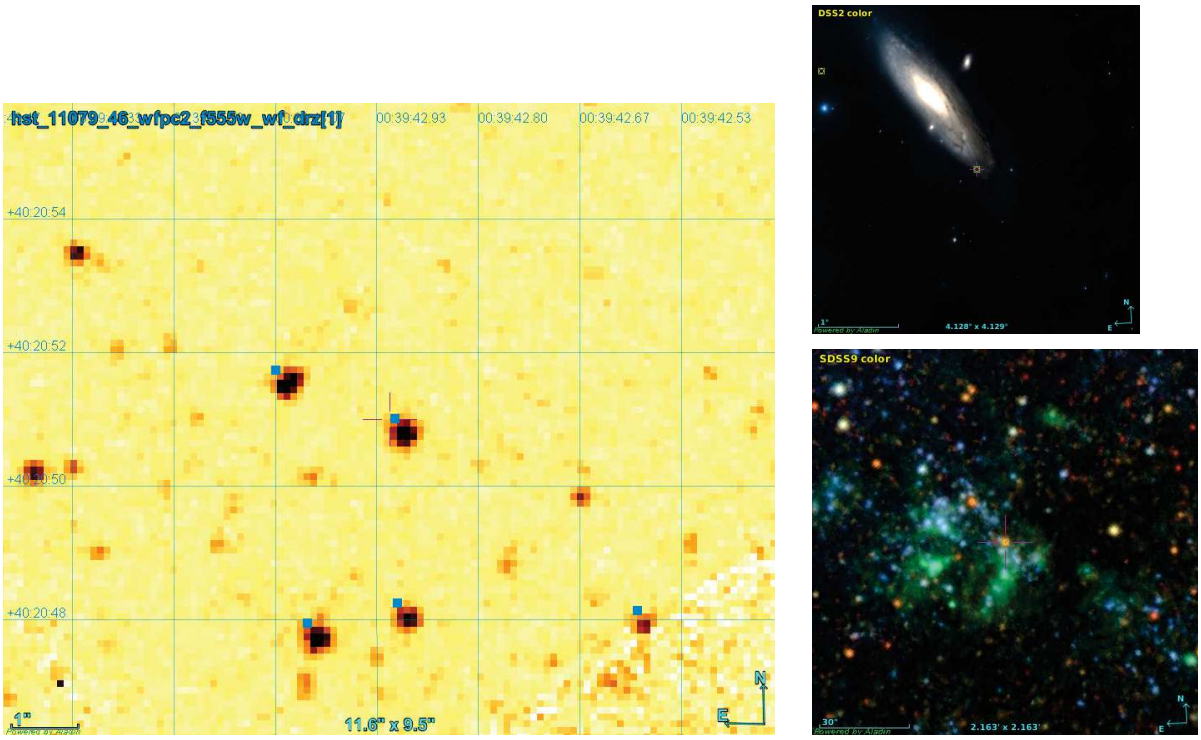


Figure 81: 2MASS J00394291+4020510 – Possible Red supergiant star in M31's HII region source_id=381119317489566464 , G=18.35, R_{FGS}=17.75, P1=0.87

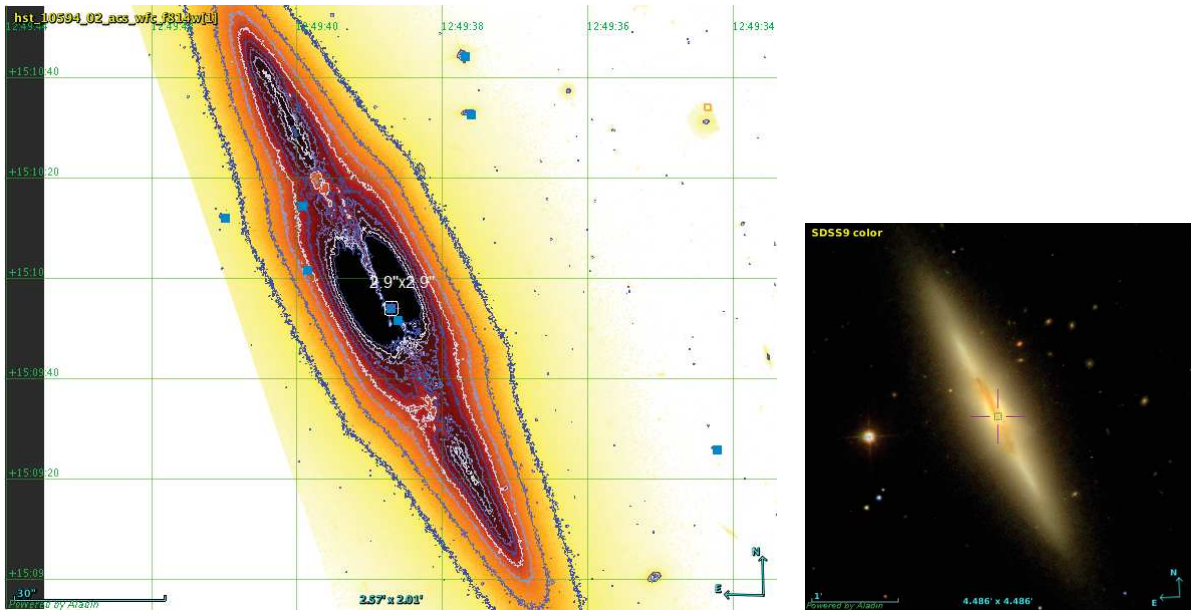


Figure 82: NGC 4710 – HII Galaxy source_id=3931025923551506944, G=18.19, R_{FGS}=17.81, P1=0.79

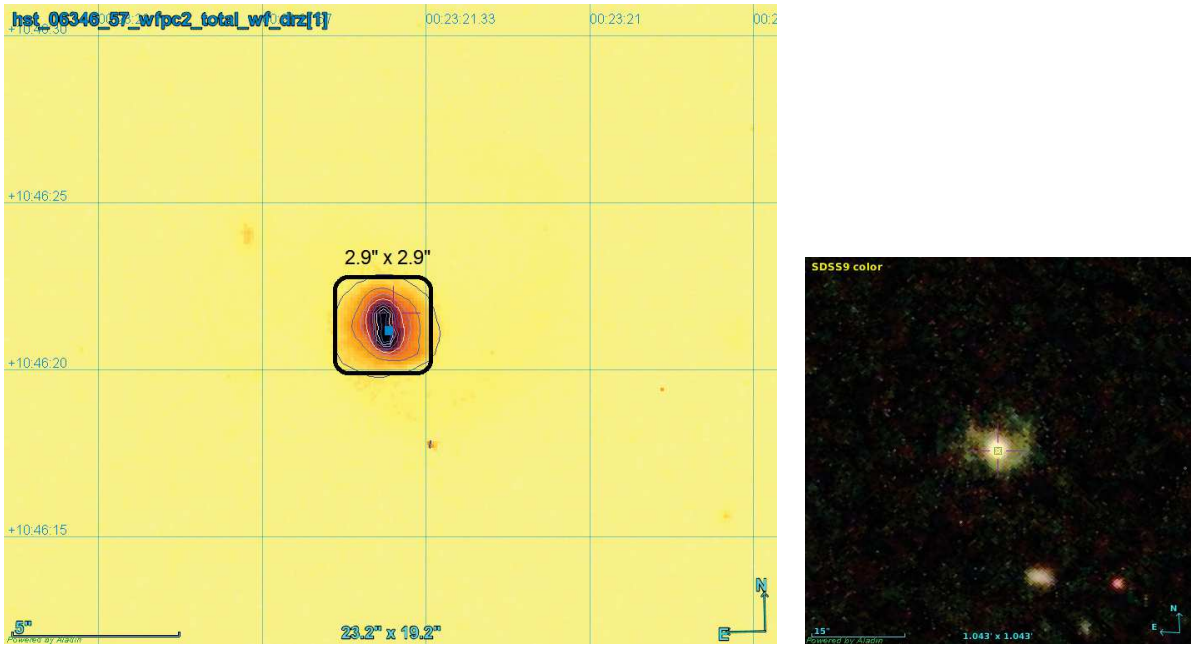


Figure 83: 2MASS J00232140+1046213 – Seyfert 1 Galaxy
source_id=2754181695917482240, G=18.40, R_{FGS}=17.90, P1=0.93

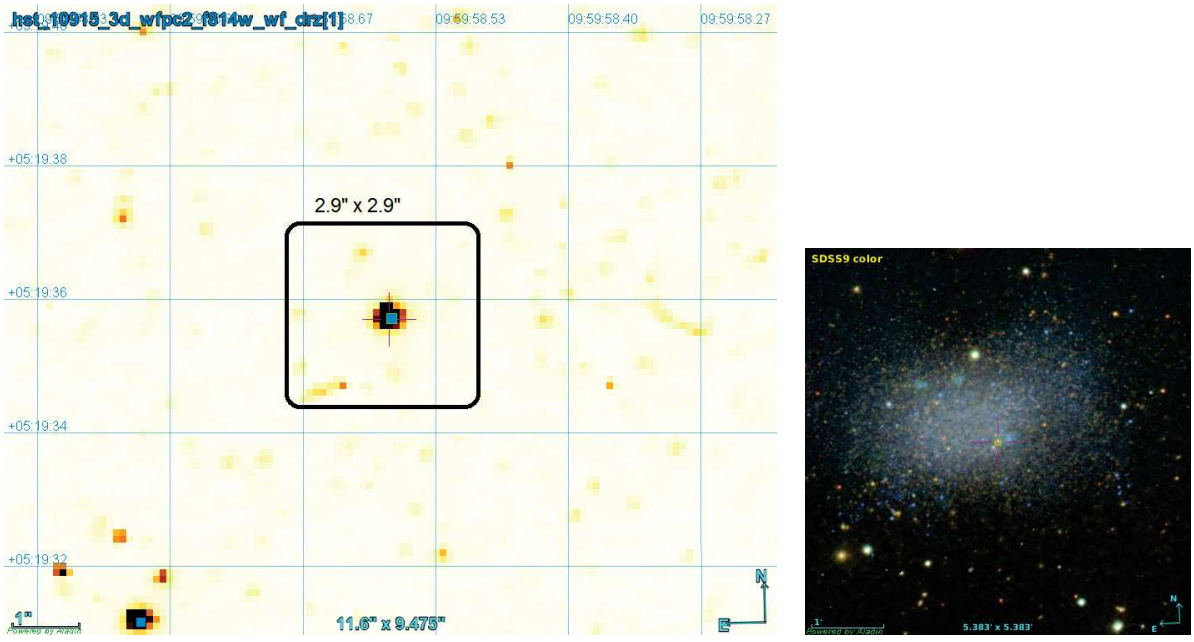


Figure 84: EV* SexB V0005 – Variable Star of irregular type in dwarf galaxy
source_id=3849400001370256384, G=18.40, R_{FGS}=17.95, P1=0.73

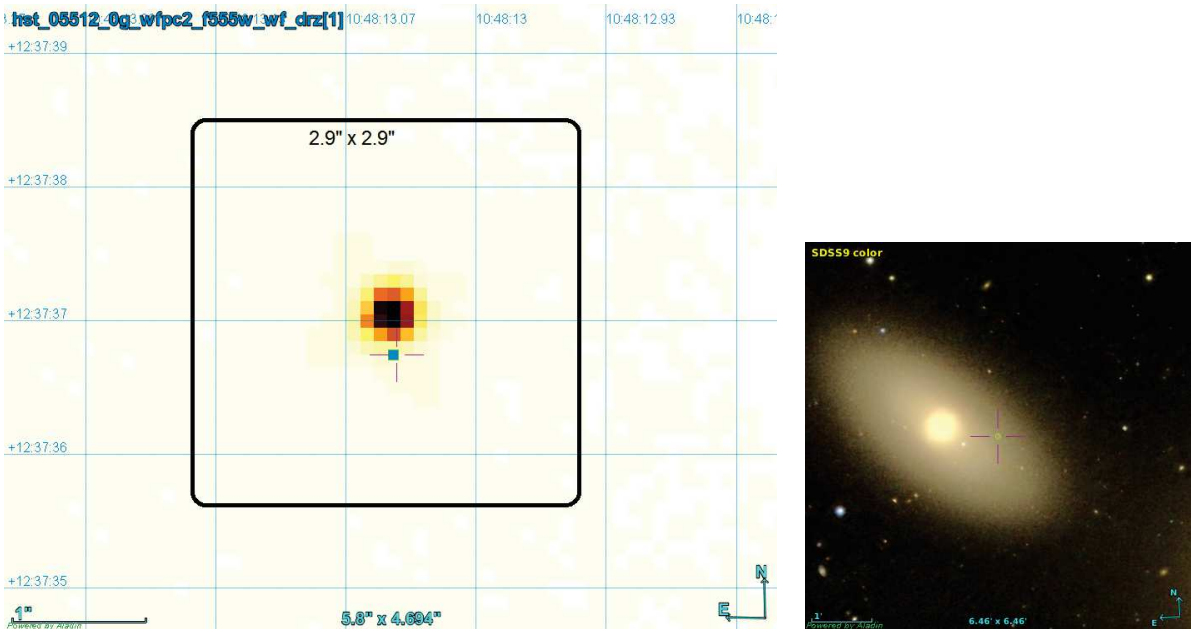


Figure 85: [CJF89] NGC 3384 k – Star
source_id=3872447654875340288, G=18.33, R_{FGS}=17.95, P1=0.82

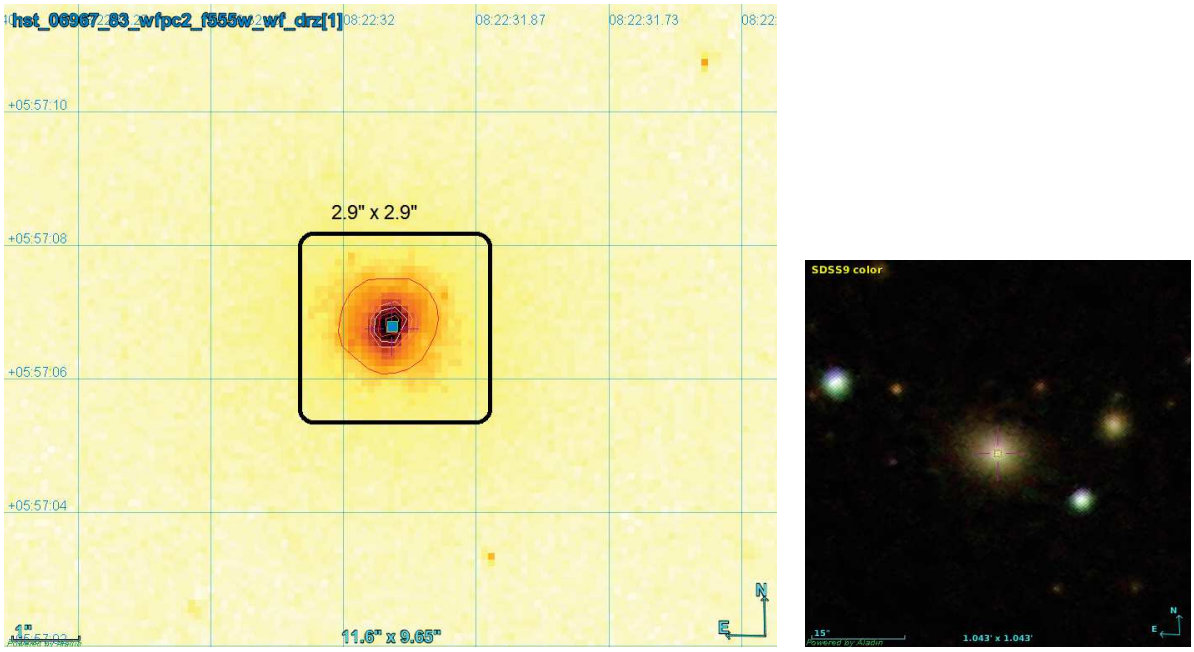


Figure 86: 3C 198.0 – Active Galaxy Nucleus
source_id=3093775585962794880, G=18.38, R_{FGS}=17.99, P1=0.94